Spring 4-17-2013

Flow and Geometry Measurements at an Active Knickpoint

Clark W. Kephart
University of Nebraska-Lincoln, ckcj10@aol.com

Flow and Geometry Measurements at an Active Knickpoint

By

Clark Willis Kephart

A THESIS

Presented to the Faculty of

The Graduate College at the University of Nebraska

In Partial Fulfillment of Requirements

For the Degree of Master of Science

Major: Civil Engineering

Under the Supervision of Professor

David Admiraal

Lincoln, Nebraska

May, 2013

Flow and Geometry Measurements at an Active Knickpoint

Clark Willis Kephart, M.S.

University of Nebraska, 2013

Adviser: David M. Admiraal

Channel degradation is an area of growing concern in areas of the Midwestern United States where there are large deposits of loess soils. Channel degradation occurs as a result of disturbances to the sediment load, bed soil configuration, and hydraulic characteristics of the stream (i.e. discharge, channel slope and geometry). These changes may occur suddenly or slowly over time. A given disturbance may be due to a large rain event, channel adjustments (i.e. dredging and straightening), and changes in land use around the stream (Chen et al. 1999).

A knickpoint is an abrupt drop in stream bed elevation over which water plunges and scours the downstream bed. The plunging water may lead to intense bed degradation and subsequent upstream migration of the knickpoint, often causing stream banks to become unstable and unsafe. Knickpoint migration problems have been particularly prevalent in the loess soil regions of western Iowa and eastern Nebraska as a result of wide spread channel straightening projects in the region. The goal of this project is to monitor the migration of an active knickpoint located on Mud Creek in Mills County, Iowa. Analysis of the knickpoint consists of: (1) acquiring time lapse images of the knickpoint every thirty minutes from a camera installed at the site, (2) periodically collecting detailed survey data of the stream channel and knickpoint, (3) collecting Large-scale Particle Image Velocimetry (LPIV) videos of the flow for a variety of high

and low flow conditions, and (4) estimating discharges in the channel using the LPIV results.

The time lapse images provide a frame-by-frame depiction of the upstream movement of the knickpoint. The images allow us to assess when the knickpoint has migrated and if its migration is associated with a particular storm event. The less frequently collected survey data provide a more accurate assessment of knickpoint position and can also be used in conjunction with LPIV videos to establish velocity distributions and a rating curve for the knickpoint. LPIV videos have been converted to bitmaps and rectified for analysis using Particle Image Velocimetry (PIV) and Particle Tracking Velocimetry (PTV) software. They are then used to examine depth, discharge, and velocity conditions for different flow events.

Acknowledgements

I would like take this opportunity to thank a few of the people that made this research experience not only successful, but enjoyable. First off I must express my deep appreciation of Dr. David Admiraal for affording me this opportunity and guiding me to the successful completion of this thesis and possible publication. The steady guidance and patience that was afforded by Dr. Admiraal promoted a positive learning environment that without-a-doubt has prepared me for the next step in my career and life.

There were a few graduate students that need to be thanked for their roles in making this research experience enjoyable.

Alex: Thanks for keeping every moment very interesting. Your enthusiasm made the stressful course work and tedious work in the lab much easier. I am so glad that you thought me so much about looking up bike stuff on the internet, and without you we never would have been able to steal the world map and hang it in our office

Miles: I am so grateful that you allowed me to spend so much time running tests in the lab each day. If it wasn't for you, I would have had to spend all that time working on my own research. I mean, who wants to that? Ha

Mohamed: Thank you for all your help getting my thesis ready, and most importantly thank you for all the FuFu.

Martin: Thank you for the 50 cases of MRE's!!

I also wanted to thank my mom and dad for all their help and support.

GO HUSKERS!!

Table of Contents

List of Figures

List of Tables

Chapter 1: **Introduction**

1.1 Background

Knickpoints are natural or man-induced formations that occur frequently in streams and rivers all over the world. A knickpoint is manifested as a sudden drop in channel bed elevation that may resemble a river rapid or (at a larger scale) a waterfall (Brush and Wolman, 1960). Knickpoints tend to induce large scale channel degradation that consequently causes headward (upstream) migration of the knickpoint. The headward migration of the knickpoint results in steepened side slopes, bank failures, and channel widening downstream of the knickpoint. These degradation processes introduce safety concerns for people and structures adjacent to the stream channels. It is important to develop a deeper understanding of the migration processes of knickpoints in order to properly assess the condition of a given stream channel and to insure the proper design of stream crossings and surrounding structures.

1.2 Objectives of Research

Extensive laboratory and flume studies concerning the behavior of knickpoints have been carried out over the years; however little research has been conducted on actively migrating knickpoints in the field. This study centers on an active knickpoint located within the deep loess area of western Iowa. This knickpoint has induced large amounts of channel degradation, and is approaching a bridge crossing upstream of the knickpoint. The end goal of this study is to acquire unique field measurements of the migration process of an active knickpoint that can help assess the condition of this and

other streams containing headward progressing knickpoints. Analysis of the knickpoint consists of the following:

1.) Acquiring time lapse images of the knickpoint over an extended period of time. The goal is to create a unique two-dimensional depiction of the headward retreat of the knickpoint front. The images aid in the determination of when the knickpoint has moved, how far it has moved, and if the movement was related to a given storm event.

2.) Periodically collecting detailed survey data of the stream channel and the knickpoint. The elevation data are used to create a series of contour plots that can more accurately assess the position of the knickpoint and visually show the stream morphology over time as a result of the presence of the knickpoint. The surveyed data are also used in conjunction with Large-scale Particle Image Velocimetry (LPIV) to establish velocity distributions and discharge estimates.

3.) Collecting LPIV videos for a variety of high and low flow conditions. These videos are analyzed using Particle Image Velocimetry (PIV) and Particle Tracking Velocimetry (PTV) software that will yield surface water velocity distributions. These velocity distributions are then used to estimate the discharge in the channel.

1.3 Thesis Overview

This thesis is a product of research conducted by the University of Nebraska-Lincoln (UNL) civil engineering department in collaboration with the University of Iowa. This project was funded by the Mid-America Transportation Center (MATC) and additional work was funded by the USGS 104b program administered by the UNL water center. The research focuses on the study of the migration behavior of knickpoints within

the deep loess area of the Midwestern United States. Altogether, the thesis consists of six chapters and three appendices (A, B, and C). Chapter 1 provides a brief introduction to the research that was conducted. Chapter 2 is a review of relevant literature pertaining to the research. Chapter 3 provides a description of the knickpoint site, the instruments used in the field, as-well-as hydrological information of Mud Creek. Chapter 4 provides an overview of the methods to carry out the knickpoint analysis. Chapter 5 presents the results obtained from the analyses. Finally, Chapter 6 is a summary of the conclusions drawn from the research process and presents some recommendations for future analysis of knickpoint migration.

Chapter 2: **Literature Review**

2.1 Introduction

Literature pertaining to channel degradation, knickpoints, and flow measurement techniques is presented in this chapter. A number of topics were reviewed; particularly work involving the basic structure of knickpoints and the concept of knickpoint migration; as well as a description of Large-scale Particle Image Velocimetry (LPIV). Also the channel degradation processes in the loess soil deposits of the Midwestern United States were reviewed, as this is the area in which the research is being conducted. Channel degradation is discussed in section two of the review. The areas of focus pertaining to knickpoint migration consist of knickpoint formation and classification, migration rate, and velocity field measurements at an overfall. These areas will be discussed in detail in the third section of the literature review. The final area of interest was flow measurement techniques, which includes the basics of Particle Image Velocimetry (PIV), Large-scale Particle Image Velocimetry, and image correction for the use of PIV software analysis. These topics will be discussed in section four.

2.2 Channel Gradation

2.2.1 Background

Channel bed conditions can be described as either: degrading, stable, or aggrading. Degradation is the gradual decline of stream bed elevation and the loss of streambed stability by way of headward progressing erosion, hill-slope failures, and channel widening. Aggradation is the gradual increase in channel bed level by way of excess sediment build-up over time. This can happen as a result of construction or removal of

vegetation in the upstream watershed, causing an increase in sediment load to the stream. For the purpose of this review only headward channel degradation will be discussed further as it is directly related to knickpoint migration.

2.2.2 Loess Soil

When examining channel bed degradation, the soil configuration of a stream bed is one of the most important characteristics to consider. Beds composed of Loess soil are of particular concern to researchers and engineers as they are very unstable. Loess is highly susceptible to erosion and facilitates the formation of steep stream banks and headward progressing knickpoints, which greatly affect the degradation of stream channels.

Channel degradation is an area of growing concern in areas of the Midwestern United States where there are large deposits of loess soil configurations. These areas are illustrated in *Figure 2.1*, which shows contours of loess depth in feet throughout the Midwest. Loess soils are unconsolidated, homogenous, and highly porous sediments that are typically yellowish brown in color. Loess is said to be one of the most highly fertile agricultural soils in nature, hence the large concentration of agriculture in the Midwest. Some of the qualities that make this soil ideal for agriculture are also what make it susceptible to erosion. Since loess deposits were formed by wind erosion, they are composed mainly of fine silts and in this region consist of fine grained particle mixtures such as silts and clays, with small amounts of coarse particles. This indicates that very little energy is required to keep these particles in suspension, and because of the limited supply of coarser grained particles, the channel bed and banks are easily eroded away (Rus et al, 2003).

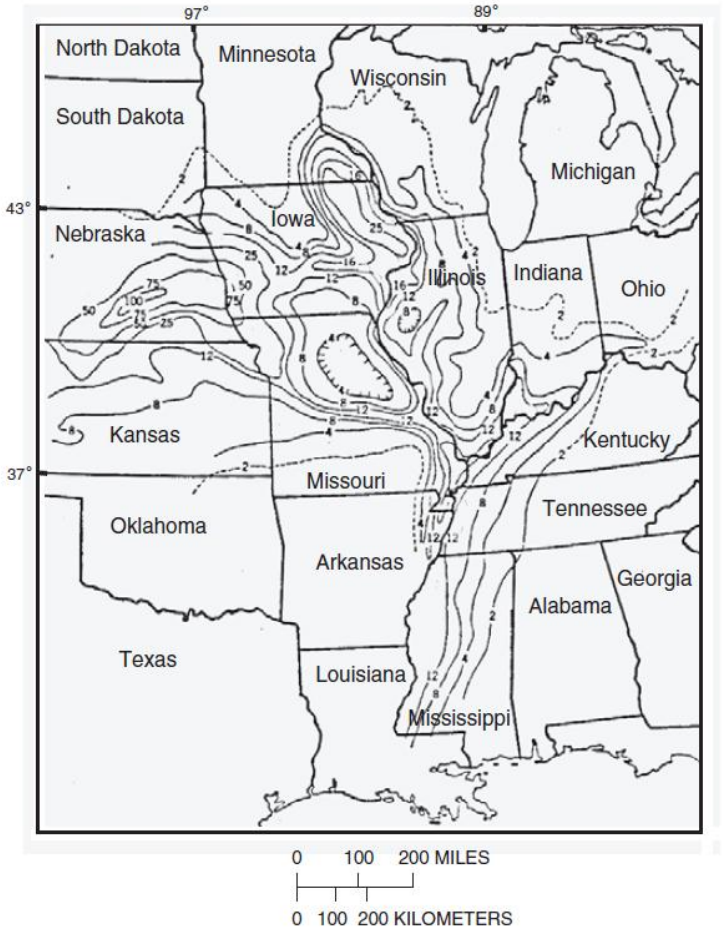

Figure 2.1: Loess soil deposits in Midwestern United States (Rus et al., 2003).

2.2.3 Channel Degradation

Channel degradation occurs as a result of disturbances to stream sediment load, bed soil configuration, and hydraulic characteristics (i.e. discharge, channel slope, and geometry). These changes may occur suddenly or slowly over time. A given disturbance may be due to a large rain event, channel adjustments (i.e. dredging and straightening), and changes in land use around the stream. It is important to examine the issue of channel degradation, as it can greatly affect the safety of stream crossings and land surrounding a given stream (Chen et al. 1999). There are a number of factors that contribute to stream bed degradation, but the degradation process can be most basically described as an imbalance between the strength of the stream bed material and the forces that act on the

stream bed. Ideally if these forces balance each other the stream is considered to be in equilibrium and no net erosion will take place. However, the disturbances that were previously discussed may cause the equilibrium to be disrupted and as the stream attempts to return to its equilibrium state, degradation of the stream bed occurs (Simon and Rinaldi, 2000; Rus et al, 2003).

Naturally, streams meander and change over time to maintain their natural equilibrium condition. The inconsistent flow path of a meandering channel presents a number of problems to the surrounding land; such as flooding and loss of effective farmland. The loess area of the Midwestern United States (*Figure 2.1*), particularly in areas of eastern Nebraska and western Iowa facilitate thousands of kilometers of unstable stream channels. In an attempt to control the meandering nature of the channels in this area, large scale channel straightening and dredging projects were initiated over the last century. Controlling the flow path of these channels has alleviated the threat of flooding and increased the productivity of agriculture surrounding the streams. These man-made adjustments have allowed for higher conveyance of flows, and though alleviating flooding problems, have greatly affected the equilibrium of many of these channels. As a result of these modifications a large number of active knickpoints have developed, inducing increasing amounts of headward channel degradation by way of steepened channel banks, bank failures, and channel widening (Rus et al., 2003). Understanding the mode by which these knickpoints are formed and how they migrate upstream is essential to ensure the stability of stream channels, and the safety of the structures and land that surround them.

2.3 Knickpoints

2.3.1 Background

Knickpoints are classically defined in literature as abrupt breaks in slope along channel beds that tend to migrate upstream (Brush and Wolman, 1960). The abrupt break in channel slope induces a sudden increase in flow velocity over the knickpoint causing the impinging flow to plunge and scour the downstream bed. This action induces large amounts of bed erosion and sediment transport that cause the channel to grow wider and deeper over time. These degradation processes cause the channel to become unstable, introducing safety concerns for people and structures surrounding the stream. The degradation of the streambed poses problems such as scour around bridge piers, dams, and pipelines; damage to roads; and loss of valuable farm land that surrounds the stream channel (Papanicolaou, 2008).

Defining the features of a knickpoint is an important first step in developing a thorough and consistent understanding of the behavior of knickpoints. The main features of a knickpoint consist of the knickpoint lip, face, and plunge pool. The lip is the point at which the drop in channel bed elevation occurs. The face extends from the lip to the base of the plunge pool. The plunge pool is a pool that forms at the base of the knickpoint as a result of water plunging over the lip and scouring the downstream bed and knickpoint face (Gardner, 1983). These features are illustrated below in *Figure 2.2*.

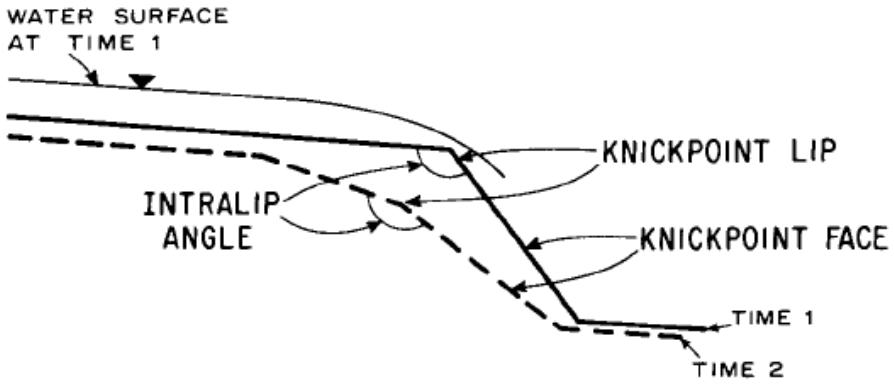

Figure 2.2: Knickpoint features (Gardner, 1983)

A knickpoint persists from a mild upstream slope followed by an abrupt change to a steep slope with a return to mild slope immediately downstream. A mild slope will typically convey flows that are subcritical in nature, whereas steep slopes will tend to sustain supercritical flows. These flow regimes are classified by the Froude number, which is a function of the flow velocity and the channel geometry. The abrupt change to steep slope followed by a return to mild (i.e. supercritical flow changing back to subcritical flow) indicates that a hydraulic jump will occur just downstream of the knickpoint, near the base. The sudden dissipation of energy caused by the hydraulic jump is what initiates the bed erosion and the upstream migration of the knickpoint. These flow characteristics are important mechanisms that greatly influence the migration process of knickpoints (Brush and Wolman, 1960).

The process of knickpoint migration (in general) is very slow. The migration may continue on for many years until the knickpoint reaches a control structure, until the channel slope is reduced to the point that it cannot displace any sediment, or until the soil structure of the stream bed changes (Brush and Wolman, 1960). The process of knickpoint migration is an area of great interest to engineers and researchers as it affects

the stability of stream channels. As water flows over the lip, erosive stresses are induced at its base; these stresses cause the soil to be displaced and a plunge pool to form. The erosion at the base of the knickpoint undercuts the face, causing a series of mass failures (Papanicolaou, 2008). These actions are the driving mechanisms that cause the knickpoint to migrate upstream and will be discussed in greater detail later in the review. *Figure 2.3* gives a visual representation of the basic knickpoint migration process.

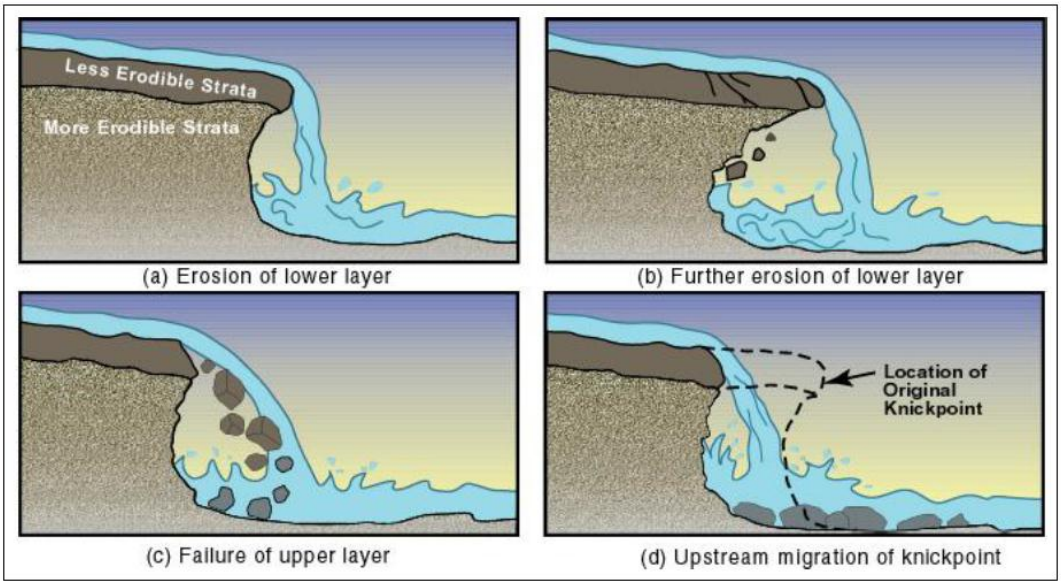

Figure 2.3: Knickpoint migration process (Papanicolaou, 2008).

Much research has been conducted by many researchers to further understand these mechanisms that drive the behavior of knickpoints. Available studies consist of knickpoint formation and classification, migration rate, and velocity field measurements at an overfall. These topics are discussed below.

2.3.2 Knickpoint Formation/Classification

The formation of a knickpoint can be initiated by a drop in base level, which is the water surface elevation of the exit pool or river that a given stream discharges into (Gardner, 1983). A drop in base level creates the abrupt break in bed slope which defines the discontinuity in the stream as a knickpoint. A drop in base level may occur due to low flow conditions in the exit stream. In some cases drops in the base level may occur frequently due to seasonal high and low flow conditions. Also the erosion caused by the presence of a knickpoint may induce a drop in base level as the knickpoint passes the mouth of connecting tributaries (Papanicolaou, 2008). These fluctuations in base level may cause new knickpoints to be continuously generated. Pending on the type of knickpoint that is formed, stresses at the lip or on the nearly vertical face of the knickpoint begin to erode the soil away and migration upstream will persist (Begin et al. 1980).

Begin et al. (1980), Gardner (1983), and Frankel et al. (2007) investigated the formation of knickpoints due to a fall in base level in laboratory constructed flumes. All three experiments allowed meandering channels to form while holding the base level in the exit pool at a constant elevation. Upon the drop in base level a knickpoint formed and began to migrate upstream. All three experiments confirmed that a drop in base level was the driving cause of knickpoint formation; however the mode at which each of the knickpoints migrated upstream was very different. Each study used a different soil structure to make up the stream bed, which resulted in very different forms of knickpoints and migration processes. Further studies have been conducted to understand the factors

that influence the mode at which knickpoints migrate upstream and to classify these different knickpoint types.

The mode of knickpoint migration is a function of the bed soil make up, the channel geometry, and the characteristics of the flow in the stream (Begin, 1980; Rus et al., 2003). The soil structures that make up the streambed are the key contributors that influence the type of knickpoint that is formed and how it will migrate upstream. The two main types of soil structures that make up a typical streambed are homogeneous and stratified soils. A homogeneous streambed consists of only one soil type throughout, and a stratified streambed consists of a combination of soils (typically a cohesive and a non-cohesive layer). A knickpoint that is formed in a homogeneous streambed will behave very differently than a knickpoint that is formed in a stratified soil.

A stratified streambed is made up of layers of different soil types. The layered stratigraphy may consist of an erosion resistant layer of soil that overtops a more erosive layer of soil (i.e. a sand layer underlying a clay layer). This soil configuration allows for a specific type of knickpoint to form and migration to take place. The flow over the lip of the knickpoint creates an impinging jet which easily erodes the non-cohesive sediment that is present at the base of the knickpoint. The erosion causes an enlarging scour hole (plunge pool) to form. This erosion undercuts the resistant layer of soil until a mass failure occurs. A mass failure occurs when the overlying layer of cohesive soil can no longer support itself due to the soil beneath it being eroded away by the stresses induced on the face by the presence of the impinging jet and plunge pool. The mass failure ensures that the nearly vertical face of the knickpoint will be maintained as the knickpoint

migrates upstream. The mass failure process will continue on until a control is reached or until the plunge pool ceases to exist; most likely by way of a change in soil type (Stein and LaTray, 2002; Brush and Wolman, 1960). In a laboratory setting, when the plunge pool was removed the undercutting of the knickpoint lip ceased and the knickpoint face began to decrease in slope until it was no longer present, resembling a knickpoint in a homogenous soil configuration (Holland and Pickup, 2006). A knickpoint that is formed and maintained by way of undercutting and mass failure is referred to as a stepped knickpoint. The main features of a stepped knickpoint are the presence of a plunge pool, and the maintained vertical face throughout the migration process. Stepped knickpoints are the most prominent form of knickpoint found in nature. The undercutting and mass failure process that occurs during the migration of stepped knickpoints is what accounts for the steepening of side slopes, channel widening, deepening, damage to bridge infrastructure, and damage to surrounding farmland.

Homogeneous streambeds consist of one soil type, either cohesive or non-cohesive. The homogeneity of the streambed causes a different type of knickpoint to form than was previously presented. Upon formation in a homogeneous soil the knickpoint will have a nearly vertical face, however the flow over the lip will not form a plunge pool, and thus undercutting will not take place. This indicates that the nearly vertical face of the knickpoint will not be maintained as the knickpoint migrates upstream and the knickpoint face will eventually decrease in slope until it is no longer recognizable as a discontinuity in the stream (Holland and Pickup, 2006). In this case the bulk of the erosion will take place at the knickpoint lip as appose to at the face in the case of a stepped knickpoint. This type of erosion causes the knickpoint to gradually decrease in slope over time

(Gardner, 1983). If the stream is made up of primarily non-cohesive material, the soil will easily be eroded and the knickpoint will quickly reduce in slope and eventually disappear. In a cohesive streambed the knickpoint will be preserved for a longer period of time as the slope slowly rotates towards the slope of the existing channel (Brush and Wolman, 1960). This type of knickpoint is referred to as a rotating knickpoint, as the slope of the knickpoint face rotates towards the existing channel slope. *Figure 2.4* shows in more detail the different soil formations that make up the different types of knickpoints found in nature.

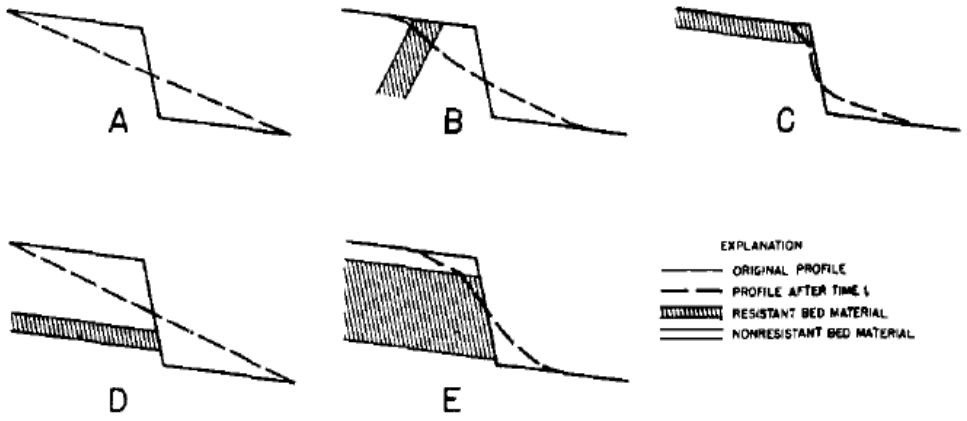

Figure 2.4: Soil configurations that affect the formations and migration of knickpoints (Brush and Wolman, 1960).

At times it may be difficult to differentiate between a stepped or rotating knickpoint. The development of a knickpoint is dependent on the stresses that act upstream and downstream of the lip. As was stated above if the bulk of the erosion acts at the knickpoint lip it is classified as a rotating knickpoint and if the bulk of the erosion takes place on the face it is said to be a stepped knickpoint. Thus, if upstream erosion dominates, it is rotating, and if downstream erosion dominates the knickpoint is stepped (Stein and Julien, 1993). The question arises; how does one determine whether upstream

erosion or downstream erosion dominates? Stein and Julien (1993) developed a relationship between upstream and downstream erosion time scales. The upstream time scale is denoted by T_u and it represents the time it takes for the upstream erosion to reach the base of the knickpoint. The downstream time scale is denoted by T_d and it represents the time it takes for the downstream erosion to reach the base of the knickpoint. Once these time scales are determined, the ratio of the upstream to downstream time scale (T_u/T_d) is used to determine which type of knickpoint is present. If T_u/T_d is less than one, then the upstream erosion is dominant and the knickpoint can be classified as a rotating knickpoint. If T_u/T_d is greater than one than downstream erosion is dominant and the knickpoint will be classified as a stepped knickpoint.

2.3.3 Knickpoint Migration

Knickpoint induced channel degradation in the highly erodible loess soils of western Iowa and eastern Nebraska cause hill-slope failures and damage to bridge infrastructure. For this reason it is important to understand the migration processes of knickpoints. The rate of knickpoint migration is of particular importance because it can help assess the stability of a particular channel or how great is the risk to surrounding structures.

Field observations of knickpoints conducted over the years have offered an insight into their natural migration behavior. Daniels, (1960) examined a knickpoint that was formed as a result of straightening efforts of Willow Creek, IA in the mid 1950's. It was documented that the knickpoint migrated upstream 2,819 m over the 5 year study period, with expedited movement upstream as a result of high flow events. It was noted that the

knickpoint migrated upstream as a result of repeated mass failure events resulting in large scale degradation of Willow Creek.

More recent field studies have centered on the migration rate of knickpoints and mechanisms driving the migration of knickpoints upstream. Simon and Thomas, (2002) and Simon et al., (2002) examined a series of knickpoints that formed in the Yalobushaa River in Mississippi as a result of channelization projects. They observed that the knickpoints migrated at rates ranging from 0.4 m/yr to 11m/yr. More importantly they found that knickpoints do not migrate at a constant rate, but rather as quick bursts upstream as a result of high flow events followed by periods of slow but consistent movement. In addition to the observed migration rates they identified a series of mechanisms driving the migration of the knickpoints. These mechanisms are as follows: The streambed being exposed during low flows result in weathering and cracking of the bed soils, detachment of streambed particles caused my excess seepage, static liquefaction of the cohesive streambeds, and a mass failure cycle caused by the stresses induced on the knickpoint face by the hydraulic jump.

Predicting the migration rate of a knickpoint can prove to be a complex task due to the large number of variables involved. The rate of migration can be described as the distance the knickpoint moves upstream divided by the time between mass failures (Robinson and Hanson, 1994; Hanson et al., 1997; Hanson et al., 2001). The migration processes for stepped and rotating knickpoints are very different. For rotating knickpoints the erosion will be most prominent at the lip. This causes the knickpoint to gradually reduce in slope until it no longer exists. Stepped knickpoints follow a pattern of mass failures that preserve the vertical face of the knickpoint as it migrates upstream. These

processes are dependent on the geometry of the channel, the stresses induced by the flow, and the soil structure of the streambed (Rus et al., 2003). Over the years the rate of knickpoint migration has been extensively researched in laboratory settings. A number of models have been developed, taking the before mentioned characteristics into count. The research carried out by Robinson, (1989), Robinson and Hanson, (1994); Hanson et al., (1997); and Hanson et al., (2001) centered on the migration behavior of knickpoints that were developed in a large scale flume. The end goal of the research was to develop an equation that accurately predicts the migration rate of knickpoints.

The stresses that are induced on a knickpoint are key contributors in the development of its migration. It is important to understand how these stresses influence the migration process of knickpoints. The stresses that are induced on the knickpoint face and channel floor are a function of the backwater height, the height of the knickpoint, and the discharge in the stream. When the initial backwater elevation is nearly the same as the knickpoint height there will be very little stress induced on the face of the knickpoint. As the backwater depth is lowered the stresses on the floor and face of the knickpoint will increase significantly and cause intensive erosion to take place (i.e. undercutting of the knickpoint face and formation of a plunge pool). This process can be seen in more detail in Figure 2.5 below.

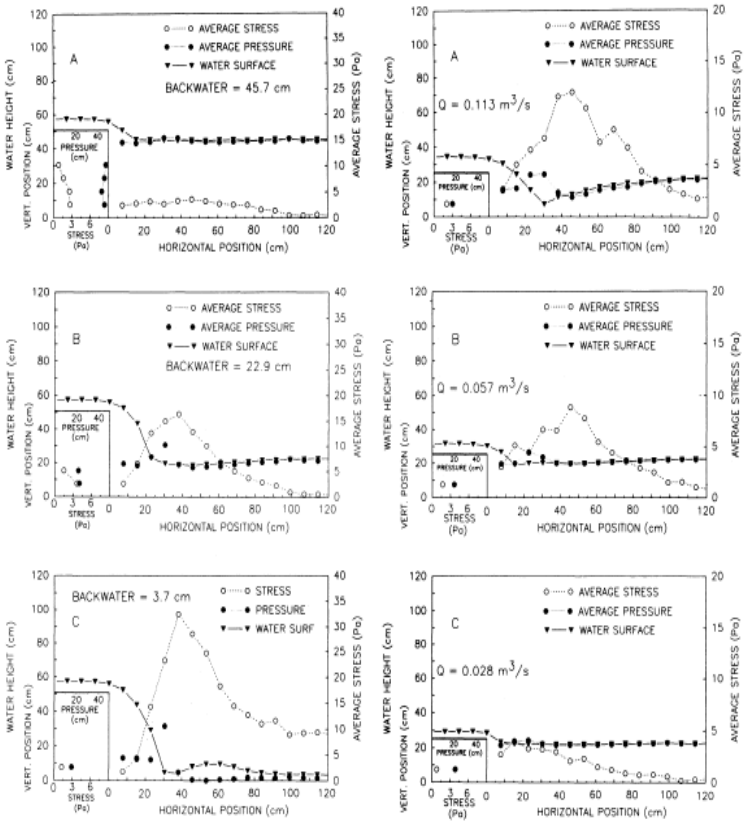

Figure 2.5: Stress on the knickpoint as the water surface elevation and height of knickpoint is adjusted

When the backwater is lowered a nappe is formed as the water plunges over the knickpoint. The plunging nappe forms a reverse roller at the base of the knickpoint which causes an increase of shear stress on the channel floor and the knickpoint face. The presence of the reverse roller is what induces the displacement of sediment and subsequent upstream migration of the knickpoint (Robinson, 1989). The nappe profile, shear stresses, and mass failure components of knickpoint migration are the three main areas of interest when attempting to model the upstream movement of a given knickpoint. In order to determine the magnitude of the shear stresses present on the channel floor and knickpoint face it is necessary to predict the nappe profile. Prediction equations for the nappe profile provide the X and Y components of the nappe trajectory, which can be used

to calculate the magnitude of the vertical and horizontal stresses acting on the knickpoint. The nappe profile components can be determined with the following relation:

$$\frac{Y}{D_a} = -.483F^{-.546}\left(\frac{X}{D_a}\right)^{1.6} + .823 \quad (2.1)$$

where F is the square of the Froude number, D_a is the approach depth, and X and Y represent the horizontal and vertical components of the nappe trajectory, respectively. Knowing the X and Y components of the nappe profile the time-averaged horizontal and vertical stresses can be determined. With the time-averaged stress components known, the excess stress acting on the knickpoint can be computed using the following equation:

$$\varepsilon = K_d(\tau - \tau_c) \quad (2.2)$$

where K_d is the erodibility coefficient, τ is the effective boundary shear stress, and τ_c is the critical shear stress for the given soil. Finally the mass failure component can be described as follows:

$$(W_s + W_w - T_v - CLsin\theta)[tan(\theta - \emptyset)] - T_h - CLcos(\theta) = 0 \quad (2.3)$$

where W_s is the weight of the soil block, W_w is the weight of water above the failure block, T_v is the vertical water force, T_h is the horizontal water force, C is the soil cohesion, L is the length of the failure plane, θ is the angle of the failure surface, and $\emptyset$ is the angle of internal friction. When the magnitudes of these forces sum to zero, a mass

failure will occur (Robinson and Hanson, 1994; Hanson et al., 2001). These concepts can be combined and simplified to form a governing equation that predicts the migration rate of a given knickpoint. The equation developed by Hanson et al. (2001) is as follows:

$$\frac{dX}{dt} = \left(\frac{H}{2E_v}\right) K_d(\tau - \tau_c) \tag{2.4}$$

where E_v is the cumulative undercutting erosion given by the following expressions:

$$E_v = \frac{-b \pm \sqrt{b^2 - 4ac}}{2a} \tag{2.5}$$

$$a = \frac{\gamma_s}{2} \tag{2.6}$$

$$b = \gamma_w B_w - \frac{\gamma_s H}{2} - 2c_u \tag{2.7}$$

$$c = c_u H + \frac{\gamma_w}{2} B_w^2 - \frac{3}{8}\gamma_s H^2 - \frac{\gamma_w}{2} D_a H \tag{2.8}$$

This model has been tested in a laboratory setting and the results are graphically represented below in Figure 2.6. It appears as though the proposed equation follows the test data very closely.

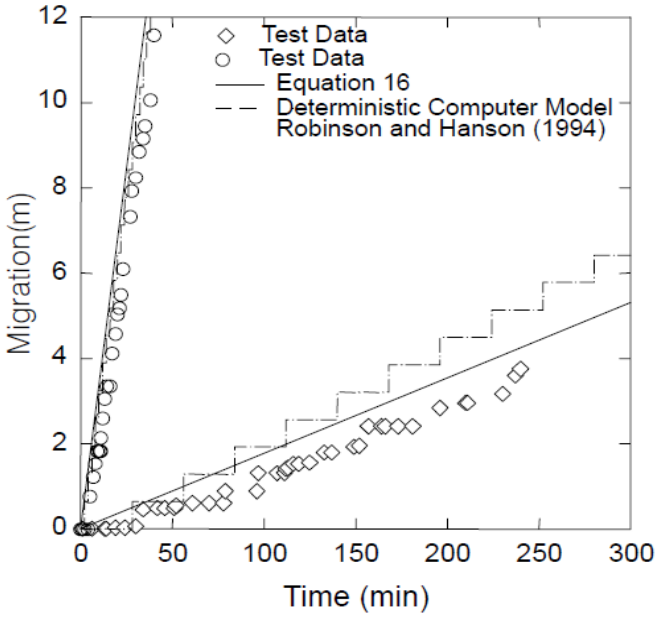

Figure 2.6: Results from knickpoint migration model developed by Robinson and Hanson (1994)

2.3.4 Velocity Field Measurements at an Overfall

Mapping the velocity fields that are induced by the flow over a knickpoint can lend insight into the driving mechanisms that initiate upstream migration. This is an area of ongoing research and will be discussed in section four of this review. The use of particle image velocimetry (PIV) techniques can be used to map velocity vectors that are present in the flow. Using these techniques the circulation patterns of the flow over a knickpoint can be thoroughly examined. A knickpoint introduces three dimensional flow characteristics, which are difficult to measure with traditional two dimensional PIV practices. Robinson et al., (2000) attempted to map the velocity vectors at the boundary of an overfall using acoustic Doppler velocimetry (ADV) techniques to account the three dimensional nature of the flow. Their findings showed that as the nappe plunges over the knickpoint and into the downstream bed, a portion of the flow is diverted upstream and downstream along the channel bed. The upstream flow typically impacts the knickpoint

face and then proceeds to move vertically upwards, undercutting the lip. This type of motion is typically referred to as a reverse roller, and is responsible for inducing the erosion that takes place along the face of the knickpoint, especially if the soil is highly erodible. The largest velocities were recorded near the channel bed as the flow was diverted downstream. The flow rushed downstream and then recirculated upstream to the nappe entry point. This action caused scour of the channel bed, which formed an enlarging plunge pool over time. *Figure 2.7* shows how the flow behaves in more detail as it plunges over a knickpoint and into a downstream bed.

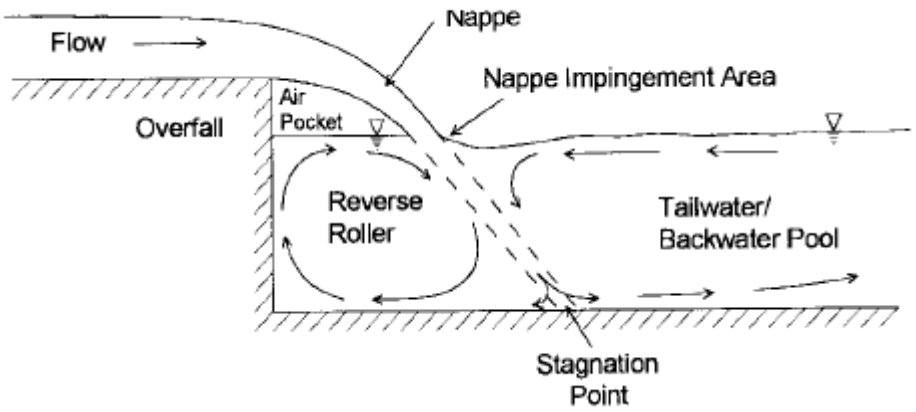

Figure 2.7: Flow behavior at and overfall.

2.4 Flow Field Measurement

2.4.1 Background

Imaging techniques such as Particle Image Velocimetry (PIV) and Particle Tracking Velocimetry (PTV) are used to visualize instantaneous velocity field measurements in a given flow. These techniques are typically used in laboratory research as well as in field applications. PIV and PTV techniques measure velocity vectors non-intrusively in two dimensional flows. This is done by determining the velocity of particles or tracers that are initially present or released in a given flow. The selection of

the tracers is highly dependent on their fluid mechanical properties (i.e. density, size, and settling velocity) (Adrian, 1991; Raffel et al., 1998). These tracers can range anywhere from bubbles present in the flow due to turbulence to breakfast cereal released on the surface of the flow.

2.4.2 Particle Image Velocimetry

The primary purpose of any PIV or PTV imaging technique is to measure the displacement of particles between two successive images. The particle displacements are measured in small regions of each image called interrogation areas. The velocity vectors are then calculated for each interrogation area by dividing the particle displacement by the separation time between images (for Large-scale PIV, the separation time is typically given as the frame rate of the camera being used) (Fujita et al., 1998).

The difference between PIV and PTV resides in the tracer particle density in a given flow. If the tracer density is low, one can track the displacement of individual particles between images; this technique is known as Particle Tracking Velocimetry (PTV). If the particle density is high then the displacement of groups of particles are tracked; this technique is known as Particle Image Velocimetry (PIV). In the case of very large imaging areas with large tracer particles, Large-scale Particle Image Velocimetry (LPIV) may be applied. LPIV will be discussed in more detail later in this section. *Figure 2.8* below illustrates three modes of particle image density given by Raffel et al., 1998.

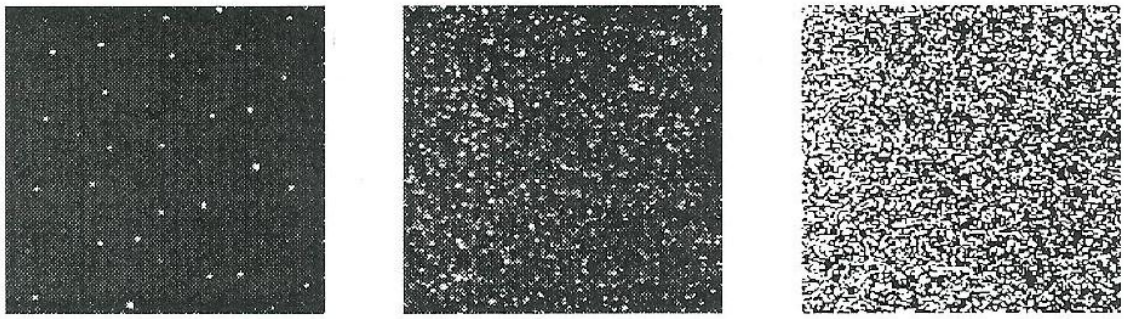

Figure 2.8: The three modes of particle image density: (a) low particle density (PTV), (b) medium particle density (PIV), and (c) very high particle density.

Determining the displacement of a group of particles can prove to be challenging and typically a statistical approach must be used. The statistical approach is carried out by determining a correlation coefficient between corresponding regions (or interrogation areas) of two consecutive images with the use of Fourier transforms. The correlation coefficient is computed for all possible displacements of particles within the aforementioned interrogation areas. The displacements that result in the highest correlation coefficients are considered to be the most likely displacement of the group of particles at any given location in the images (Meselhe et al., 2002). This method is visually described with the use of Figure 2.9, below. The correlation coefficient R_{ab} is defined by the following equation given by Fujita et al., 1998:

$$R_{ab} = \frac{\sum_{i=1}^{MX}\sum_{j=1}^{My}\{(a_{ij}-\bar{a}_{ij})(b_{ij}-\bar{b}_{ij})\}}{\left\{\sum_{i=1}^{MX}\sum_{j=1}^{MY}(a_{ij}-\bar{a}_{ij})^2\sum_{i=1}^{MX}\sum_{j=1}^{MY}(b_{ij}-\bar{b}_{ij})\right\}^{1/2}} \quad (2.9)$$

Where, MX and MY are the sizes of the interrogation areas, and a_{ij} and b_{ij} are the particle intensities within the two interrogation areas. Once a displacement is determined it can be divided by the separation time to estimate the velocity of the flow.

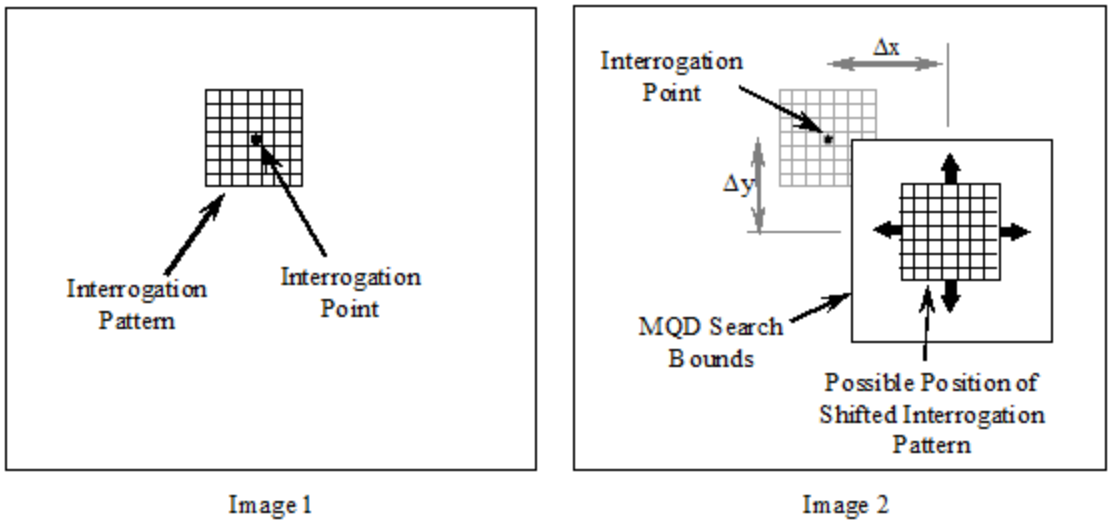

Figure 2.9: PIV process using a statistical correlation approach

2.4.3 Large-scale Particle Image Velocimetry

Typically PIV and PTV measurement techniques are carried out in laboratory settings, where the lighting and flow environment are relatively simple. In the laboratory the lighting, seeding, scale, and recording can all be carefully controlled by the user. More recently, image velocimetry has been applied in field settings. With advances in flow visualization technologies, more and more PIV investigations have been applied in the field. In a field setting, the scale is much larger than that of a laboratory, thus this PIV technique is known as Large-scale Particle Image Velocimetry (LPIV). A typical LPIV arrangement is shown in Figure 2.11 (Muste et al., 2008).

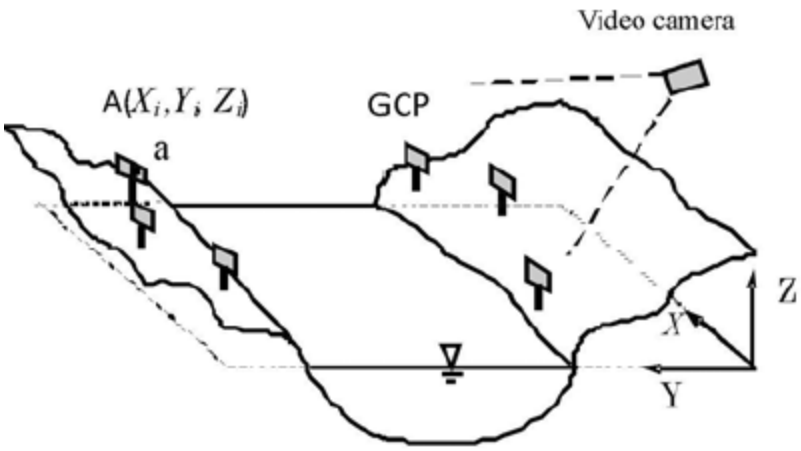

Figure 2.10: Large-scale particle image velocimetry (LPIV) system setup (after Muste et al, 2008).

Conducting PIV measurements in the field offers a number of unique challenges. In the field it is often impossible to set up the camera from directly overhead (as can be done in a typical laboratory environment) and thus the camera is aligned at an oblique angle to the field of view. Obliqueness introduces spatial distortion into the PIV images. This distortion can be dealt with by implementing a series of correction equations that will change the orientation of the image to appear as if it would if the camera was placed directly above the field of view (which is favorable for PIV calculations) and undistorted (Meselhe et al., 2002; Muste et al., 2008). This process of image correction is called Oblique Correction.

2.4.4 Oblique Correction

Oblique correction is a technique used to change the orientation of a given image to make it easier to properly determine distances and velocities. In LPIV the large scale and oblique angle of the camera setup introduce spatial distortions within the sets of images that are to be processed. This distortion is unfavorable to traditional PIV processing. By utilizing oblique correction techniques the orientation of a given oblique image can be

rectified so that it appears as if it were viewed from directly overhead and undistorted, making determining distances and velocities possible (Fujita et al., 1998). Oblique images can be rectified or aligned using the following oblique correction equations developed by Fujita et al., 1998:

$$X = \frac{b_1 x + b_2 y + b_3}{b_4 x + b_5 y + 1} \tag{2.10}$$

$$Y = \frac{b_6 x + b_7 y + b_8}{b_4 x + b_5 y + 1} \tag{2.11}$$

In which, x and y are the coordinates of a given calibration point in the image (given in pixels), and X and Y are the surveyed coordinates of that given calibration point (given in meters). The oblique correction coefficients (b_1 through b_8) are determined by carrying out a least squares optimization method with the following equations:

$$TB = Z$$

where:

$$T = \begin{matrix} x_1 & y_1 & 1 & -x_1X_1 & -y_1X_1 & 0 & 0 & 0 \\ \vdots & \vdots & \vdots & \vdots & \vdots & \vdots & \vdots & \vdots \\ x_N & y_N & 1 & -x_NX_N & -y_NX_N & 0 & 0 & 0 \\ 0 & 0 & 0 & -x_1Y_1 & -y_1Y_1 & x_1 & y_1 & 1 \\ \vdots & \vdots & \vdots & \vdots & \vdots & \vdots & \vdots & \vdots \\ 0 & 0 & 0 & -x_NY_N & -y_NY_N & x_N & y_N & 1 \end{matrix}$$

and:

$$B = [b_1, b_2, \ldots b_8]^T \quad Z = [X_1, X_2, \ldots . X_N, Y_1, Y_2, \ldots . Y_N]^T$$

It is important to note that there must be at least four surveyed coordinate points for the optimization to reach an acceptable solution (Fujita et al., 1998).

2.5 Summary

Studies pertaining to the issues of channel degradation, knickpoints, and flow measurement techniques were discussed in this chapter. The bulk of the chapter consisted of past work dealing with the migration processes of knickpoints. Aside from a few field observations, it is apparent that a large portion of the research dealing with the migration behavior and morphology of knickpoints has been conducted in laboratory settings where the hydrodynamic forces can be controlled. The laboratory studies discussed in this chapter are highlighted by the work carried out by Robinson and Hanson, 1994; Hanson et al., 1997; and Hanson et al., 2001 who developed a knickpoint retreat model for a knickpoint migrating in a large scale flume. Several laboratory flume studies have analyzed the stability and morphology of knickpoints, as well as work examining the behavior of hydraulic stresses acting on the lip and face of a knickpoint. Based upon the results of this literature review, it is apparent that there are limited available studies concerning the migration behavior of knickpoints in field settings. The laboratory studies discussed in this review provide a solid foundation into the migration behavior of knickpoints. Because of the difficulties associated with measuring flow fields at active knickpoints, there are fewer studies describing flow behavior of knickpoints in field settings. This thesis is intended to provide a unique set of data offering insight into the migration behavior of a real, actively migrating knickpoint in a field setting.

Chapter 3: **Site Description**

3.1 Knickpoint Location

The knickpoint chosen for this study is within the deep loess area of the Midwestern United Sates (*Figure 2.1*), with loess depths ranging from 50 to 75 feet. It is located on Mud Creek, which is a tributary stream of the West Nishnabotna River located in northeast Mills County, Iowa. Mills County is located in the Southwest corner of Iowa, and the study site is near the town of Henderson, Iowa. The site was selected because it was readily accessible and because it was a part of an ongoing study being conducted jointly with the University of Iowa. The site also has a history of active knickpoints. Mud Creek has a stream length of 25.75 km with a watershed area of 97.5 km^2.

This location of the Midwestern United States promotes a climate that is characterized by hot summers, cold winters, and wet springs. The average summer temperature in this area is 30°C (86°F) and is accompanied with periodic large thunderstorms. The winter average temperature is -4°C (24.8°F) with significant snow accumulation and periods of freeze and thaw. The average annual precipitation is approximately 846 mm/yr with the majority of the precipitation falling in the spring and summer months (April – September) (Papanicolaou, 2008). Over the course of this study the precipitation was recorded from the Iowa Environmental Mesonet (2013), which can be accessed at <mesonet.agron.iastate.edu>. The Precipitation data are presented in Figure C1, and the cumulative rainfall data are presented in Figure C2. These figures are presented in Appendix C.

The Mud Creek knickpoint is an active knickpoint, but it is currently approaching a concrete grade stabilization structure just downstream from a bridge on Elderberry Avenue. The study site is surrounded by farmland for crops such as corn and soybeans, as well as range land for grazing cattle. *Figure 3.1* shows the knickpoint in question and the surrounding area at the study site.

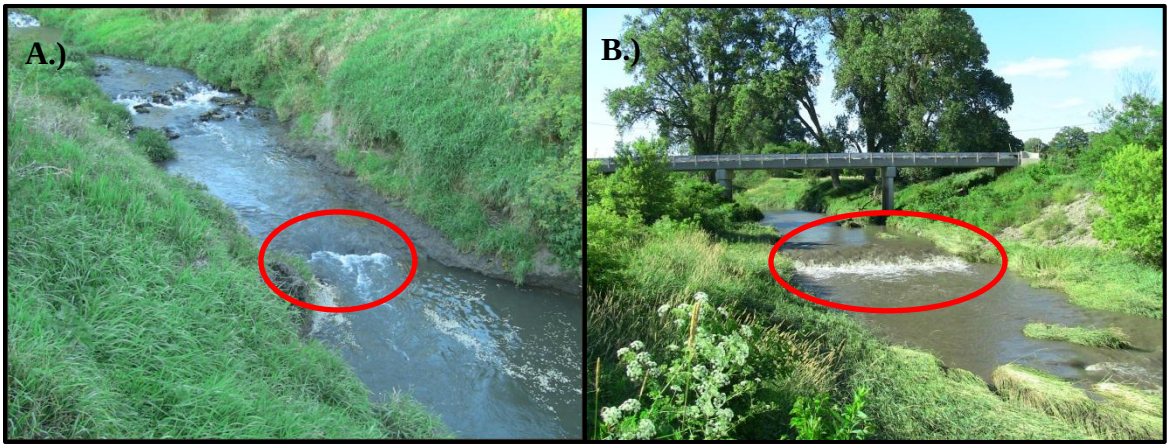

Figure 3.1: A.) Mud Creek knickpoint at study site. B.) Image of the study area showing the grade stabilization structure and Elderberry Ave. Bridge.

3.2 Site Condition

Mud Creek is an erodible channel that meanders southward where it eventually drains into the West Nishnabotna River. The soil structure in this area consists of highly erodible loess soil, which is a common soil type in areas of eastern Nebraska and western Iowa. At the site the channel has a measured width of 19 meters with steep channel banks ranging from 4-5 meters high. The average flow depth at the site was approximately 24 cm over the study period. As a result of efforts to straighten many channels in this area, a large number of active knickpoints have developed, causing intense channel degradation. As a result, Mud Creek has become increasingly canyon-like over the years with the presence of deep, steep channel walls. The Mud Creek knickpoint has induced channel degradation including; steepening of side slopes, channel widening, and bank failures that

are easily identifiable at the site. Evidence of the channel degradation gathered during site visits over the course of the study are pictured below in *Figure 3.2*.

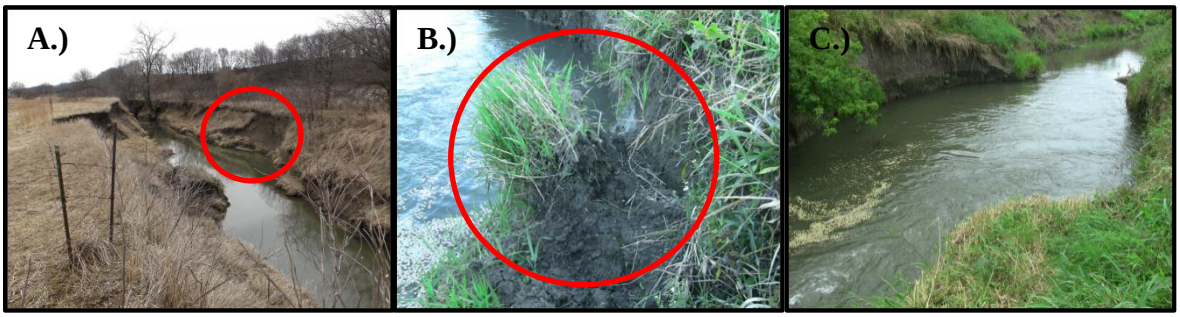

Figure 3.2: Evidence of channel degradation caused by passage of knickpoint: A.) Steep side slopes B.) Bank failures C.) Channel widening

3.3 Field Equipment

Throughout the duration of the study, a number of instruments were used to gather data in the field. A time lapse camera and a digital camcorder were used to capture images of the knickpoint and to create videos of various flow conditions. Also survey equipment was used to gather elevation data of the stream channel and the knickpoint.

3.3.1 Time Lapse Camera

The knickpoint was continuously monitored throughout the research process using a time lapse camera installed at the site. The purpose of continuously monitoring the knickpoint is to develop a set of images that provide a unique two-dimensional representation of the knickpoint migration over the duration of the study period. The camera used was a Moultrie Plotstalker time lapse camera. An image of this camera is provided in *Figure 3.3*. The applicable settings present on the camera consist of the time lapse interval, photo quality, and the time/date. Also the camera is capable of taking video, which may prove useful in later studies. The time lapse interval was set to 30 minutes, meaning that an image of the knickpoint was taken every 30 minutes. The photo

quality was set to 3264 x 2448, and the date and time were set accordingly and imprinted on each image. The images taken from the camera were stored on a 16 GB SD card and downloaded to a laptop during each site visit.

Figure 3.3: Moultrie Plotstalker time lapse camera

The camera was installed at the site on June 27, 2011 and is still in operation. The camera was placed in a field security lock box and mounted on a wooden post located on the right descending bank of the stream. The field installation of the time lapse camera is shown in *Figure 3.4*. Two issues arose with this particular camera setup. First, when images were downloaded, the camera position sometimes changed slightly, and second, changes in temperature, humidity, and soil conditions affected the camera alignment to some extent. These issues and the methods used to address them are discussed further in Chapter 4.

Figure 3.4: Time lapse camera installation at site

3.3.2 Digital Video Camera

Particle Image Velocimetry (PIV) techniques were used to analyze the flow in the approach reach of the channel upstream of the knickpoint. PIV techniques are discussed in greater detail in Chapter 4. The camera used to gather the PIV data at the site was a Canon Vixia HF200 HD digital camcorder 1080P. An image of the camera is shown in *Figure 3.5*. The Canon Vixia HF200 has multiple capabilities and settings that made this camera ideal for this particular study. The camera has the ability to take photos as well as videos. The camcorder settings feature a high definition image sensor that can capture videos that are 1920 x 1080 pixels. An important setting to take note of is the frame rate. This camera allows for three different frame settings: 60i, PF30, and PF24. These settings can be adjusted for any given need. For this project the frame rate was set to PF30, which means 30 frames per second. This information is essential to the quality of the PIV analysis and results. The videos taken in the field are stored on an SD card and later converted into bitmap images that can be used in the PIV analysis.

Figure 3.5: Canon Vixia HF200 HD digital camera.

During the site visits the camera was set up on a tripod on the right descending bank (near the time lapse camera). Each visit, two to three five minute videos of the knickpoint were taken in order to capture the current flow field of the water surface.

3.3.3 Survey Equipment

Survey data were required for a number of applications throughout the research process. It was important to acquire elevation data of the stream channel and knickpoint to more accurately assess the amount of knickpoint migration that had taken place. The survey data were also utilized in the PIV analysis. The role of the survey data in the PIV analysis will be discussed in Chapter 4.

Over the duration of the study period, two models of survey equipment were used. The instruments used to carry out the required surveying tasks at the site were a Sokkia Set5A Electronic Total Station, and a TopCon GPS based system. The survey equipment was set up in the center of the Elderberry Avenue bridge to overlook the stream. This allowed for a clear view of the knickpoint and surrounding features of the stream. When the Set5A was used, the survey data were recorded using a Sokkia SDR 31 Electronic Field Book. The field book connects directly to the total station, and the surveyed points

are automatically stored and later downloaded to a computer. The use of the electronic field book made it convenient to record large amounts of data during each site visit.

3.4 Historical Stage Data

Periodic stage data were collected at the site from a stage sensor that was installed on the Elderberry Avenue bridge during the early months of 2012. The sensor is operated by the Iowa Flood Center and can be accessed at the Iowa Flood Center website: www.iowafloodcenter.org. Figure 3.6 shows the placement of the sensor on the side of the bridge, which is located at an elevation of approximately 321.42 m (5.88 m above the channel bed). The sensor was used during the latter portion of the project to collect stage levels in the stream, which were used to estimate discharges. The discharge calculation methods will be described in section 3.5.

Figure 3.6: Iowa Flood Center stage sensor

The data provided by the stage sensor were given as a distance from the stage sensor to the water surface. This presented a challenge in relating the stage readings to water surface elevations above the crest of the grade stabilization structure. During each site survey, a series of data points of the water surface were collected upstream of the

grade stabilization structure and below the stage sensor. Then the elevation of the stage sensor could be determined, thus allowing conversion of each reading from the stage sensor into a stage elevation so that we could provide a rating curve for the grade stabilization structure. The first reading from the stage sensor was collected on March 25, 2012 and a reading has been collected every 15 minutes to date. A record of the stage elevations over time are presented in Figure C3 located in Appendix C. Also the crest elevation of the grade stabilization structure was plotted to offer context for each stage reading. Stage readings begin on March 25, 2012 and end on January 7, 2013. The data will continue to be downloaded from the Iowa Flood Center website to keep the stage record up to date.

3.5 Grade Stabilization Structure

The grade stabilization structure pictured in Figure 3.1B is located 18 m south of the Elderberry Avenue bridge. During the September 25, 2012 site visit a detailed survey of the site was conducted using the TopCon GPS survey equipment. A cross section of the grade stabilization structure and the upstream water surface elevation was obtained from this survey. The cross section of the stabilization structure is given in Figure 3.7. The east positions given on the x-axis are relative to an arbitrary benchmark set at the southwest corner of the Elderberry Avenue Bridge, which was set to (0,0).

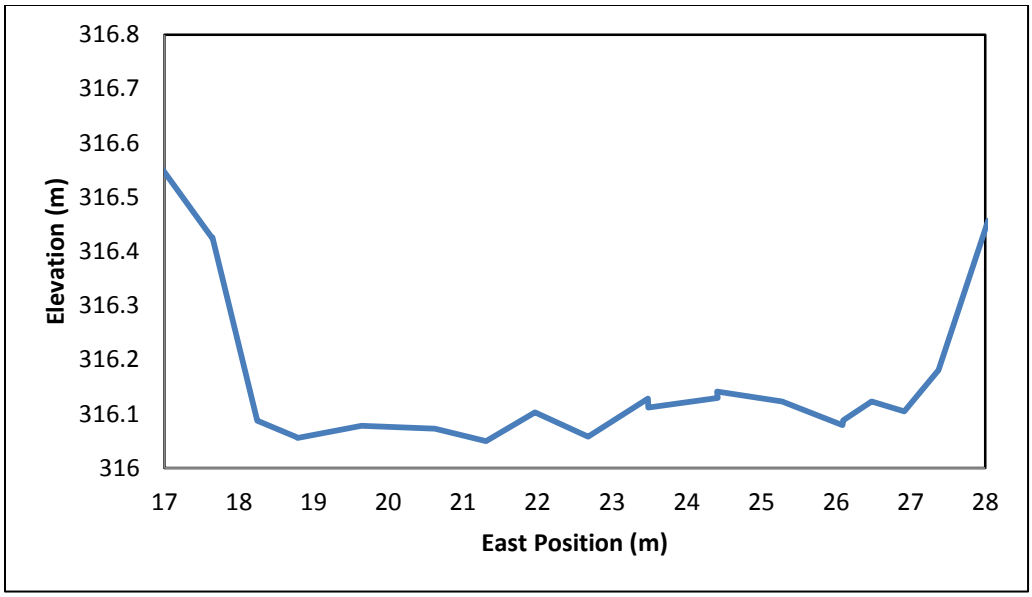

Figure 3.7: Cross section of grade stabilization structure

From this cross section we were able to obtain the geometric information needed to estimate the flow in Mud Creek in conjunction with stage elevations provided by the stage sensor. The survey data provided the crest elevation and length of the grade stabilization structure. Also the water surface elevation upstream of the structure was recorded. The average crest elevation was determined to be 316.11 m, the length was 8.60 m, and the upstream water surface elevation was 316.17 m. In addition to the survey information, the reading from the stage sensor was 5.25 m (17.23 ft).

The information obtained from this cross section along with the periodic stage data downloaded from the stage sensor was used to calculate the discharge in Mud Creek. It was assumed that the grade stabilization structure acted as a broad crested weir, meaning that a broad crested weir equation could be used to calculate the flow over the structure. The broad crested weir equation used for calculation is given by Admiraal, (2007) as follows:

$$Q = C_D\sqrt{g}LH^{1.5} \quad (3.1)$$

Where, C_D is the weir coefficient, L is the length of the weir, H is the height of the water above the weir, and g is gravity (9.81 m/s^2). The weir coefficient was given as 0.461 after Admiraal, (2007), as the stabilization structure most closely resembles a rectangular weir profile. However, further calibration of the weir coefficient will be needed in the future, as the discharges yielded by this value were slightly high when compared to the results from the discharge calculations that were obtained using the LPIV calculations (presented in Chapter 5). The calculated discharges obtained from equation 3.1 and the stage elevations are presented in the hydrograph available in Figure C4 in Appendix C. Adjustment of the weir coefficient will yield more accurate discharge values that can be compared with the discharges calculated by the LPIV simulations to further develop a rating curve for the study site.

Chapter 4: **Methodology**

4.1 Introduction

This chapter describes the methodology used for the analysis of data collected during the research process. The areas that will be discussed in further detail are the: time lapse analysis, survey data acquisition, LPIV analysis, and discharge estimation. In addition to the four main areas of analysis required for this project, a description of Flow Field Captor MD, the software used for LPIV analysis, will be presented, as it relates to the work done in this thesis.

4.2 Flow Field Captor MD

Flow Field Captor MD (FFCMD) is analysis software that was used to do PIV calculations and a number of other processes that aided in data processing and presentation. The software was developed by the advisor of this research, Dr. David Admiraal. For the purposes of the current Mud Creek knickpoint analysis, Flow Field Captor MD was utilized for correcting images (i.e. oblique correction), velocity distribution calculations, and image alignment techniques. The important parameters and tools that were used are discussed in further detail in this section.

4.2.1 Separation Time

The separation time is an important parameter used in PIV and PTV calculations. This time represents the time between two consecutive PIV images. In LPIV, the separation time is generally calculated from the frame the rate of the camera (typically 30 frames per second). In PIV analyses, the velocities of particles that are present in the flow

are calculated by computing the ratio of the particle displacement and the separation time between a set of images. It is very important to take note of the camera separation time (or frame rate) before beginning PIV measurements, because some cameras have different frame rate settings. The separation time for the camera used in the Mud Creek analysis was 0.033 seconds.

4.2.2 Pixel to Distance Ratio

The pixel to distance ratio is another important parameter, not only for the calculation of velocities, but also for image resolution. The pixel to distance ratio offers a link between object coordinates measured using survey equipment and the corresponding coordinates within the image. For the Mud Creek knickpoint analysis the pixel to distance ratio was dependent on how the oblique image correction was applied. Using FFCMD, the resolution of rectified images can be set by selecting an appropriate pixel to distance ratio in the *Properties of Corrected Oblique Images Window* (*Figure 4.1*). A recommended maximum resolution is provided by the software, but the resolution should also be large enough to capture the tracer particles that are present in seeded flows.

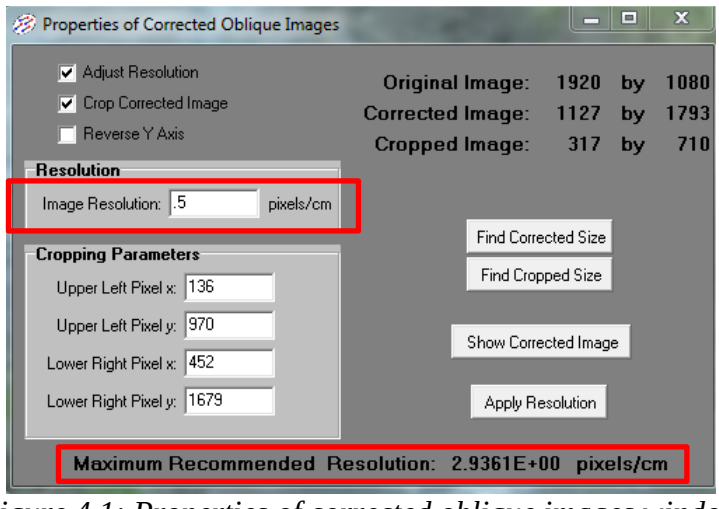

Figure 4.1: Properties of corrected oblique images window

4.2.3 Oblique Correction

Oblique correction is a technique applied to an image to change the orientation of the image so that the pixel to distance ratio is uniform everywhere within the image. In the case of the current Mud Creek analysis, the time lapse camera and the PIV camera were set up on a bank of the stream, and not directly above the knickpoint. By utilizing oblique correction techniques, the orientations of the images provided by the cameras were rectified so that they appeared as if viewed from directly overhead. Oblique images were rectified using Equations 2.10 and 2.11 developed by Fujita et al., (1998).

FFCMD provides a framework for applying Equations 2.10 and 2.11 and for rectifying the images. Within the *Oblique Image Correction Window* (*Figure 4.2*) the object coordinates (the surveyed coordinates) can be entered in the X(m) and Y(m) columns. These are the raw survey data acquired from the field. The corresponding image coordinates can then be entered in the x (pix) and y (pix) columns. These coordinates are the pixel locations of where the surveyed data appear within the image. For instance, when applying LPIV, markers are placed at the edge of the stream at multiple points. The actual positions of the markers are recorded using survey equipment, and then the location of each of the markers is found in an image of the stream. These are the object coordinates and the image coordinates, respectively. Figure 4.2 shows the oblique calibration points – both the object coordinates and the image coordinates – and the corresponding rectification coefficients b_1 though b_8, for one of the LPIV runs.

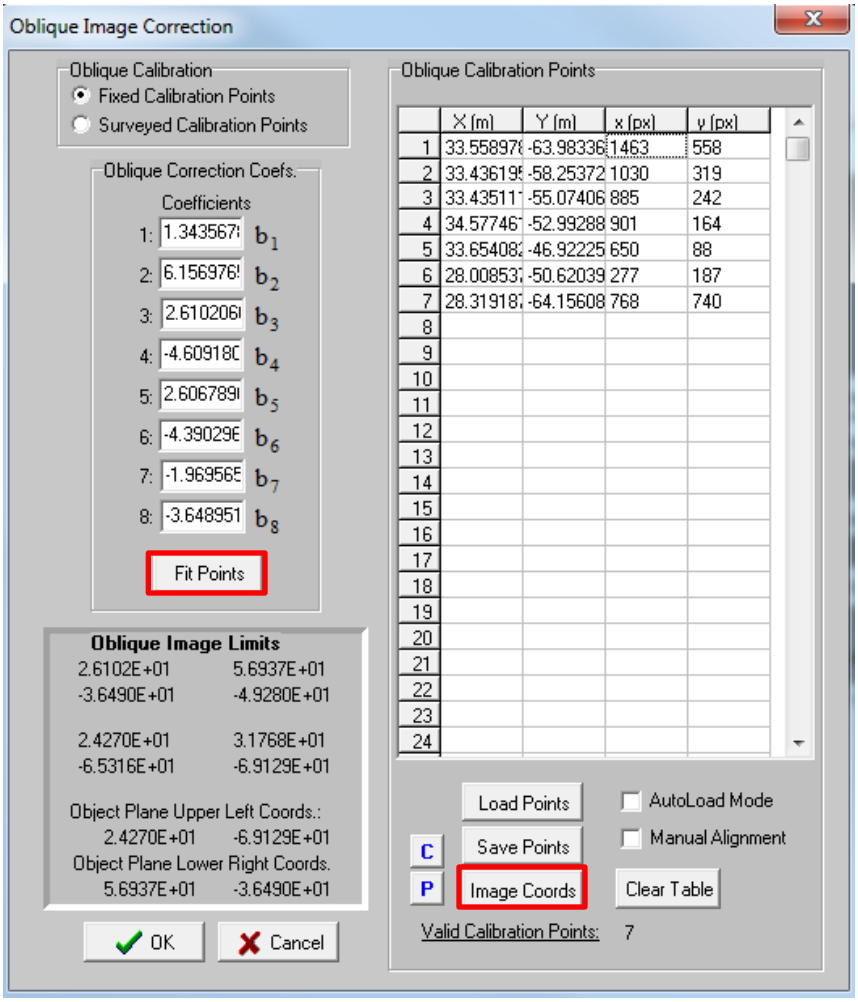

Figure 4.2: Oblique image correction window

Fortunately, in FFCMD, image coordinates can be located interactively by clicking on the *Image Coords* button and loading an image in which each survey point can be viewed. This action will access the *Interactive Oblique Correction Window* (*Figure 4.3*). By clicking on the object coordinate located within the *Interactive Oblique Correction Window* an image coordinate will be paired with its corresponding object coordinate within the *Oblique Image Correction Window*. Once each image coordinate is determined, FFCMD has an algorithm that determines the oblique correction coefficients by least squares paired with an LU decomposition equation solver.

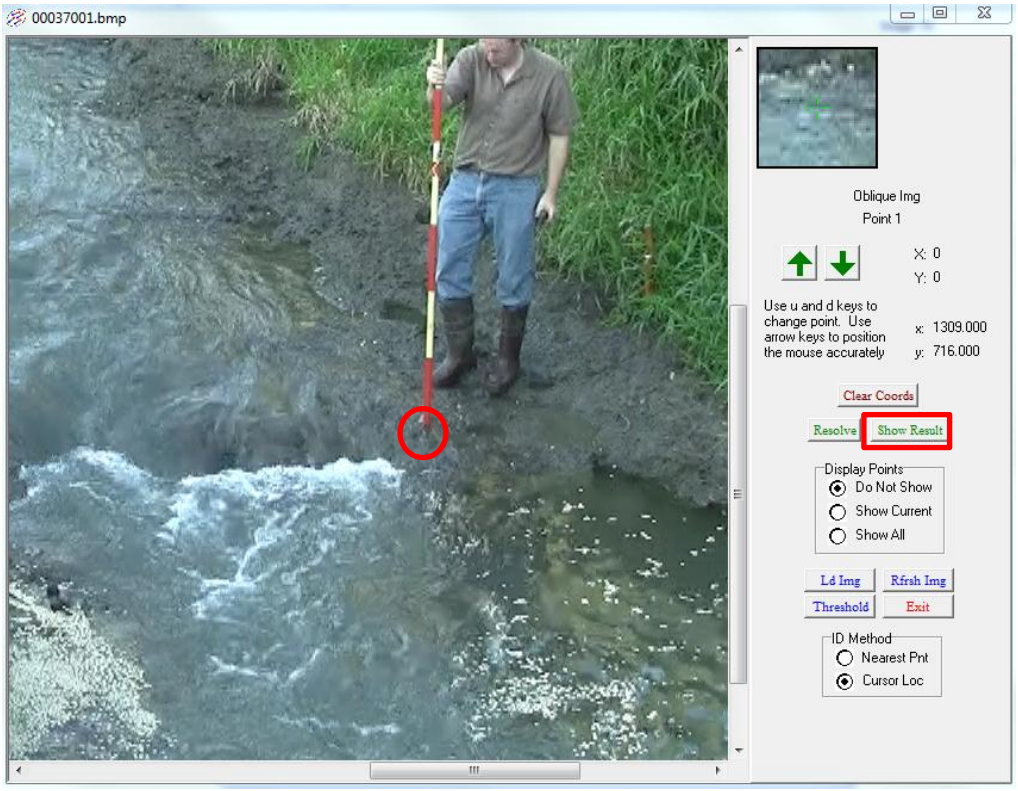

Figure 4.3: Interactive oblique correction window. One calibration point is circled in the image.

With the oblique correction coefficients known, every image in a sequence of images can be rectified. Within the *Interactive Oblique Correction* window, the *Show Results* button (highlighted in Figure 4.3) can be pressed and the *Properties of Corrected Oblique Images window* (*Figure 4.1*) will appear. This window contains resolution and cropping options for the corrected image. Image resolution and/or cropping parameters can be adjusted until an appropriate final image size is determined. The user can see how settings will affect the final image size by choosing *Find Corrected Size*. If the *Show Corrected Image* button is pressed, the image will be corrected based on the previously determined correction coefficients and the image resolution settings and the new image will appear in a new window. If the final image size is not optimal, new image settings

can be applied. The final pixel to distance ratio must be recorded, since it is necessary to use the ratio when calculating velocities in subsequent analyses.

Upon correction, the image will be adjusted from its original form and may be quite large. This is a result of the rectification process. Parts of the image that do not contain flow regions can be cropped using FFCMD. Note that one of the assumptions that is made by the algorithm when rectifying oblique images is that the entire image lies within the same plane as the water surface and all of the calibration points. Since the images collected with the time-lapse camera and the LPIV camera are recording three-dimensional features, when rectified, these three-dimensional figures will appear very distorted. Only the water surface containing the calibration points will appear undistorted. The final image can be saved by clicking on the file menu and selecting S*ave Image As*, but most oblique corrections will be done using a batch process once the appropriate image correction parameters have been determined.

The oblique correction tool can also be used to correct unwanted rotation for a set of images. If the *Manual Alignment* checkbox is selected in the *Oblique Image Correction* Window (*Figure 4.2*) a calibration image (the image being corrected) and a guide image (an image that the calibration image is being aligned with) can be simultaneously loaded into the *Interactive Oblique Correction* Window (*Figure 4.3*). Once the guide and calibration images are loaded, a series of stationary base points can be identified within each of the images by navigating between the two images. For instance, a small branch on a tree or a rock in a fixed position might serve as a stationary point. With multiple base points spatially distributed throughout the images, the oblique

correction algorithm can be applied to align the calibration image with the guide image. The goal of this procedure is to align all of the images belonging to a set of time lapse images to a guide image with known coordinates. Then, all of the images in a time-lapse set will have the exact same alignment, and subsequent geometric measurements in any of the aligned images will be relative to the same datum.

4.2.4 Batch Processes

It is typical in PIV processing to have a large number of files to process. The batch process table in FFCMD allows the processing of multiple files or multiple pairs of files simultaneously. In order to apply the selected processes, all parameters (e.g., oblique correction coefficients, cropping sizes, etc.) were first selected. Then, the set of files that was to be batch processed was entered into the batch operations table (*Figure 4.4*). The Batch Operations Table offers a wide variety of different processes ranging from Image Velocimetry to Multi-File MQD. During the Mud Creek knickpoint analysis, batch operations were utilized for oblique correction and multi-file MQD. *Figure 4.4* below provides some insight into how the batch process table is utilized for oblique image correction.

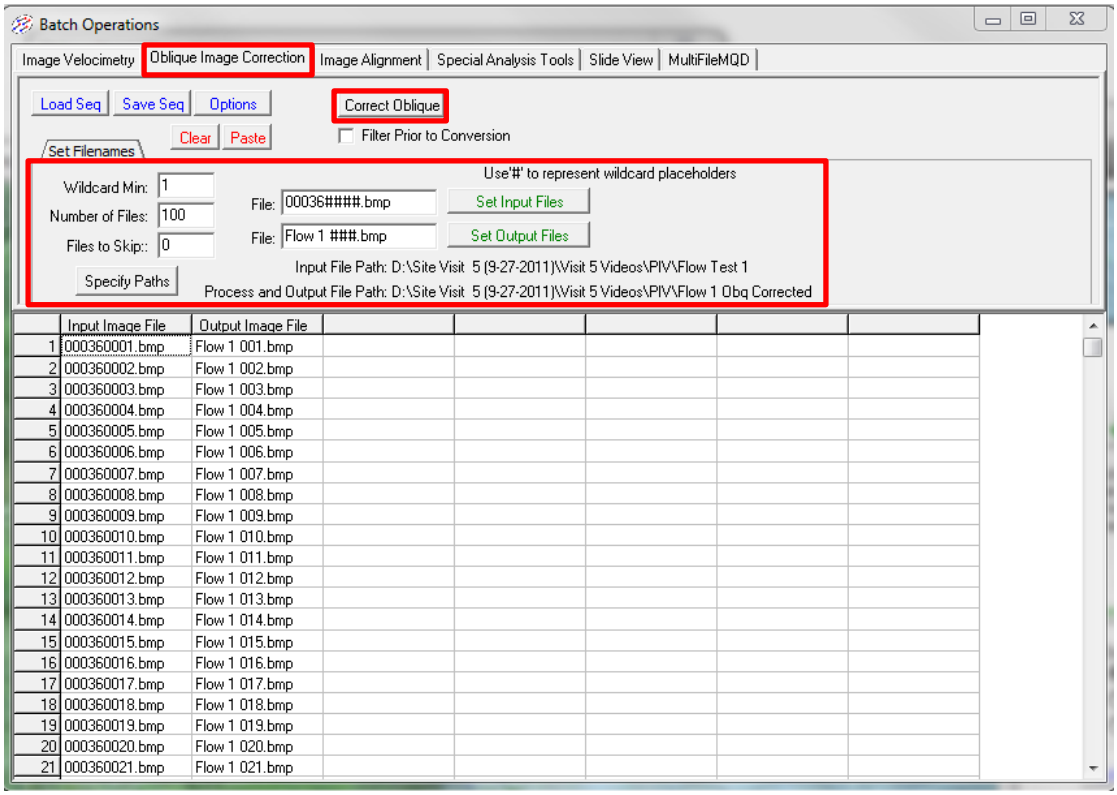

Figure 4.4: Batch operations table (oblique correction)

4.2.5 Masks and Filters

Masks and filters can be utilized during data processing to enhance or aid in obtaining valid PIV results. Masks are used to block out areas of an image that bias results. Areas that may require the use of a mask include flow boundaries and areas in which objects like grass or tree branches block the flow surface. Filters can be used to filter out colors in an image that may make it difficult to locate tracers or particles present in the flow. The *Universal Mask and Filters Window* (*Figure 4.5*) can be accessed in the Tools menu of FFCMD. Within this window, an image can be loaded, and a mask or filter can be applied to the image. For the Mud Creek analysis, Universal Mask and HSL (Hue-Saturation-Luminance) Filters were used.

Within the mask and filters window, drawing tools built into the FFCMD program were used to identify parts of the PIV images that were not part of the surface flow field.

Areas that were masked were ignored by the PIV algorithms (essentially, they were assumed to have zero intensity). Once a mask was completed for a given set of PIV images, it was stored and saved. After a valid mask was developed, it was activated by selecting the *Enable Universal Masking* option in the Tools menu.

The *HSL Filters* were applied by first checking the *Use HSL Filter* checkbox and then adjusting the Hue, Saturation, and Luminance bars to appropriate settings. For example, in some cases the hue bar was adjusted to exclude all colors in the image that were not red. This proved to be useful when attempting to identify particles in the flow or certain features of an image (such as a highlighted knickpoint front). For example, for the present research it was useful to track the knickpoint crest. To do this, time lapse images were organized in order and the knickpoint crest was traced in each image. The trace color was a homogeneous color (e.g., bright red), and everything else in the time-lapse images could be filtered out using the hue filter as shown in Figure 4.5.

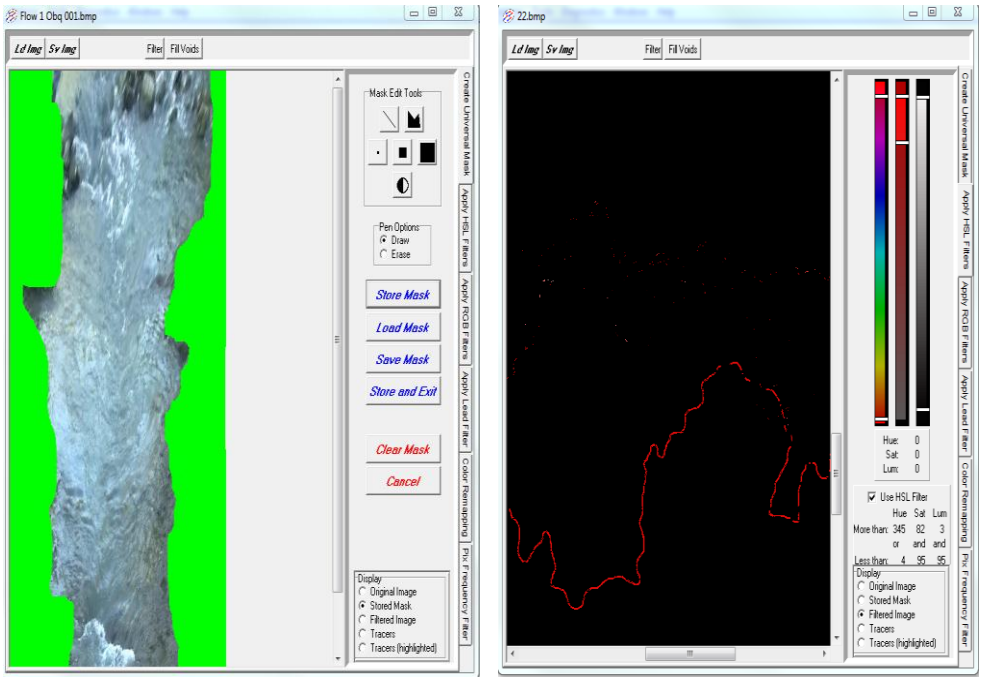

Figure 4.5: Universal mask and filters window showing a hand drawn flow boundary mask (left) and a knickpoint front that was first traced and then filtered using the hue filter to eliminate the background image (right).

4.2.6 Multiple File Minimum Quadratic Difference Method

The Multiple file Minimum Quadratic Difference (MQD) Method developed for the work presented in this thesis is a modified PIV algorithm that improves the signal-to-noise ratio between sequences of pairs of PIV images. Typically in field operations implementing Large-scale Particle Image Velocimetry (LPIV) small numbers of particles and small differences in intensity between flow tracers and the background weaken the signal used for PIV calculations. An adjustment to the traditional PIV calculation technique is necessary to reduce background noise. The main difference between a traditional PIV approach and the Multifile MQD method is that the correlation coefficient (or objective function) is computed for a series of image pairs simultaneously. The use of multiple image pairs improves the signal-to-noise ratio of the correlation, but simultaneously averages flow measurements over time.

The algorithm is applied by choosing an interrogation area; this is a square area with a side length of 8, 16, 32, 64, 128, or 256 pixels. When an interrogation location is chosen, the interrogation area is shifted by all possible x and y displacements within a user specified range. For each shift, the difference between the pixel intensity in a first, shifted LPIV image and a second unshifted LPIV image is determined for all pixels within the interrogation area. These differences are squared and summed over the interrogation area. The minimum quadratic difference algorithm finds the image shift that produces the smallest difference between image intensities for a small region of the image, and thus, the optimal displacement in that region of the image. For multifile analysis, the minimum quadratic difference procedure is repeated for every pair of images, and the quadratic differences for each possible image shift of every pair are combined prior to finding the minimum quadratic difference in order to reduce background noise. This procedure works well, but it should be noted that it eliminates any unsteady components of the flow.

There are multiple ways to carry out the new MQD procedure. The first being to pre-identify interrogation points and to calculate combined arrays for each pre-defined point from a preselected sequence of image pairs. A second way is to identify the region in which the interrogation points will be found and to preprocess all of the preselected image pairs so that when an interrogation point is later identified, all of the necessary correlation information is already stored in memory. Storing every possible image shift in memory is very memory intensive, but makes it easier to calculate velocity vectors at random locations. The second method is illustrated below in Figure 4.6.

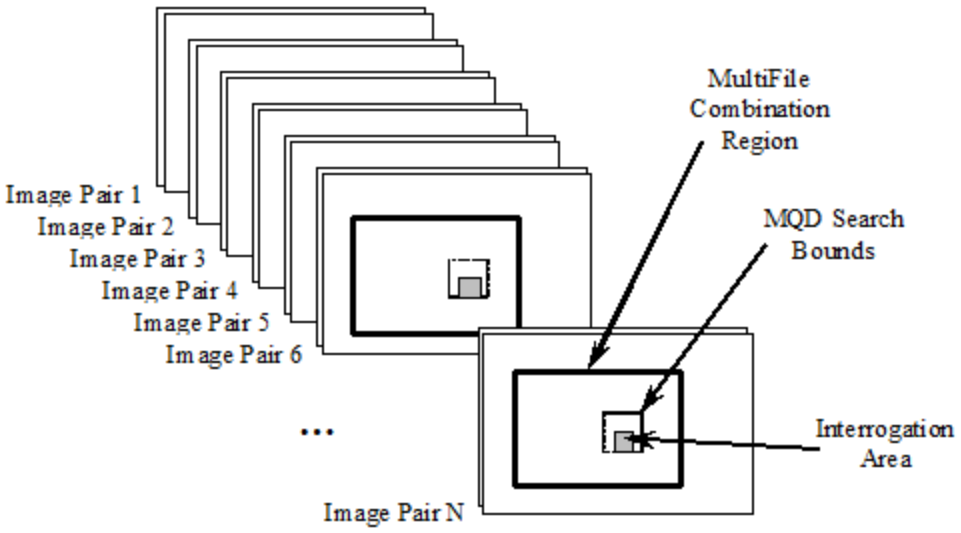

Figure 4.6: Multifile MQD approach

The Multi-File MQD tool can only be accessed in the Batch Operations Table (*Figure 4.4***)** because by definition, the Multi-File MQD method is a batch method that is applied to sequences of image pairs. Within the Multi-File MQD tab a series of image file names and locations can be entered, much the same way as for the oblique correction process described earlier.

Once the image files are entered in the Batch Operations Table; processing can begin by accessing *the Multifile MQD dialog* (Figure 4.7) by clicking the Load First Image button. Within this dialog box the user can adjust the scaling options, processing options, and the display options. Also the locations of interrogation points can be defined within the dialog, either by generating a grid of interrogation points or by loading custom arrays of points.

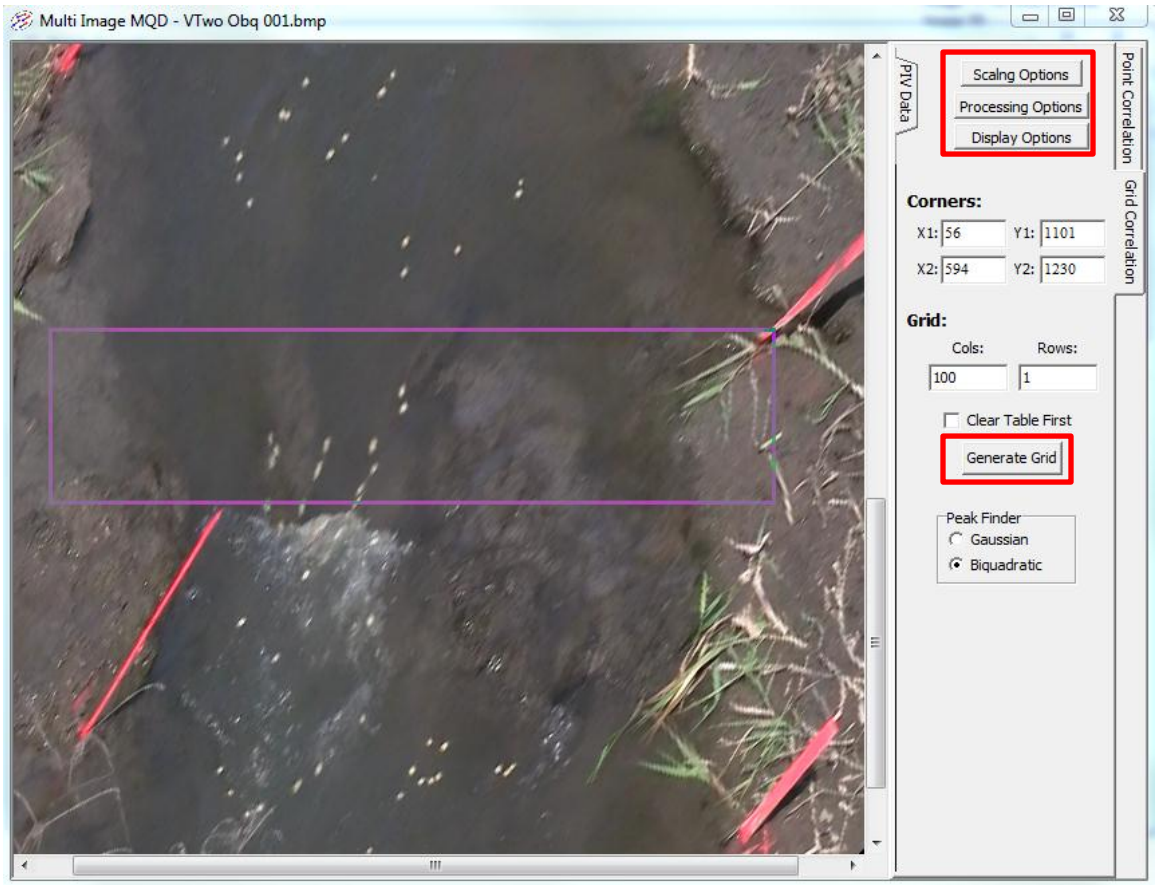

Figure 4.7: Multifile MQD dialog box

Information required to complete the MQD process include scaling options like the separation time and the pixel to distance ratio. Other MQD processing options are important and can be adjusted within the *Processing Options dialog box* (Figure 4.8). Within this box the Multi-File MQD search bounds and interrogation area can be adjusted for each calculation.

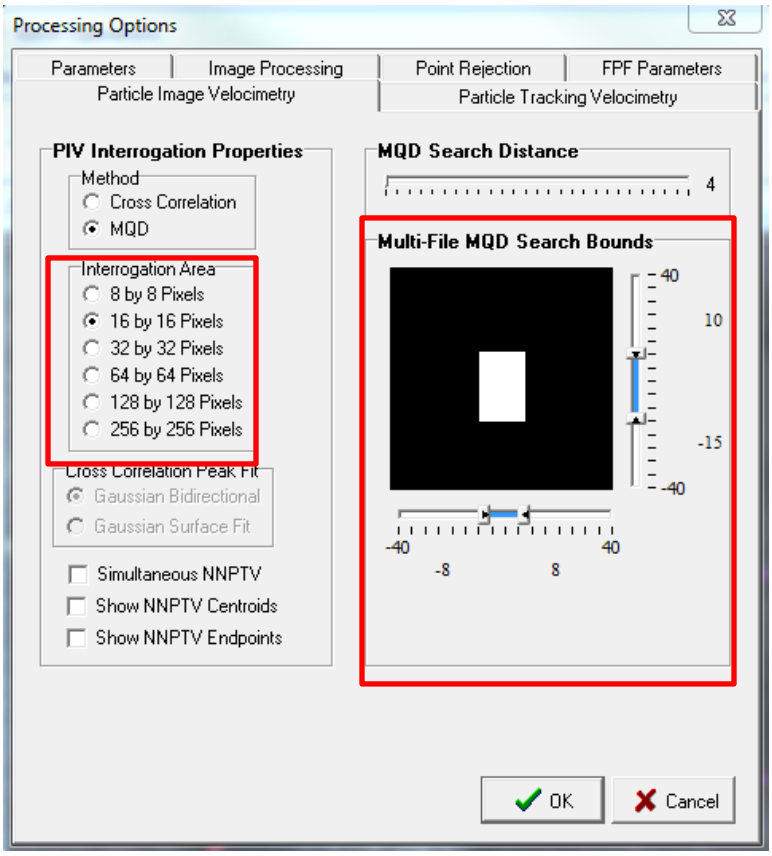

Figure 4.8: Processing options dialog box

4.2.7 Multi-Plot Window

The Multi-Plot tool of FFCMD can be utilized to overlay or align images. *The Multi-Plot Window* (*Figure 4.9*) can be accessed in the View menu. Within the *Multi-Plot Window*, two images can be loaded and viewed. Typically the first image loaded is the guide image, and the second image is the image being aligned. There are two ways to view the images simultaneously, either with the composite or mesh function. The composite function shows the brightest pixels from each image, and the mesh function shows every other pixel in each image. The use of these functions is dependent on the application and the contents of the images being used. For the Mud Creek study the mesh function proved to be best. The image that needs to be aligned can be adjusted by pressing the arrow keys until it is aligned with the guide image. The image shift is

reported in the window and can be recorded if aligning a series of images is necessary. Once the images are aligned the image to which the offset was applied can be viewed and saved.

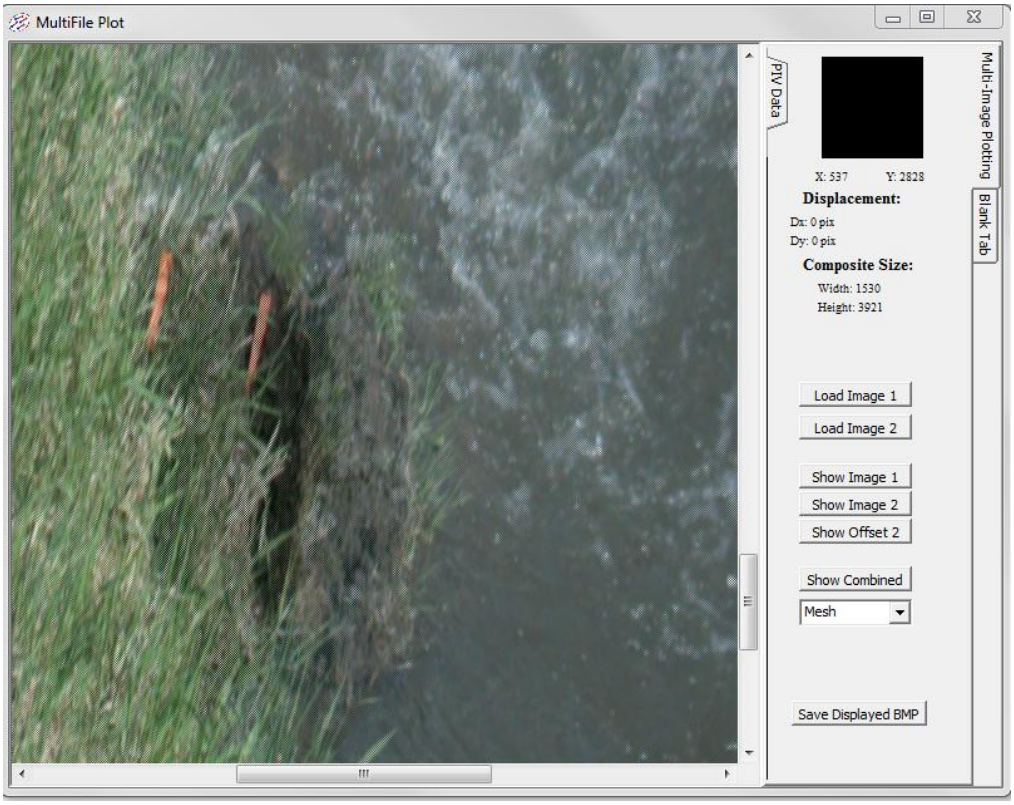

Figure 4.9: Multi-plot window showing two overlapping images. Note the offset of the orange stake in the two meshed images.

4.3 Time Lapse Analysis

A time lapse camera was installed at the Mud Creek study site to continually monitor the headward progression of the knickpoint front over the study period. The images from the time lapse camera were used to create a two-dimensional overhead representation of the knickpoint migration. As was discussed in Chapter 3, the camera was installed on the right descending bank of the channel and was programed to capture an image of the knickpoint every thirty minutes. After nightfall the images were too dark to make any useful observations, so only images taken during the daylight hours were

considered to be useful for the analysis. As the time lapse analysis of the knickpoint progressed it was determined that the thirty minute image capture rate was unnecessary, and though it is still advantageous to gather the data at a high frequency (in attempts to capture high-flow events and to allow selection of optimal images), one image per day was determined sufficient for monitoring knickpoint progression. Of the images collected, 499 images have been reviewed from July 14, 2011 to November 28, 2012.

4.3.1 Image Corrections

As mentioned in Chapter 3, images collected with the time-lapse camera had to be corrected because of three things: (1) slight changes in the alignment of the camera when data were downloaded, (2) minor shifts in the camera position from day to day caused by temperature and humidity changes, and (3) the obliqueness of the images. To create an accurate representation of the knickpoint retreat, each image had to be aligned appropriately. In order to properly align the images, each one of the corrections listed above had to be applied.

First, upon downloading the images from the camera, the design of the camera made it difficult to return it to its exact previous position. Thus, slight rotation of the camera resulted in a shift in orientation between the final image in one data set and the first image in the next data set. The rotation was corrected for by using oblique correction techniques provided in FFCMD and utilizing the *Oblique Image Correction Window* (Figure 4.2) and checking the *Manual Alignment* box to correct all of the time-lapse images. Stationary base points were identified near the stream in each image set, and the images were then corrected so that the base points were aligned. The same oblique correction coefficients were applied to all images collected during the period between

two sequential site visits because camera misalignment only happened when data were downloaded.

The oblique correction procedure eliminated the rotation between images; but there were still minor shifts in the camera orientation between images. It is believed that these minor shifts were caused by thermal expansion of the camera mount and changes in moisture content of the soil supporting the camera mount. With the elimination of rotation, these minor shifts were mainly x and y translations. To correct these minor shifts the Multi-Plot tool was utilized. With the use of the *Multi-Plot Window* (*Figure 4.9*), successive images were loaded and aligned by aligning stationary objects that appeared in all of the images. Orange stakes were placed at the site to offer a consistent set of stationary base points throughout each set of images. Note that these minor shifts were corrected after the images had been rectified.

The final adjustment that was necessary was to correct the images for obliqueness; that is, the camera was set up at an angle and not directly above the knickpoint. In order to properly determine the amount of knickpoint retreat, the images had to be rectified to make them appear as if they were being viewed from directly overhead. To correct for obliqueness the *Oblique Image Correction Window* (Figure 4.2) was utilized again. This time, however, the *Manual Alignment* box was left unchecked. Twelve calibration points collected during the September 27, 2011 site visit were used to carry out the oblique correction calculations for the time lapse analysis. The calibration points are given in Appendix A (Table A1). These calibration points were identified with markers to make them readily identifiable within the time lapse images.

As an example of the image rectification process; *Figure 4.10* shows the oblique, unaligned images downloaded from the time lapse camera for the dates of September 15, 2011, December 3, 2011, and February 12, 2012. The corresponding rectified images are shown in *Figure 4.11*.

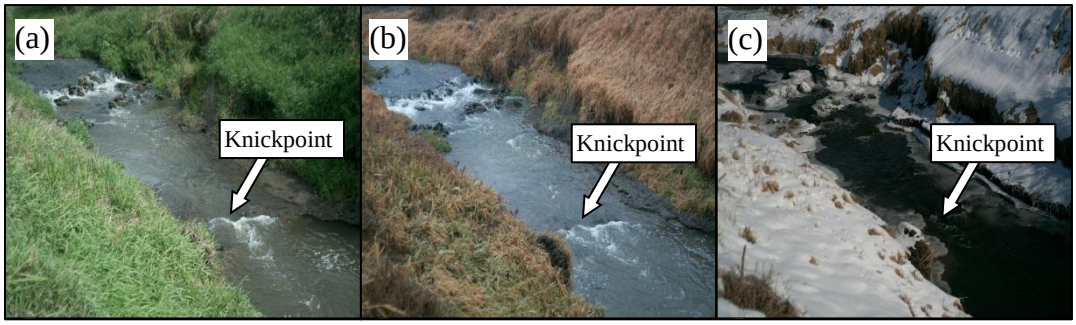

Figure 4.10: Time-lapse images collected on (a) September 15, 2011, (b) December 3, 2011, and (c) February 12, 2012

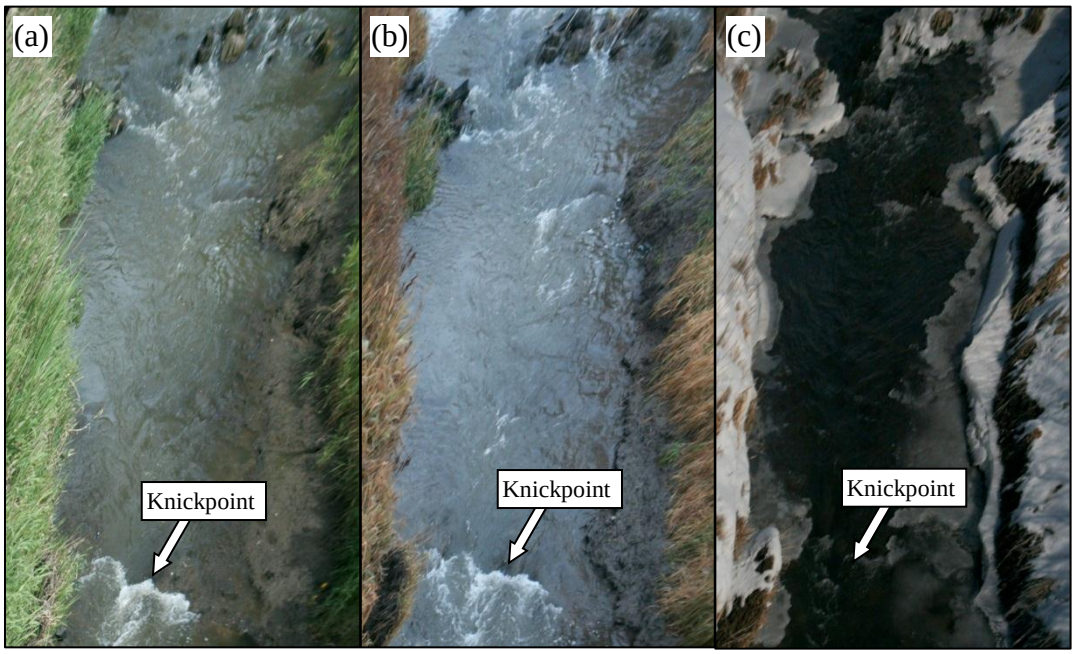

Figure 4.11: Rectified time-lapse images from (a) September 15, 2011, (b) December 3, 2011, and February 12, 2012

4.3.2 Knickpoint Front Tracking

After the time-lapse images were aligned and rectified, the knickpoint front was identified and highlighted in each image. The exact location of the knickpoint front was

not always easily identifiable due to variations in flow rate. The vertical face of the knickpoint is somewhat three-dimensional, and what is actually observed in each time-lapse image is the location of the hydraulic jump above the knickpoint (see Figure 4.10). However, at low flows, the hydraulic jump occurs at the crest of the knickpoint. For the majority of the study period, the stream had relatively low flows, which made the crest of the knickpoint face easy to identify. The knickpoint crest was highlighted with a bright red color using a drawing program. By applying an HSL Filter in FFCMD (Figure 4.5), pixels with colors that didn't match the exact color of the highlighted knickpoint front were painted black, leaving only the highlighted knickpoint front visible in the image. By overlaying each of the filtered images using the Multi-Plot tool (Figure 4.9), the gradual headward progression of the knickpoint could be easily observed in a two-dimensional fashion.

4.4 Survey Data

Survey data of the banks and stream were collected during each site visit. The survey data were used to provide calibration points for rectifying Large-scale Particle Image Velocimetry (LPIV) videos and the time lapse images, as-well-as stage information of the channel. In addition, a series of more detailed surveys were carried out on the dates of September 27, 2011, March 21, 2012, and September 25, 2012. These more extensive surveys contained more detailed information about the changes in the stream bathymetry that occurred over the duration of the study period. The observation of the change in stream bathymetry provides insight into the mechanisms associated with the migration of the Mud Creek knickpoint.

4.5 Surface Water Velocity Distributions Using LPIV

Surface water velocity distributions of Mud Creek were determined using Large-scale Particle Image Velocimetry (LPIV) techniques. The velocity distributions were calculated along the approach reach of the channel upstream of the knickpoint. During each visit to the site, a series of videos was taken that captured sequences of the flow. The videos were collected using a digital video camera (Figure 3.5) that was set up on the right descending bank near the time lapse camera mount. Again, like the time lapse camera, the digital video camera was set up at an angle to the knickpoint and not directly above the knickpoint. The videos were converted into sequences of bitmaps with image separation times of 1/30th of a second. Using the surveyed calibration points, the bitmaps were corrected for obliqueness (rectified) using the *Oblique Image Correction Window* (Figure 4.2).

Figure 4.12: LPIV images: (a) original bitmap and (b) rectified image

The low flows were seeded with particles (slightly buoyant cereal) to aid in the LPIV analysis. The high flows were left unseeded, as there was an abundance of highly

visible bubbles present on the water surface. The surface velocities were calculated at a series of cross sections upstream of the knickpoint. The cross sections were developed where detailed elevation data of the stream were known from the collected survey information. For each cross section, interrogation points were selected at regular intervals from bank to bank. The average velocities were calculated at each of the interrogation points using the *Multi-File MQD* tool (Figure 4.7) for 100 to 200 pairs of images.

This particular field environment introduced challenges to traditional PIV approaches. First, large blades of grass and branches overhanging the flow significantly increased the signal to noise ratio, throwing off the PIV calculations. In other words, grass and branches interfered with visibility of some parts of the water surface, causing erroneous results. This issue was resolved by masking all areas of the image that had vegetation in them, including the banks and any parts of the image where vegetation was between the camera and the water surface. This was done utilizing the *Universal Mask and Filters Window* (*Figure 4.5*) described in Section 4.2.5. Second, the number of tracers present in the flow was very low. By applying the multi-file averaging approach that was described in Section 4.2.6, the signal to noise ratio was significantly improved, which vastly improved the results of the velocity calculations.

4.6 Discharge Estimation

Determining discharges in the stream was the final objective of the knickpoint analysis. This was done by using the surface velocity distributions obtained from the LPIV analysis to calculate a depth-averaged velocity at a series of interrogation points across the stream. The depth-averaged velocities were then used to compute the discharges through each cross section using the following equation:

$$Q = \sum U_i A_i \tag{4.1}$$

Where Q is the discharge at a cross section, A_i is the effective flow area associate with each interrogation point, and U_i is the depth averaged velocity for a given subarea associated with each interrogation point.

The depth-averaged velocities for each subarea were estimated by assuming the $1/7^{th}$ power law was valid for each interrogation point. Therefore, it was assumed that the flow in the approach reach of the channel was uniform. The $1/7^{th}$ power law is given by Chow, (1959) as follows:

$$\frac{u}{U_{max}} = \left(\frac{y}{H}\right)^{\frac{1}{7}} \tag{4.2}$$

Where u is the velocity at a distance y from the streambed, U_{max} is the surface velocity (obtained from LPIV), and H is the depth in the channel. By integrating equation 4.2, the depth averaged velocity for each interrogation point was found to be $7/8^{th}$ of the surface

velocity. By implementing the 1/7th power law, a new discharge calculation can be expressed as follows:

$$Q = \sum \frac{7}{8} U_{max,i} A_i \tag{4.3}$$

The depth-averaged velocity for each interrogation point was then calculated, and multiplied by the effective flow area associated with the point to get the discharge flux associated with each point. All of the discharge fluxes were then summed form each subarea in the cross section to get the discharge in the channel. *Figure 4.13*, below, illustrates the procedure used to estimate the discharge in the channel.

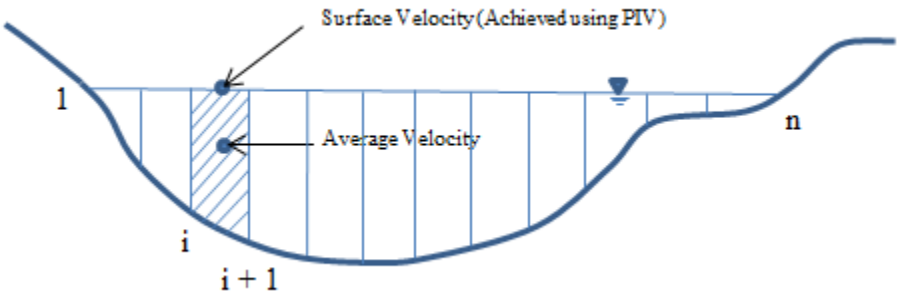

Figure 4.13: Depiction of subareas associated with interrogation points used for discharge calculations

Chapter 5: **Results and Discussion**

5.1 Introduction

This chapter presents the results from the time lapse images, surveys, surface water velocity analyses, and discharge estimates that were performed on the data retrieved at the Mud Creek knickpoint site. The data were obtained and analyzed using the equipment and methods described in the previous chapters.

5.2 Time Lapse Analysis

For 499 days the position of the knickpoint front was continually observed using the time lapse images collected at the site. The images were collected between July 14, 2011 and November 28, 2012. The knickpoint fronts were identified and highlighted in each image. Nine of the front locations observed throughout the study period were overlain and placed on a rectified bitmap of the knickpoint (Figure 5.1). The time spacing between the front locations in Figure 5.1 was not uniform, but an effort was made to allow significant time between observations (approximately two months) and to present observations in each season of the year. Presenting the front position in this way offers a unique two dimensional representation of the headward retreat of the knickpoint over the observation period. Some of the front locations shown in the image overlap. The knickpoint crest is not always clearly identified because the depth of the water changes over time, and the knickpoint crest can erode downward as well as upstream – downward erosion of the crest can be perceived as downstream migration of the knickpoint due to the oblique angle of the camera.

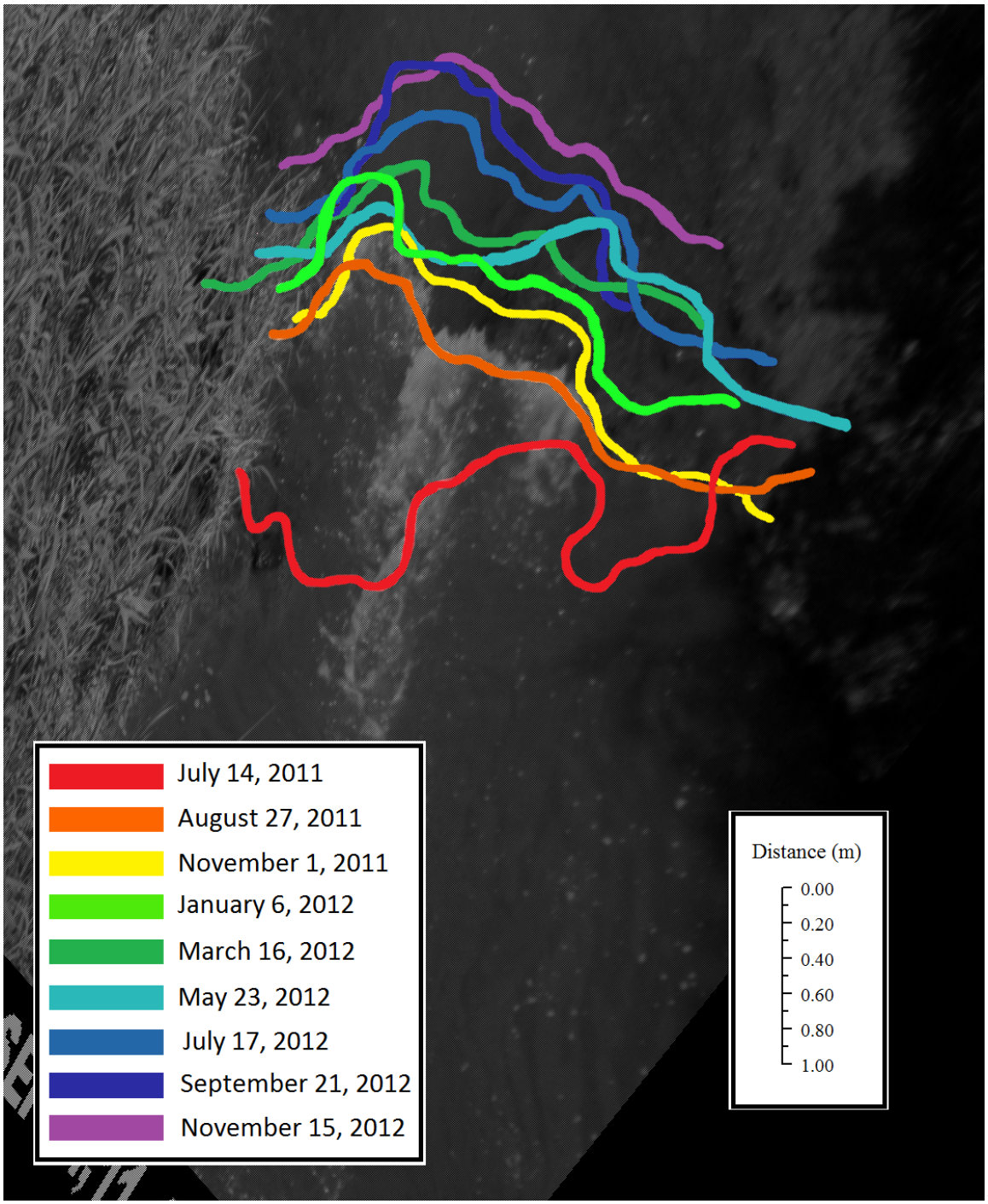

Figure 5.1: Two dimensional representation of the knickpoint retreat over the duration of the study period.

Upon observing the movement of the knickpoint front over the duration of the study period (Figure 5.1), it is apparent that most of the time, the migration is very slow, moving only 2 meters over the 1.5-year study period. The data recorded thus far indicate

that the migration upstream slows significantly in the fall and winter months, and increases during the spring and summer. Figure 5.2 graphically shows the progression of the knickpoint upstream over the duration of the study period.

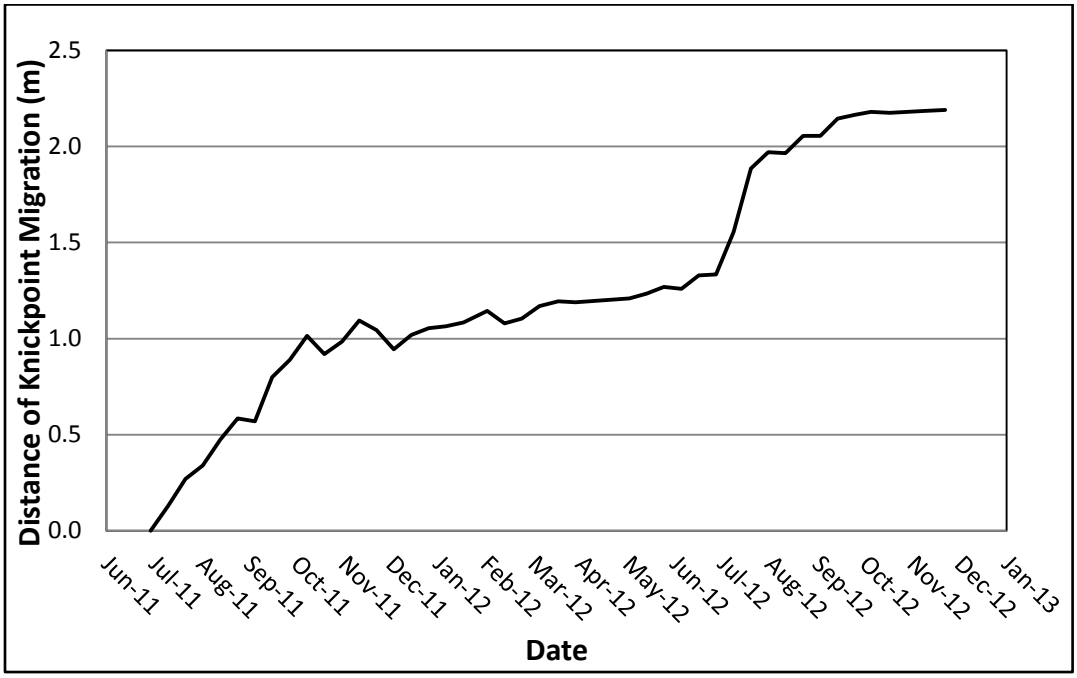

Figure 5.2: Distance of knickpoint migration over the study period.

Figure 5.2 was developed by recording the upstream most point of the knickpoint lip in each of the time lapse images. It should be noted that there is uncertainty involved with the location of the knickpoint lip presented in Figure 5.2. In each of the time lapse images the actual lip of the knickpoint is submerged by the flow and what is actually observed is the position of the leading edge of the hydraulic jump. As the flow in the stream fluctuates, the position of the hydraulic jump changes, causing inconsistences in the plot, and in some cases indicating that the knickpoint has migrated downstream. Nevertheless, Figure 5.2 clearly illustrates the migration rate of the knickpoint has varied throughout the study period.

Another possible reason for the apparently slower movement of the front may be a change in the mode of knickpoint erosion in combination with the time-lapse analysis technique. Only the upper surface of the knickpoint can be seen in the time-lapse images, and when the location of the knickpoint front is determined, it is the location of the crest. It is possible that the mode of knickpoint migration changes with the onset of the lower stream flows and freezing that take place during the winter months. The lower flows may cause the bulk of the erosion to shift from the knickpoint face to the knickpoint lip (i.e. causing the knickpoint to migrate in a rotating fashion). If this is the case, observing the movement of the knickpoint front in the way shown in Figure 5.1 does not completely capture the erosion behavior of the knickpoint front. The results may indicate that the knickpoint front is not eroding (or eroding slowly); when in reality the knickpoint front is being undercut during the winter months, and then retreating upstream in the spring and summer when higher flows are present in the channel to carry away loose sediment at the lip of the knickpoint.

Nevertheless, the knickpoint front has significantly migrated upstream over the course of the time lapse analysis. By examining the highlighted fronts in *Figure 5.1* and the knickpoint progression in Figure 5.2, it is apparent that the knickpoint front has moved upstream approximately 2.2 meters over the 499 day study period. The most significant front movement appears to have occurred near the beginning of the study period migrating at 0.0102 m/day. The migration upstream then slowed in the winter months to 0.0009 m/day, and speeded up again in the spring and summer. The average migration rate over the duration of the study period was determined to be 0.0044 m/day.

Table 5.1 below provides a summary of the varied migration rate of the knickpoint throughout the 499 day study period.

Table 5.1: Summary of varied migration rates of the knickpoint

Season	Time Period	Migration Rate (m/day)
Summer and fall	July-October (2011) (100 days)	0.0102
Winter and spring	November - July (2012) (232 days)	0.0009
Summer and early fall	June -September (2012) (99 days)	0.0089
Fall and early winter	October - November (2012) (68 days)	0.0007
All Seasons	Study Period (499 days)	0.0044

5.3 Survey Analysis

To further examine the morphology of the knickpoint front and the stream channel, extensive survey data were collected on the dates of September 27, 2011, March 21, 2012, and September 25, 2012. The elevation data collected during these surveys were used to create the series of contour plots presented in *Figure 5.4*. The east and north positions given on the x and y axes of the plots are relative to an arbitrary benchmark located at the southwest corner of the Elderberry Avenue Bridge set to (0,0). The elevations given in the contour plots are relative to the World Geodetic System 84 (WGS 84) datum. The same benchmarks were used for all of the contour plots so that the elevations could be directly compared with one another.

During the collection of the survey data, two separate sets of survey equipment were used. For the surveys collected on September 27, 2011 (a) and March 21, 2012 (b) a Sokkia Set 5A total station was used to gather the elevation data. For the September 25, 2012 (c) survey a new TopCon GPS based survey system was acquired and used to gather the elevation data (note that the letter next to the date refers to the specific contour

plot in Figure 5.4). There were some problems with the Set 5A system, and the data collected using the new TopCon system were assumed to be more accurate than those collected using the Set 5A. The inaccuracies in the Set 5A data were observed by comparing data collected at each of the bridge corners, which were points that should not change between surveys. The bridge corner elevations did not match up with the TopCon elevation points; they were considerable lower. To properly align the elevations of the three contour plots some adjustments to the Set 5A elevations needed to me made. First the GPS survey equipment utilized the WGS 84 datum, whereas the total station used an arbitrary datum set at 152.439 m (500 ft). In order to align the elevations in each contour plot, the elevations in surveys (a) and (b) needed to be increased by 169.541 m (556.094 ft). This adjustment worked quite nicely for the survey conducted on March 21, 2012 (b); however, the data collected on September 27, 2011 (a) still seemed very low compared to contour plots (b) and (c). It is believed this was due to equipment and user error. This inconsistency in data was adjusted by locating a cross section of the stream channel where the elevations were known for all of the surveys, and in a location close to the knickpoint, but at a cross-section that was known to have been stable over the study period. Comparison of the cross sections collected with the three surveys allowed us to accurately adjust the datums for the Set 5A surveys.

Figure 5.3 is a plot of the cross section that was chosen, and which is located at North -57.00 m. This cross section was chosen because very little (if any) erosion has taken place at this location during the study period. By examining the elevation data collected at this cross section during surveys (a) and (c), it was determined that the data collected on September 27, 2011 (a) was approximately 10 cm below the data collected

with the GPS survey equipment on September 25, 2012 (c). By adding 10 cm to each elevation data point collected during the September 27, 2011(a) survey, the three contour plots could be compared side by side, and the upstream progression of the knickpoint could be examined more clearly. It is important to note that during the September 27, 2011 (a) survey a smaller number of data points were collected compared to the surveys collected on March 21, 2012 (b) and September 25, 2012 (c). This is evident in the reduced amount of detail shown in *Figure 5.4* (a).

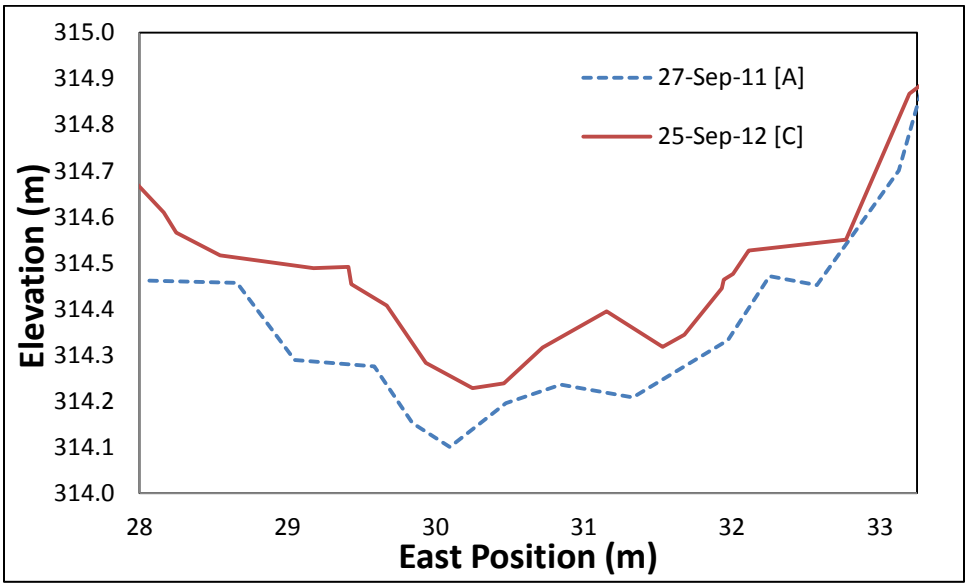

Figure 5.3: Surveyed channel cross sections at north -57.00 m

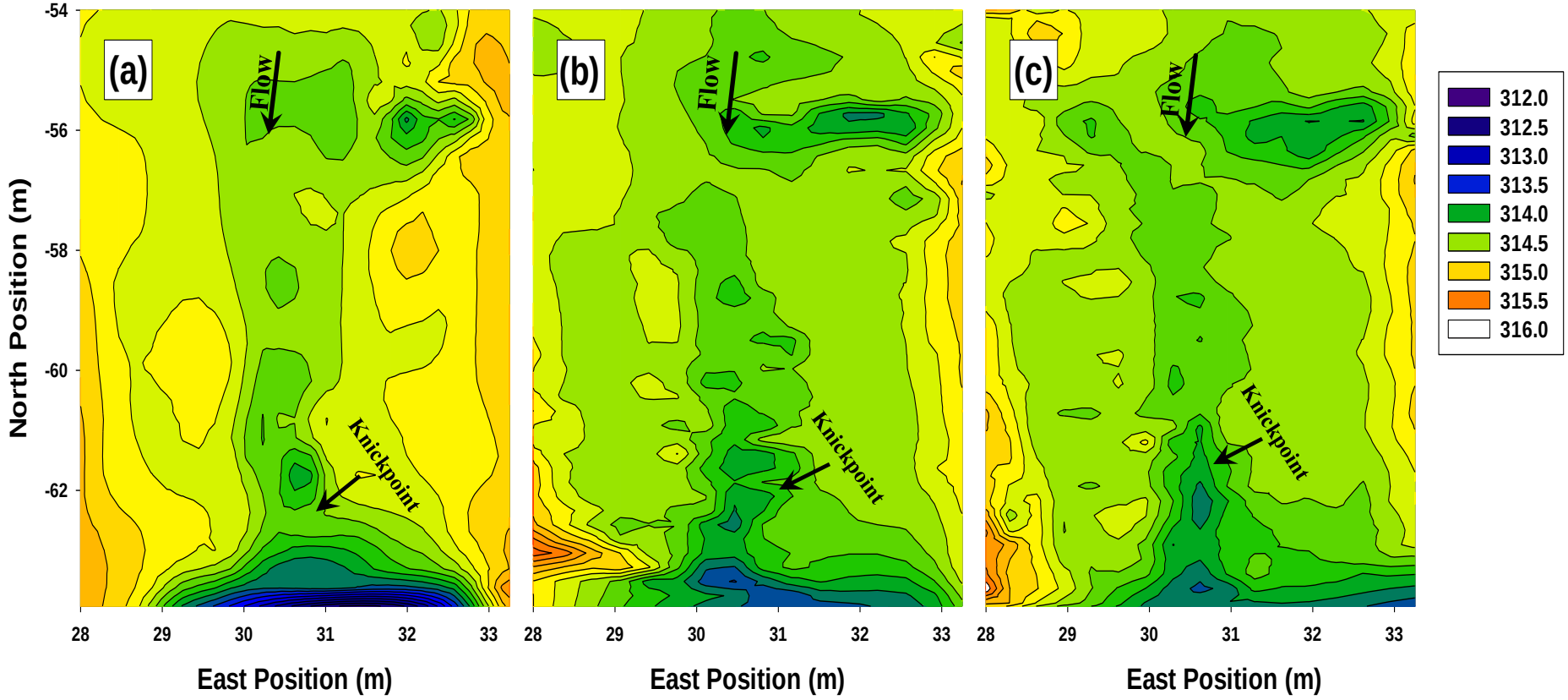

Figure 5.4: Contour plots of Mud Creek knickpoint: (a) September 27, 2011, (b) March 21, 2012, (c) September 25, 2012

The three contour plots were able to illustrate the morphology of the stream channel and knickpoint throughout the period of analysis, as well as highlight important features of the channel that may be affecting the migration of the knickpoint. To offer context to the three contour plots presented in Figure 5.4, the flow direction is marked by an arrow and the face of the knickpoint is labeled in each plot.

As observed during the time lapse analysis (*Figure 5.1*), the contour plots confirm that measurable upstream migration of the knickpoint front has occurred over the duration of the study period. However, the contour plots also show significant widening of the knickpoint face and that the downstream plunge pool is deepening and widening as well. Also, upstream of the primary knickpoint on the left descending bank a enlarging secondary scour hole is forming. Upon further examination of the contour plots, it was determined that the main channel itself is approximately 4.5 meters wide, but there also appears to be a deep, narrow trench forming at the center of the channel . This trench is approximately 1 meter wide and extends upstream from the primary knickpoint to the upstream scour hole. The trench has increased in depth over the study period and appears to have a significant impact on the morphology of the knickpoint and stream channel, as the knickpoint appears to be working its way upstream within the confines of trench. The trench appears to be a mechanism by which knickpoint migration can occur much more rapidly than by direct erosion of the knickpoint face.

5.4 Surface water Velocity Observations with LPIV

During each visit to the site, a series of videos were taken of the flow surface upstream of the knickpoint. The videos were converted into bitmap images. The Oblique images were then rectified using surveyed calibration points that were gathered at the

edges of the water surface. The calibration points and oblique correction coefficients can be viewed in Tables A1-A8 available in Appendix A. Tables A1 and A2 correspond to the time lapse survey data collected on September 27, 2011. Tables A3-A8 present the information relating to the three LPIV surveys. A multi-file minimum quadratic difference algorithm was applied to determine average velocities at interrogation points spaced across a series of cross sections. The chosen cross section locations and processing information varied slightly for each data set. The cross section locations for each LPIV calculation are available in Tables 5.3, 5.4, and 5.5. These locations are relative to the location of the knickpoint

The processing information for the LPIV data sets collected on September 27, 2011 and March 21, 2012 were nearly identical. The image scale was set at 2.0 pix/cm, the separation time was given as 0.0333 s, the interrogation area was set at 16 pix by 16 pix, and the search bounds were set as 16 pix by 27 pix. 50 interrogation points were used across each cross section with a pixel spacing of 18 pix and 20 pix, respectively. For each of these two data sets, 100 pairs of images were used for processing. The processing information for the September 25, 2012 LPIV data set was slightly different than the previous two data sets. This was because the scale of the video taken at the site was considerably larger than the previous two videos, as the water surface in the stream was very low due to drought conditions. For this reason the image scale for this data set was set to 3.0 pix/cm, providng a higher level of resolution. The separation time remained 0.0333 s, the interrogation area was set at 16 pix by 16 pix, and the search bounds were set to 16 pix by 27 pix. 100 interrogation points were used across each cross section with a pixel spacing of 7 pixels. For this data set, 200 image pairs were used for processing.

The higher resolution and increased number of image pairs allowed for a greater level of accuracy in the calculation of the surface water velocity distributions for this data set. Table 5.2 offers a summary of the processing information used for each set of LPIV data collected at the site.

Table 5.2: Summary of LPIV Processing Information used for each data set

	September 27, 2011	**March 21, 2012**	**September 25, 2012**
Separation Time (s)	0.0333	0.0333	0.0333
Image Resolution (pix/cm)	2.0	2.0	3.0
Interrogation Area (pix^2)	16x16	16x16	16x16
Search Bounds (pix by pix)	16x27	16x27	16x27
Interrogation Points	50	50	100
Pixel Spacing (pix)	18	20	7
Image Pairs	100	100	200

The velocity distributions for each LPIV analysis are presented in Figures 5.5, 5.6, and 5.7. Figure 5.5 corresponds to the September 27, 2011 site visit, Figure 5.6 corresponds to the March 21, 2012 site visit, and Figure 5.7 corresponds to the September 25, 2012 site visit.

Figure 5.5: Surface water velocity distributions created from LPIV data collected on September 27, 2011 site visit.

Figure 5.6: Surface water velocity distributions created from LPIV data collected on March 21, 2011 site visit.

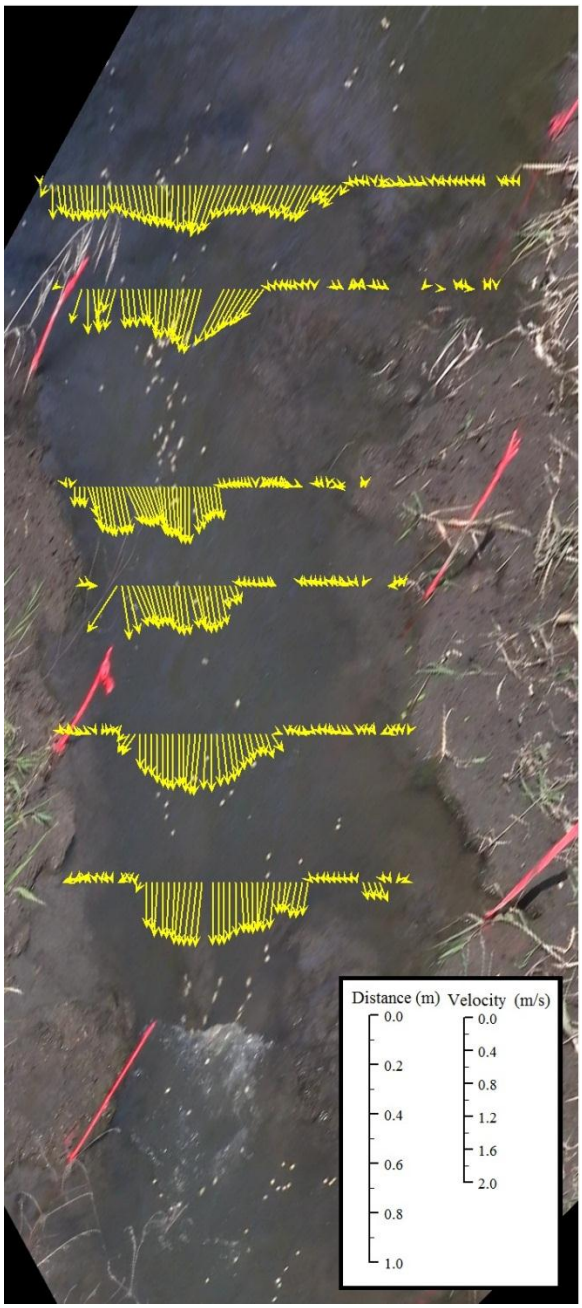

Figure 5.7: Surface water velocity distributions created from LPIV data collected on September 25, 2012 site visit.

Although the width of the water surface varies from observation to observation, the highest surface velocities are in the center of the channel. For the lower flows, there are areas of stagnation or rotation near the channel banks. This may be as a result of water being diverted to the deeper, narrower trench. The highest velocities for all flows were observed within the bounds of the 1 meter wide region directly above the trench that has developed upstream of the knickpoint. The higher velocities associated with this region result in an increase in shear stress within the trench. It is very likely that the concentrated flows will continue to deepen, lengthen, and widen the trench until a mass failure occurs; At this point the knickpoint front will likely quickly move upstream within the confines of the trench.

5.5 Discharge Estimation

Using the average surface velocities obtained from the LPIV techniques, volumetric discharges through each cross section were estimated. The surface velocities were converted into mean velocities using the $1/7^{th}$ power law. The mean velocities were then multiplied by the subarea associated with the velocity to obtain a discharge flux. Each flux was then summed to get a discharge for the entire cross section. Tables B1-B20 illustrate the steps of the discharge estimation in more detail. These tables are available in Appendix B. Tables B1–B7 correspond to the September 27, 2011 survey, Tables B8–B14 correspond to the March 21, 2012 survey, and Tables B15-B20 correspond to the survey carried out on September 25, 2012. Each table presents the position and elevation of each interrogation point, the channel depth at each interrogation point, the area of each subarea, and the effective area related to each interrogation point (note, the effective area is defined by the sum of one half of the two subareas on either side of a given

interrogation point). The tables also present the surface water velocities obtained from the LPIV analysis, the depth-averaged velocities ($7/8^{th}$ of the surface velocity), and finally the calculated discharges for each subarea. A summary of cross section locations, flow areas, and volumetric discharges for the channel are presented in Tables 5.3, 5.4, and 5.5 for the three flow tests below.

Table 5.3: Summary of Discharge Calculations and Cross Section Geometry: September 27, 2011 LPIV Data

Cross Section	Distance Upstream of Knickpoint (m)	Flow Area (m^2)	Discharge (m^3/s)
a	0.40	-	-
b	1.60	0.705	0.351
c	2.15	0.657	0.316
d	2.85	0.582	0.244
e	3.73	0.481	0.310
f	4.45	0.776	0.342
g	6.75	0.977	0.290
h	8.85	0.679	0.293

Table 5.3 presents the discharge calculations determined from the LPIV data collected on September 27, 2011. The flow condition in the stream appeared to be a typical base flow condition for Mud Creek, since the water covered most of the non-vegetated bed. The discharge at cross section (a) was not calculated because of its proximity to the knickpoint; the hydraulic jump at the knickpoint face prevents accurate LPIV measurements in addition to the flow not being uniform in the vicinity of the face, meaning the $1/7^{th}$ power is not valid in this region. The remaining cross sections produced a consistent set of results, aside from the results at cross sections (b) and (f), which seem a bit higher than the other measurements. Cross section (b) is still located quite close to the knickpoint and cross section (f) is located just downstream of the

secondary scour hole described above. In these areas flow structures associated with the secondary scour hole and the primary knickpoint may be affecting the motion of tracers present in the flow and used for the LPIV calculations. The assumption of uniform flow in the channel is not ideal at some of these locations. The average discharge for the first test date was *0.306 m^3/s* with a standard deviation of *0.036 m^3/s*.

Table 5.4 presents the results from the discharge calculations performed on the LPIV data collected on March 21, 2012. The flow condition in the stream on this date was slightly higher that than the flow calculated previously, as there was a light but consistent drizzle falling throughout the data collection period. Much like the previous calculation, cross section (b) appears to be a bit high because of its proximity to the knickpoint. Cross section (h) is also suspiciously high. Cross section (h) is located just upstream of the secondary scour hole, and the $1/7^{th}$ power law may not be valid at this cross section because of the presence of the secondary scour hole. The remaining cross sections are more consistent, and the average discharge is *0.387 m^3/s* with a standard deviation of 0.045 m^3/s.

Table 5.4: Summary of Discharge Calculations and Cross Section Geometry: March 21, 2012 LPIV Data

Cross Section	Distance Upstream of Knickpoint (m)	Flow Area (m^2)	Discharge (m^3/s)
a	0.15	-	-
b	0.75	0.413	0.448
c	1.45	0.472	0.332
d	2.25	0.578	0.412
e	2.95	0.505	0.401
f	3.75	0.485	0.336
g	4.45	0.613	0.396
h	6.45	0.871	0.539

Table 5.5 shows the results from the discharge calculations carried out using the LPIV data collected at the study site on September 25, 2012. On this date the observed flow in Mud Creek was very low, due to the increased drought conditions in the Midwest during the previous months leading up to the data collection. In an attempt to avoid inconsistencies in the LPIV data, cross sections that would not be affected by the knickpoint or by the secondary scour hole were selected for analysis. The results from this calculation yielded more consistent results, particular in the approach reach to the knickpoint. Cross sections e and f yielded discharges that were slightly higher than in the other cross sections. This is believed to be because of limitations in the LPIV video taken at the site, and also due to the presence of the developing trench in the approach reach of the channel. The average discharge for this flow was determined to be *0.098 m^3/s*, with a standard deviation of 0.026 m^3/s. As expected the discharge in the stream was much lower than the previous two flows, because of the extreme drought conditions in the Midwest.

Table 5.5: Summary of Discharge Calculations and Cross Section Geometry: September 25, 2012 LPIV Data

Cross Section	Distance Upstream of Knickpoint (m)	Flow Area (m^2)	Discharge (m^3/s)
a	0.60	0.180	0.097
b	1.20	0.237	0.081
c	1.80	0.218	0.067
d	2.20	0.224	0.088
e	3.00	0.260	0.128
f	3.42	0.302	0.130

The three flows that were calculated represent a typical base flow, an increased base flow, and a low flow condition for Mud Creek. The discharges for the three flow events were 0.098, 0.306, and 0.387 m^3/s with corresponding stage elevation

measurements upstream of the concrete weir of 316.17, 316.21, and 316.26 meters. By plotting the stage vs. discharge for these three flow conditions a rating curve for the site was created (Figure 5.8). The flows in Mud Creek during each data collection period were relatively low, with very little variation. More data will need to be collected to create a more reliable rating curve for the site. It will be important in the future to gather LPIV data for a high flow event and possibly a large storm event. With the collection of these data, a more accurate hydrologic record of Mud Creek can be created.

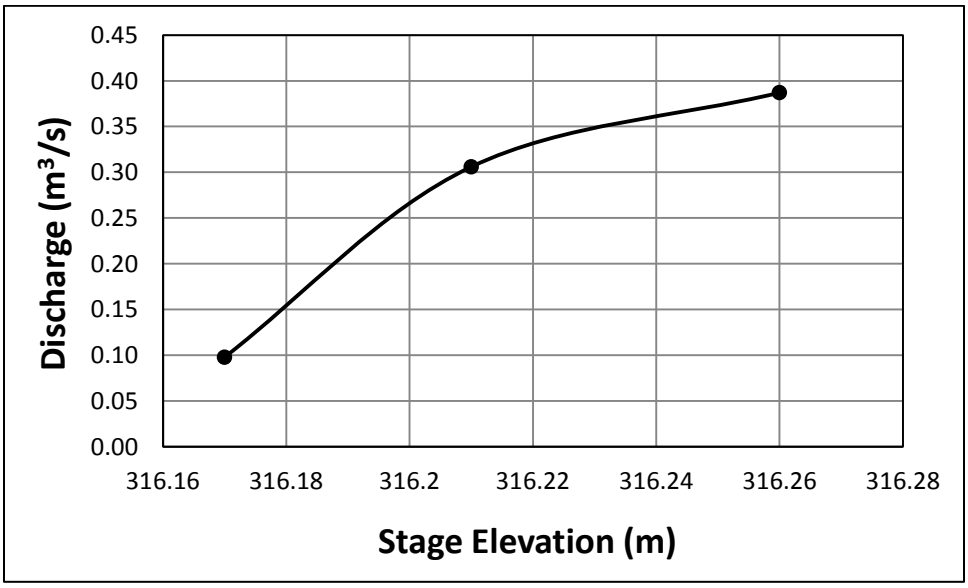

Figure 5.8: Rating curve of stage vs. discharge for the three calculated flows

5.6 Stage and Hydrologic Records

Over the course of the study period the precipitation records and the stage in Mud Creek were continually monitored. The daily precipitation amounts and cumulative rainfall for Mud Creek are presented in Figures C1 and C2, available in Appendix C. For 2011, 896 mm of rainfall was recorded; 2012 had 692 mm of rainfall; and 2013 has had 6.10 mm to date (24 days). Over the duration of the study period the study site has had 1595 mm of rainfall. Using the precipitation data, a runoff hydrograph for the Mud Creek

watershed was created. This hydrograph is presented in in Figure C3 located in Appendix C. This hydrograph indicates that this watershed is quite flashy in nature, meaning that with the onset of precipitation a sharp increase in flow occurs in the stream.

Figure C4 (Appendix C) shows the stage elevation in Mud Creek during the latter portion of the study period. There were 6 significant flow events in March, April, and May of 2012; and a prolonged period of low stage in Mud Creek during the summer of 2012. The corresponding stage readings ranged from 316.12 m to 317.20 m. The period of low stage coincides with the extreme drought conditions that were documented in the Midwest during 2012. 2012 saw 692 mm of rainfall, which is 154 mm less than the annual average. With the use of the stage information the discharge over the weir was calculated using equation 3.1. The results of the discharge calculations are presented in Figure C5, also located in Appendix C. The discharges in Mud Creek ranged from 0.1 m^3/s to 14.0 m^3/s, with the highest flows taking place in the late summer and early spring of 2012 and the lowest flows taking place in mid-summer and winter. These discharge calculations worked quite well for the low flows when compared to the discharges calculated using the LPIV results, however adjustments will need to be made for the higher flows, as the weir length (L in equation 3.1) changes with the onset of high flows. Again prolonged drought conditions greatly influenced the stage records, meaning that observation of the stage in the stream will need to be continued for an accurate hydrologic record of Mud Creek to be created.

Observing the recorded knickpoint front movement with the calculated flow as shown in Figure 5.9, the relationship between the migration of the knickpoint front and the discharge in the stream can be examined.

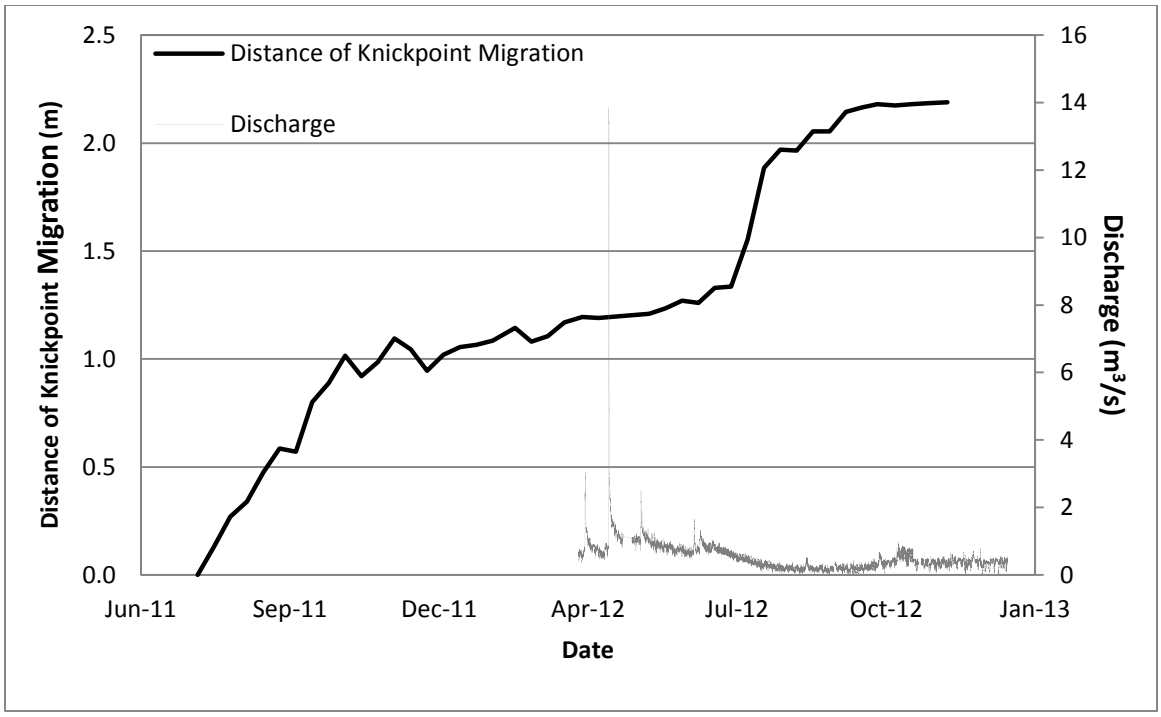

Figure 5.9: Distance of knickpoint migration compared with the calculated discharge in Mud Creek

As mentioned previously, there was an extended period of low flow in Mud Creek during the summer of 2012. During these low flow conditions the majority of the flow engulfed the aforementioned trench, causing the majority of the erosive stresses from the flow to act within the confines of the trench and on a small portion of the knickpoint face. These concentrated low flows certainly influence the migration behavior of the knickpoint. Evidence of this can be seen as an increase in front moment during the extended period of low flow experienced during the summer of 2012. It is only during high flow conditions that the flow is more evenly distributed across the entire channel, and though the magnitude of the shear stresses acting on the channel may be larger for these high flows, they occur for such a brief period of time that they do not appear to be strongly correlated to the headward progression of the knickpoint. In March, April, and

May of 2012 there were periods of increased flow events in Mud Creek, during which, the movement of the knickpoint front slowed significantly.

Chapter 6: **Conclusions**

6.1 Knickpoint Retreat

The results of the time lapse and survey analyses lend some insight into the mode of knickpoint migration. The mode of knickpoint migration changes with the change in season. Slowed headward retreat of the knickpoint front in the fall and winter months observed in this study may indicate that other forms of knickpoint erosion, not observed in the time-lapse photos, are taking place. It is also possible that the 2012 winter was too mild to provide a representative picture of knickpoint erosion. The 2013 winter will provide additional data for comparison with the previous year, but that will not be available for this thesis.

Over the study period, the study area was in a severe drought, and stream flow was much lower than usual. The hydrographical data provided by the bridge-mounted sensor at the site showed that there were 6 large storms or increased flow events during 2012 that had estimated flow rates ranging from 0.50 m^3/s to14.00 m^3/s. During the remainder of the year, the base flows were quite low, and ranged from 0.1 to 0.3 m^3/s. During the study time period, the knickpoint migrated 2.2 meters upstream, with the migration rate rising in the spring and summer and slowing in the fall and winter. The average migration rate observed for the 499 day study period was determined to be 0.0044 m/day. Though the migration rate varied from season to season, overall the rate of knickpoint migration was relatively steady over the study period with no large, punctuated knickpoint failures.

Overall, the migration of the Mud Creek knickpoint appears to be quite slow, when compared to other related studies. Daniels, (1960) observed a headward progressing knickpoint in Willow Creek, IA over a 5 year period. The Willow Creek knickpoint migrated upstream 2,819 meters over the course of the 5 year study period, which is much more than the Mud Creek knickpoint which migrated 2.2 meters upstream over the 2 year study period. Simon and Thomas (2002) and Simon et.al., (2002) also observed larger migration rates for a series of knickpoints that had developed along the Yalobushaa River in Mississippi. They observed migration rates ranging from 0.4 m/yr (0.001m/day) to 11 m/yr (0.030 m/day), whereas the Mud Creek knickpoint exhibited migration rates ranging from 0.0007 m/day to 0.01 m/day.

Though the Mud Creek knickpoint study observed what appears to be a slowed rate of knickpoint migration, all three studies observed periods of varied migration rates. The Willow Creek and Yalobussa River studies attributed the quick pulses of the knickpoint upstream to the onset of high flow events. In the case of the current Mud Creek study it appears as though the large flow events are not correlated to expedited movement of the knickpoint. As shown in Figure 5.9 (page 82), during the onset of high flow events there was very little headward progression of the knickpoint upstream. It was during the prolonged period of low flow that the larger migration rates were observed. This may be as a result of soil conditions in the area, as well as the dry weather patterns observed during the study period. However, the presence of the deeper narrower trench that has developed upstream of the Mud Creek knickpoint appears to be greatly affecting its migration behavior, by temporarily reducing headward migration at the knickpoint face,

but potentially leading to rapid changes in the location of the knickpoint face in the future.

6.2 Trench Development

Throughout most of the year, especially during dry periods, the channel flow was mostly confined to a trench that progressed upstream from the knickpoint face. Low flows persisted most of the time, and the bulk of the flow traveled through the trench, causing an uneven distribution of erosion on the bed and on the face of the knickpoint, consequently slowing its headward progression. It was only during larger flow events that the flow was more evenly distributed within the channel and over the knickpoint face. The result was that low flows had a significant impact on the morphology of this particular channel (see Figure 5.9). The impact was observed as the development of the trench between surveyed contour plots. The trench appeared to be the mechanism that was driving the migration of the knickpoint. Comparing the contour plots in Chapter 5 (page 69), it appears that most of the erosion took place within the narrower region of the channel and in the location where the trench crosses the knickpoint face. Thus, the knickpoint is slowly migrating upstream within the confines of the trench, a process that is slowly deepening, widening, and lengthening the trench, but it is altogether possible that development of the trench will cause a rapid, punctuated mass failure of the knickpoint face to occur. If this happens, the knickpoint will quickly erode upstream until it reaches a location where the bed material is more stable.

This migration process will continue until the grade stabilization structure (the concrete weir upstream of the knickpoint) is reached. When the study began at the site in early 2011, evidence of the trench-based migration behavior of the knickpoint was

present, though we did not realize it at the time. *Figure 6.1* shows evidence of a trench and large plunge pool that existed downstream of the present knickpoint location, and through which the knickpoint had passed previously. It appears as though the knickpoint remained stationary for a long period as the previous plunge pool and trench developed. Then, a rapid mass failure occurred, and the knickpoint quickly retreated upstream within the confines of the trench until it reached more stable bed material. Other than photos like the one given in Figure 6.1, evidence of the previous trench and plunge pool of the knickpoint are now gone because of mass wasting of the downstream channel banks. The continuing upstream migration of the knickpoint and other knickpoints like it has resulted in a channel that is very incised, leading to extensive mass wasting of the channel banks.

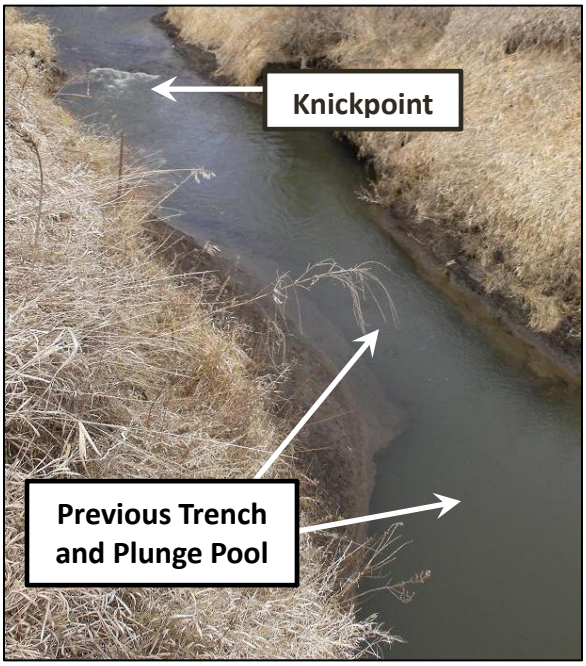

Figure 6.1: Image of knickpoint on March 18, 2011 with evidence of previous trench and plunge pool downstream of knickpoint.

Based on the current development of the secondary plunge pool and trench; we think that it is likely that when a mass failure of the knickpoint face occurs the knickpoint

will quickly retreat upstream until it reaches the secondary scour hole. At this point the trench based migration process may begin again.

6.3 Future Work

The purpose of any research project is to develop a deeper understanding of a particular topic, and to create a starting point for future projects to build upon. The Mud Creek knickpoint study focused on the collection of time lapse data, survey analysis, LPIV calculations, and discharge estimation. To push this research forward it is important to continue the current analysis techniques by continuing to collect time lapse images from the site, adding another detailed survey of the knickpoint and trench, recording more LPIV data, and estimating the discharge for high flow conditions. With the addition of more discharge measurements a more reliable rating curve for the Mud Creek study site can be created. In addition we can further develop the relationship between the discharge in the channel and the rate of knickpoint migration.

Expanding the time lapse analysis to include video collection is an appropriate first step in building on the work already presented in this thesis. Introducing an automated video capture system at the site will prove useful in collecting LPIV videos of the water surface for large flow events or capturing any punctuated movements of the knickpoint upstream while we are away from the site. The Moultrie Plotstalker time lapse camera that is currently being used for this study offers a setting that collects videos at specified time intervals. This will prove useful; however, it may be necessary to acquire a camera that can be remotely triggered by the user or triggered by increased stage in the stream. The current time lapse camera does not offer this type of setting, but it may be possible to modify it to do so.

The next step for this research is to begin an examination of the shear stresses acting on the streambed (both average and local). By developing a local shear stress profile along the streambed, a deeper understanding of the morphology in the stream and the migration behavior of the knickpoint can be achieved.

References

Admiraal, D., "Weir, Sluice Gate, and Culvert Literature Related to G304/G306 Control Structures: A Literature Review." Prepared for the Operations and Hydro Data Management Division of The South Florida Water Management District, September 2007.

Adrian, R.J., "Particle-Imaging Techniques for Experimental Fluid Mechanics." Annual Review of Fluid Mechanics, 23, 1991, pp. 261-304

Begin, Ze'ev B. Schumm, Stanley A. Meyer, David F. "Knickpoint Migration due to Baselevel Lowering." Journal of the Waterway Port and Ocean Division, Vol. 106, No. 3. August 1980, pp. 369-388.

Brush, Lucien M. Jr. Wolman, M Gordon. "Knickpoint Behavior in Non-Cohesive Material: A Laboratory Study." The Geological Society of America Bulletin, Vol. 71, No. 1, January 1960, pp. 59-74

Chen, A.H., Rus, D.L., Stanton, C.P. "Trends in Channel Gradation in Nebraska Streams, 1913-95" USGS, Water Resources Investigations Report 99-4103, 1999

Chow, Ven Te, Open Channel Hydraulics, McGraw-Hill, 1959

Daniels, R.B.. Entrenchment of the Willow Drainage Ditch, Harrison County, Iowa. *American Journal of Science*. 258:161-176, 1960

Daniels, R.B., and R.H. Jordan. Physiographic history and the soils, entrenched stream systems and gullies, Harrison County, Iowa. U.S. Department of Agriculture Technical Bulletin 1348, 1966

Frankel, Kurt L. Pazzaglia, Frank J. Vaughn, Jordan D. "Knickpoint evolution in a vertically bedded substrate, upstream-dipping terraces, and Atlantic slope bedrock channel." The Geological Society of America Bulletin, Vol. 119, No. 3-4, March/April 2007, pp. 476-486.

Fujita, I., Muste, M., and Kruger, A. "Large-scale particle image velocimetry for flow analysis in hydraulic engineering applications." Journal of Hydraulic Research, Vol 36, No. 3, 1998, pp. 397-414.

Gardner, Thomas W. "Experimental study of knickpoint and longitudinal profile evolution in cohesive, homogeneous material." The Geological Society of America Bulletin, Vol. 94, No 5, May 1983, pp. 664-672

Hanson, G. J. Robinson, K. M. Cook, K.R. " Headcut Migration Analysis of a Compacted Soil" Transactions of the ASAE, Vol. 40, No. 2, 1997, pp. 355-361.

Hanson, G.J. Robinson, K. M. Cook, K. R."Prediction of Headcut Migration using a Deterministic Approach." Transactions of the ASAE, Vol. 44, No. 3, May/June 2001, pp. 525-531.

Holland, W. N. Pickup, G. "Flume Study of Knickpoint Development in Stratified Sediment." The Geological Society of America Bulletin, Vol. 87, No. 1, January 1976, pp. 76-82.

Iowa Environmental Mesonet (2013) http://mesonet.agron.iastate.edu.

Meselhe, E.A., Bradley, A.A., Kruger, A., Muste, M.V.I., "Low Flow Measurement in Streams Using Video Imagery." Water Resources Research, Vol. 38, No. 12, 2002.

Muste, M., Fujita, I., Hauet, A. "Large-Scale Particle Image Velocimetry for Measurements in Riverine Enviroments." Water Resources Research, Vol. 44, No. 19, 2008.

Papanicolaou, T. "The Effects of Headcut and Knickpoint Propagation on Bridges in Iowa" TR-541 Iowa Department of Transportation, October 2008

Raffel, M. Willert, C. Kompenhans, J., Particle Image Velocimetry: A Practical Guide. Springer-Verlag Berlin Heidelberg, 1998.

Robinson, K. M. "Hydraulic Stresses on an Overfall Boundary." Transactions of the ASAE, Vol. 32, No. 4, 1989, pp. 1269-1274.

Robinson, K. M. Hanson, G. J. "A deterministic headcut advance model." Transactions of the ASAE, Vol. 37, No. 5, 1994, pp. 1437-1443.

Robinson, K.M. Cook, K. R. Hanson, G.J. "Velocity Field Measurements at an Overfall" Transactions of the ASAE, Vol. 43, No. 3, May/June 2000, pp. 665-670.

Rus, D.L. Dietsch, B.J. Simon, A. "Stream Adjustment and Channel Widening in Eastern Nebraska" USGS, Water Resources Investigations Report 03-4003, 2003

Simon, Andrew. Rinaldi, Massimo. "Channel instability in the loess area of the Midwestern United States." Journal of the American Water Resources Association, Vol. 36, No. 1, 2000. pp. 133-150.

Simon, A. and R.E. Thomas, Processes and forms of an unstable alluvial system with resistant, cohesive streambeds. *Earth Surface Processes and Landforms*. 27:699-718, 2002.

Simon, A., R.E. Thomas, A.J.C. Collison, and W. Dickerson, Erodibility of cohesive streambeds in the Yalobusha River system. Research Report No. 26. USDA-ARS National Sedimentation Laboratory: Oxford, MS, 2002.

Stein, O. R. Julien, P. Y. "Criterion delineating the mode of headcut migration." ASCE Journal of Hydraulic Engineering, Vol. 119, No. 37, 1993, pp. 37-50.

Stein, Otto R. LaTray, Bean A. "Experiments and modeling of headcut migration in stratified soils." Water Resources Research, Vol. 38, No. 12, 11 December 2002.

Appendices

Appendix A: Oblique Correction Information

Time Lapse Surveys:

September 27, 2011 Survey:

Table A1: Time Lapse Calibration Points September 27, 2011 Survey

	Object Coordinates		Image Coordinates	
Number	**X(m)**	**Y(m)**	**x(px)**	**y(px)**
1	31.83	-61.79	2725	1496
2	32.16	-60.21	2515	1321
3	31.99	-58.93	2287	1228
4	32.25	-57.04	1904	988
5	32.46	-55.34	1768	904
6	32.70	-53.47	1607	819
7	34.07	-51.60	1712	673
8	33.80	-48.63	1373	573
9	29.48	-52.44	743	921
10	29.26	-59.05	1429	1335
11	29.61	-61.16	1810	1620
12	29.80	-62.21	2055	1755

Table A2: Time Lapse Oblique Correction Coefficients: September 27, 2011

Oblique Correction Coefficients	
b1	2.14E-04
b2	1.11E-02
b3	3.27E+01
b4	-1.13E-04
b5	5.80E-04
b6	3.52E-03
b7	-4.71E-02
b8	-3.61E+01

LPIV Surveys:

September 27, 2011 Survey:

Table A3: LPIV Calibration Points September 27, 2011 Survey

	Object Coordinates		Image Coordinates	
Number	**X(m)**	**Y(m)**	**x(px)**	**y(px)**
1	31.83	-61.79	1310	716
2	32.16	-60.21	1219	597
3	31.99	-58.93	1100	534
4	32.25	-57.04	1017	443
5	32.46	-55.34	959	383
6	32.70	-53.47	892	315
7	34.07	-51.60	964	247
8	33.80	-48.63	824	177
9	29.48	-52.44	464	348
10	29.26	-59.05	683	616
11	29.61	-61.16	868	744
12	29.80	-62.21	979	823

Table A4: LPIV Oblique Correction Coefficients**:** September 27, 2011

Oblique Correction Coefficients	
b1	1.74E-02
b2	5.52E-02
b3	2.75E+01
b4	1.44E-04
b5	2.28E-03
b6	-1.55E-02
b7	-1.73E-01
b8	-3.04E+01

March 21, 2012 Survey:

Table A5: LPIV Calibration Points March 21, 2012 Survey

	Object Coordinates		Image Coordinates	
Number	**X (m)**	**Y (m)**	**x (px)**	**y (px)**
1	32.75	-61.99	1753	711
2	32.62	-59.99	1409	549
3	32.68	-58.60	1233	438
4	32.90	-56.93	1098	332
5	32.67	-54.97	859	243
6	32.86	-54.15	824	189
7	33.85	-52.51	873	82
8	28.80	-62.43	712	1047
9	28.62	-55.74	49	465
10	29.64	-52.57	85	261

*Note, that calibration point 8 is located at the knickpoint on the right descending bank.

Table A6: LPIV Oblique Correction Coefficients: March 21, 2012

Oblique Corrections Coefficients	
b1	8.88E-03
b2	1.99E-02
b3	3.07E+01
b4	1.28E-04
b5	8.77E-04
b6	-1.13E-02
b7	-6.76E-02
b8	-4.67E+01

September 25, 2012 Survey:

Table A7: LPIV Calibration Points September 25, 2012 Survey

	Surveyed Position		Pixel Location	
Number	X (m)	Y (m)	x (px)	y (px)
1	29.811	-58.363	153	663
2	29.920	-59.877	566	794
3	29.971	-61.551	1067	985
4	31.932	-57.409	692	211
5	31.424	-59.225	965	440
6	31.608	-60.626	1412	499
7	31.610	-61.780	1797	631

*Note, that calibration point 1-4 are located on the right descending bank upstream to downstream and calibration points 5-7 are located on the left descending bank upstream to downstream

Table A8: LPIV Oblique Correction Coefficients: September 25, 2012

Oblique Corrections Coefficients	
b1	4.82E-03
b2	9.78E-03
b3	3.20E+01
b4	1.10E-04
b5	4.50E-04
b6	-9.67E-03
b7	-3.26E-02
b8	-5.37E+01

Appendix B: Discharge Calculation Tables

Table B1: Cross Section (b) September 27, 2011 LPIV Discharge Calculation

X (m)	ELV (m)	Depth (m)	Area (m^2)	Effective Area (m^2)	[1]Vel. (m/s)	[2]Avg V (m/s)	Discharge (m^3/s)
29.10	145.09	0.00	0.000	0.000	0.00	0.00	0.000
29.13	144.99	0.10	0.003	0.006	0.00	0.00	0.000
29.22	144.99	0.10	0.009	0.010	0.00	0.00	0.000
29.31	144.98	0.11	0.010	0.010	0.14	0.12	0.001
29.40	144.98	0.11	0.010	0.011	0.05	0.04	0.000
29.49	144.97	0.12	0.011	0.011	0.02	0.02	0.000
29.58	144.96	0.13	0.011	0.011	0.02	0.02	0.000
29.67	144.96	0.13	0.012	0.012	0.03	0.03	0.000
29.76	144.95	0.14	0.011	0.012	0.06	0.06	0.001
29.85	144.95	0.14	0.013	0.013	0.15	0.13	0.002
29.94	144.93	0.15	0.014	0.018	0.15	0.14	0.002
30.03	144.85	0.24	0.022	0.026	0.46	0.40	0.010
30.12	144.76	0.33	0.030	0.034	0.77	0.68	0.023
30.21	144.67	0.42	0.038	0.040	0.43	0.38	0.015
30.30	144.62	0.47	0.042	0.043	0.63	0.55	0.024
30.39	144.61	0.48	0.043	0.043	0.67	0.58	0.025
30.48	144.60	0.49	0.044	0.044	0.70	0.61	0.027
30.57	144.60	0.49	0.044	0.045	0.78	0.68	0.030
30.66	144.59	0.50	0.045	0.043	0.85	0.74	0.032
30.75	144.64	0.45	0.041	0.038	0.89	0.78	0.030
30.84	144.69	0.40	0.036	0.034	0.85	0.75	0.025
30.93	144.74	0.35	0.032	0.029	0.88	0.77	0.022
31.02	144.79	0.30	0.027	0.025	0.85	0.74	0.019
31.11	144.83	0.26	0.024	0.022	0.87	0.77	0.017
31.20	144.87	0.22	0.020	0.018	0.74	0.65	0.012
31.29	144.90	0.19	0.017	0.015	0.71	0.62	0.009
31.38	144.94	0.15	0.014	0.013	0.52	0.45	0.006
31.47	144.95	0.14	0.013	0.013	0.37	0.32	0.004
31.56	144.95	0.14	0.012	0.012	0.42	0.37	0.004
31.65	144.96	0.13	0.011	0.011	0.14	0.12	0.001
31.74	144.97	0.12	0.011	0.010	0.11	0.09	0.001
31.83	144.98	0.11	0.010	0.009	0.17	0.15	0.001
31.91	144.99	0.10	0.009	0.009	0.24	0.21	0.002
32.00	145.00	0.09	0.009	0.008	0.30	0.26	0.002
32.09	145.00	0.09	0.008	0.004	0.22	0.20	0.001
32.11	145.09	0.00	0.000	0.000	0.00	0.00	0.000
Cross Section Area (m^2) =			0.705	**Cross Sectional Discharge (m^3/s) =**			0.351

Table B2: Cross Section (c) September 27, 2011 LPIV Discharge Calculation

X (m)	ELV (m)	Depth (m)	Area (m^2)	Effective Area (m^2)	[1]Vel. (m/s)	[2]Avg V (m/s)	Discharge (m^3/s)
29.58	145.09	0.00	0.000	0.000	0.00	0.00	0.000
29.67	145.07	0.02	0.002	0.005	0.08	0.07	0.000
29.76	144.99	0.10	0.009	0.013	0.11	0.10	0.001
29.85	144.91	0.18	0.016	0.019	0.28	0.25	0.005
29.94	144.86	0.23	0.021	0.023	0.33	0.29	0.007
30.03	144.82	0.27	0.024	0.026	0.35	0.31	0.008
30.12	144.78	0.31	0.028	0.029	0.31	0.27	0.008
30.21	144.74	0.35	0.031	0.034	0.21	0.19	0.006
30.30	144.69	0.40	0.036	0.039	0.31	0.27	0.011
30.39	144.63	0.46	0.041	0.044	0.44	0.39	0.017
30.48	144.57	0.52	0.047	0.047	0.68	0.59	0.027
30.57	144.57	0.52	0.047	0.047	0.91	0.80	0.037
30.66	144.57	0.52	0.047	0.047	0.66	0.58	0.027
30.75	144.57	0.52	0.047	0.045	0.78	0.69	0.031
30.84	144.60	0.49	0.044	0.041	0.77	0.68	0.028
30.93	144.67	0.42	0.038	0.035	0.82	0.72	0.025
31.02	144.73	0.36	0.033	0.030	0.90	0.79	0.023
31.11	144.79	0.30	0.027	0.026	0.73	0.64	0.017
31.20	144.82	0.27	0.025	0.023	0.69	0.61	0.014
31.29	144.84	0.25	0.022	0.021	0.47	0.41	0.009
31.38	144.87	0.22	0.020	0.018	0.34	0.29	0.005
31.47	144.91	0.18	0.016	0.014	0.34	0.30	0.004
31.56	144.95	0.14	0.012	0.010	0.49	0.43	0.004
31.65	145.00	0.09	0.008	0.007	0.11	0.10	0.001
31.74	145.03	0.06	0.005	0.005	0.05	0.05	0.000
31.83	145.04	0.05	0.004	0.004	0.16	0.14	0.001
31.91	145.05	0.04	0.003	0.003	0.00	0.00	0.000
32.00	145.06	0.03	0.003	0.002	0.01	0.00	0.000
32.09	145.07	0.02	0.002	0.001	-0.10	-0.09	0.000
32.10	145.09	0.00	0.000	0.000	0.00	0.00	0.000
Cross Section Area (m^2) =			0.657	**Cross Sectional Discharge (m^3/s) =**			0.316

Table B3: Cross Section (d) September 27, 2011 LPIV Discharge Calculation

X (m)	ELV (m)	Depth (m)	Area (m^2)	Effective Area (m^2)	[1]Vel. (m/s)	[2]Avg V (m/s)	Discharge (m^3/s)
29.47	145.09	0.00	0.000	0.000	0.00	0.00	0.000
29.49	144.97	0.12	0.002	0.008	0.09	0.08	0.001
29.58	144.95	0.14	0.013	0.013	0.00	0.00	0.000
29.67	144.94	0.15	0.014	0.014	0.00	0.00	0.000
29.76	144.92	0.17	0.014	0.015	0.07	0.07	0.001
29.85	144.91	0.18	0.017	0.018	0.15	0.13	0.002
29.94	144.87	0.22	0.020	0.022	0.05	0.04	0.001
30.03	144.82	0.27	0.024	0.026	0.05	0.05	0.001
30.12	144.78	0.31	0.028	0.030	0.11	0.10	0.003
30.21	144.73	0.36	0.032	0.033	0.84	0.73	0.024
30.30	144.72	0.37	0.034	0.034	0.97	0.85	0.029
30.39	144.71	0.38	0.035	0.035	0.91	0.79	0.028
30.48	144.70	0.39	0.035	0.036	1.03	0.90	0.032
30.57	144.69	0.40	0.036	0.036	1.03	0.90	0.032
30.66	144.70	0.39	0.035	0.033	0.98	0.85	0.028
30.75	144.74	0.35	0.031	0.030	0.53	0.46	0.014
30.84	144.77	0.32	0.029	0.028	0.35	0.31	0.009
30.93	144.79	0.30	0.027	0.027	0.41	0.36	0.009
31.02	144.81	0.28	0.026	0.025	0.29	0.25	0.006
31.11	144.83	0.26	0.024	0.022	0.16	0.14	0.003
31.20	144.87	0.23	0.020	0.019	0.19	0.16	0.003
31.29	144.90	0.19	0.017	0.015	0.40	0.35	0.005
31.38	144.94	0.15	0.014	0.013	0.63	0.55	0.007
31.47	144.96	0.13	0.012	0.011	0.30	0.26	0.003
31.56	144.97	0.12	0.011	0.010	0.05	0.05	0.000
31.65	144.98	0.11	0.010	0.009	0.04	0.03	0.000
31.74	145.00	0.10	0.009	0.008	0.04	0.04	0.000
31.83	145.01	0.08	0.008	0.007	0.04	0.03	0.000
31.91	145.02	0.07	0.006	0.003	0.01	0.01	0.000
31.99	145.09	0.00	0.000	0.000	0.00	0.00	0.000
Cross Section Area (m^2) =			0.582	**Cross Sectional Discharge (m^3/s) =**			0.244

Table B4: Cross Section (e) September 27, 2011 LPIV Discharge Calculation

X (m)	ELV (m)	Depth (m)	Area (m^2)	Effective Area (m^2)	[1]Vel. (m/s)	[2]Avg V (m/s)	Discharge (m^3/s)
29.10	145.10	0.00	0.000	0.000	0.00	0.00	0.000
29.40	144.99	0.11	0.033	0.022	0.05	0.05	0.001
29.49	144.97	0.13	0.012	0.013	0.09	0.08	0.001
29.58	144.95	0.15	0.013	0.015	0.24	0.21	0.003
29.67	144.92	0.18	0.016	0.017	0.21	0.19	0.003
29.76	144.89	0.21	0.018	0.020	0.27	0.23	0.005
29.85	144.86	0.24	0.022	0.023	0.34	0.30	0.007
29.94	144.83	0.28	0.025	0.026	0.65	0.57	0.015
30.03	144.79	0.31	0.028	0.029	0.79	0.69	0.020
30.12	144.76	0.34	0.031	0.032	0.86	0.76	0.024
30.21	144.74	0.36	0.033	0.032	0.89	0.78	0.025
30.30	144.76	0.34	0.030	0.029	0.88	0.77	0.022
30.39	144.79	0.31	0.028	0.027	1.01	0.88	0.024
30.48	144.82	0.29	0.026	0.025	1.05	0.91	0.023
30.57	144.83	0.27	0.025	0.024	1.00	0.88	0.021
30.66	144.84	0.26	0.023	0.023	0.89	0.78	0.018
30.75	144.86	0.25	0.022	0.021	1.07	0.94	0.020
30.84	144.88	0.22	0.020	0.019	0.99	0.86	0.016
30.93	144.91	0.19	0.017	0.016	1.05	0.92	0.015
31.02	144.94	0.16	0.014	0.013	1.08	0.95	0.012
31.11	144.97	0.13	0.012	0.011	1.10	0.96	0.010
31.20	144.99	0.11	0.010	0.009	1.19	1.04	0.010
31.29	145.01	0.09	0.008	0.008	1.17	1.02	0.008
31.38	145.03	0.08	0.007	0.006	1.00	0.87	0.005
31.47	145.05	0.05	0.005	0.004	0.68	0.59	0.002
31.56	145.07	0.03	0.003	0.001	0.47	0.41	0.001
31.65	145.10	0.00	0.000	0.000	0.38	0.34	0.000
31.40	145.10	0.00	0.000	0.000	0.00	0.00	0.000
Cross Section Area (m^2) =			0.481	**Cross Sectional Discharge (m^3/s) =**			0.310

Table B5: Cross Section (f) September 27, 2011 LPIV Discharge Calculation

X (m)	ELV (m)	Depth (m)	Area (m^2)	Effective Area (m^2)	[1]Vel. (m/s)	[2]Avg V (m/s)	Discharge (m^3/s)
28.99	145.11	0.00	0.000	0.000	0.00	0.00	0.000
29.13	144.92	0.19	0.027	0.022	0.39	0.34	0.008
29.22	144.92	0.19	0.017	0.017	0.05	0.05	0.001
29.31	144.92	0.20	0.018	0.018	-0.12	-0.11	-0.002
29.40	144.91	0.20	0.018	0.018	0.06	0.05	0.001
29.49	144.91	0.20	0.018	0.018	0.07	0.06	0.001
29.58	144.91	0.20	0.018	0.020	0.08	0.07	0.001
29.67	144.87	0.24	0.022	0.023	0.11	0.10	0.002
29.76	144.83	0.28	0.024	0.027	0.20	0.17	0.005
29.85	144.79	0.33	0.029	0.030	0.30	0.26	0.008
29.94	144.77	0.34	0.031	0.032	0.47	0.41	0.013
30.03	144.75	0.36	0.033	0.033	0.45	0.40	0.013
30.12	144.74	0.37	0.034	0.033	0.38	0.33	0.011
30.21	144.76	0.35	0.032	0.031	0.46	0.41	0.012
30.30	144.78	0.33	0.030	0.029	0.61	0.53	0.015
30.39	144.81	0.31	0.027	0.026	0.76	0.67	0.018
30.48	144.83	0.28	0.025	0.025	0.83	0.72	0.018
30.57	144.84	0.27	0.025	0.024	1.04	0.91	0.022
30.66	144.85	0.26	0.024	0.023	0.94	0.82	0.019
30.75	144.86	0.25	0.023	0.022	0.99	0.86	0.019
30.84	144.87	0.24	0.022	0.022	0.93	0.81	0.018
30.93	144.86	0.25	0.022	0.022	0.90	0.78	0.018
31.02	144.86	0.25	0.023	0.023	0.89	0.78	0.018
31.11	144.85	0.26	0.023	0.023	0.87	0.76	0.018
31.20	144.85	0.26	0.024	0.024	0.93	0.82	0.019
31.29	144.84	0.27	0.024	0.024	0.95	0.83	0.020
31.38	144.85	0.26	0.024	0.023	0.85	0.75	0.017
31.47	144.87	0.24	0.022	0.021	0.50	0.44	0.009
31.56	144.89	0.23	0.020	0.020	0.42	0.37	0.007
31.65	144.90	0.21	0.019	0.018	0.22	0.19	0.003
31.74	144.92	0.19	0.017	0.016	0.19	0.16	0.003
31.83	144.94	0.17	0.016	0.015	0.22	0.19	0.003
31.91	144.95	0.16	0.013	0.013	0.13	0.11	0.001
32.00	144.97	0.14	0.013	0.012	0.26	0.23	0.003
32.09	144.99	0.12	0.011	0.010	-0.04	-0.04	0.000
32.18	145.01	0.10	0.009	0.005	-0.17	-0.15	-0.001
32.21	145.11	0.00	0.000	0.000	0.00	0.00	0.000
Cross Section Area (m^2) =			0.776	**Cross Sectional Discharge (m^3/s) =**			0.342

Table B6: Cross Section (g) September 27, 2011 LPIV Discharge Calculation

X (m)	ELV (m)	Depth (m)	Area (m^2)	Effective Area (m^2)	[1]Vel. (m/s)	[2]Avg V (m/s)	Discharge (m^3/s)
28.97	145.12	0.00	0.000	0.000	0.00	0.00	0.000
29.04	144.94	0.18	0.012	0.015	0.03	0.03	0.000
29.13	144.93	0.19	0.017	0.018	0.06	0.05	0.001
29.22	144.92	0.20	0.018	0.019	0.05	0.05	0.001
29.31	144.90	0.22	0.020	0.020	0.06	0.05	0.001
29.40	144.88	0.24	0.021	0.022	0.02	0.01	0.000
29.49	144.86	0.25	0.023	0.024	0.05	0.04	0.001
29.58	144.85	0.27	0.025	0.026	0.09	0.08	0.002
29.67	144.81	0.30	0.027	0.028	0.13	0.11	0.003
29.76	144.78	0.33	0.028	0.031	0.05	0.04	0.001
29.85	144.75	0.37	0.033	0.034	-0.01	-0.01	0.000
29.94	144.74	0.38	0.034	0.034	-0.05	-0.05	-0.002
30.03	144.73	0.38	0.035	0.035	-0.13	-0.11	-0.004
30.12	144.73	0.39	0.035	0.035	-0.06	-0.06	-0.002
30.21	144.73	0.39	0.035	0.035	0.00	0.00	0.000
30.30	144.73	0.39	0.035	0.035	0.09	0.08	0.003
30.39	144.73	0.39	0.035	0.035	0.13	0.11	0.004
30.48	144.73	0.39	0.035	0.035	0.33	0.29	0.010
30.57	144.73	0.39	0.035	0.035	0.42	0.37	0.013
30.66	144.73	0.39	0.035	0.035	0.54	0.47	0.017
30.75	144.73	0.39	0.035	0.035	0.67	0.58	0.021
30.84	144.73	0.39	0.035	0.035	0.51	0.45	0.016
30.93	144.73	0.39	0.035	0.035	1.12	0.98	0.034
31.02	144.74	0.38	0.034	0.034	1.26	1.11	0.038
31.11	144.74	0.38	0.034	0.033	1.24	1.09	0.036
31.20	144.76	0.36	0.033	0.032	1.29	1.12	0.036
31.29	144.77	0.35	0.031	0.031	0.81	0.70	0.022
31.38	144.78	0.34	0.030	0.029	0.55	0.48	0.014
31.47	144.81	0.31	0.028	0.027	0.55	0.48	0.013
31.56	144.83	0.29	0.026	0.024	0.32	0.28	0.007
31.65	144.86	0.26	0.023	0.022	0.07	0.06	0.001
31.74	144.89	0.23	0.021	0.020	-0.07	-0.06	-0.001
31.83	144.91	0.20	0.018	0.017	0.08	0.07	0.001
31.91	144.94	0.18	0.015	0.014	0.12	0.11	0.002
32.00	144.97	0.15	0.014	0.012	0.12	0.10	0.001
32.09	145.00	0.12	0.011	0.009	0.05	0.04	0.000
32.18	145.03	0.09	0.008	0.007	-0.01	-0.01	0.000
32.27	145.06	0.06	0.005	0.003	-0.03	-0.03	0.000
32.33	145.12	0.00	0.000	0.000	0.00	0.00	0.000
Cross Section Area (m^2) =			0.977	**Cross Sectional Discharge (m^3/s) =**			0.290

Table B7: Cross Section (h) September 27, 2011 LPIV Discharge Calculation

X (m)	ELV (m)	Depth (m)	Area (m^2)	Effective Area (m^2)	[1]Vel. (m/s)	[2]Avg V (m/s)	Discharge (m^3/s)
29.37	145.12	0.00	0.000	0.000	0.00	0.00	0.000
29.40	145.03	0.09	0.003	0.006	-0.02	-0.01	0.000
29.49	145.03	0.09	0.008	0.009	0.01	0.01	0.000
29.58	145.02	0.10	0.009	0.010	-0.08	-0.07	-0.001
29.67	145.01	0.11	0.010	0.010	0.13	0.11	0.001
29.76	145.00	0.12	0.010	0.011	0.18	0.16	0.002
29.85	144.99	0.13	0.012	0.012	-0.09	-0.07	-0.001
29.94	144.98	0.14	0.013	0.013	0.04	0.04	0.001
30.03	144.97	0.15	0.013	0.014	0.22	0.20	0.003
30.12	144.96	0.16	0.014	0.015	0.04	0.04	0.001
30.21	144.95	0.17	0.015	0.015	0.13	0.11	0.002
30.30	144.94	0.18	0.016	0.016	0.32	0.28	0.005
30.39	144.94	0.18	0.017	0.017	0.28	0.25	0.004
30.48	144.93	0.19	0.017	0.020	0.33	0.29	0.006
30.57	144.86	0.26	0.023	0.027	0.47	0.41	0.011
30.66	144.79	0.33	0.030	0.026	1.16	1.02	0.027
30.75	144.86	0.26	0.023	0.021	1.83	1.60	0.034
30.84	144.91	0.21	0.019	0.022	1.65	1.45	0.032
30.93	144.85	0.27	0.024	0.026	0.65	0.57	0.015
31.02	144.80	0.32	0.028	0.028	0.20	0.17	0.005
31.11	144.80	0.32	0.028	0.028	0.61	0.53	0.015
31.20	144.80	0.32	0.029	0.029	0.83	0.73	0.021
31.29	144.80	0.32	0.029	0.029	1.75	1.53	0.044
31.38	144.80	0.32	0.029	0.029	1.53	1.34	0.038
31.47	144.80	0.32	0.029	0.029	0.52	0.46	0.013
31.56	144.80	0.32	0.029	0.029	0.13	0.11	0.003
31.65	144.80	0.32	0.029	0.028	0.43	0.38	0.011
31.74	144.83	0.29	0.026	0.025	0.28	0.24	0.006
31.83	144.86	0.26	0.024	0.022	0.03	0.03	0.001
31.91	144.88	0.24	0.020	0.019	0.06	0.05	0.001
32.00	144.91	0.21	0.018	0.017	-0.01	0.00	0.000
32.09	144.94	0.18	0.016	0.014	-0.19	-0.16	-0.002
32.18	144.97	0.15	0.013	0.012	-0.07	-0.06	-0.001
32.27	145.00	0.12	0.010	0.009	0.03	0.03	0.000
32.36	145.03	0.09	0.008	0.008	-0.06	-0.05	0.000
32.45	145.03	0.09	0.008	0.009	-0.05	-0.04	0.000
32.54	145.02	0.10	0.009	0.009	0.03	0.03	0.000
32.63	145.02	0.10	0.009	0.010	-0.06	-0.05	-0.001
32.72	145.01	0.11	0.010	0.005	-0.23	-0.20	-0.001
32.78	145.12	0.00	0.000	0.000	0.00	0.00	0.000
Cross Section Area (m^2) =			0.679	**Cross Sectional Discharge (m^3/s) =**			0.293

Table B8: Cross Section (b) March 21, 2012 LPIV Discharge Calculation

X (m)	ELV (m)	Depth (m)	Area (m^2)	Effective Area (m^2)	[1]Vel. (m/s)	[2]Avg V (m/s)	Discharge (m^3/s)
28.50	144.93	0.00	0.000	0.000	0.00	0.00	0.000
28.89	144.91	0.02	0.007	0.004	0.01	0.01	0.000
28.98	144.91	0.02	0.002	0.002	0.18	0.16	0.000
29.08	144.91	0.02	0.002	0.002	0.51	0.45	0.001
29.17	144.91	0.02	0.002	0.003	0.69	0.60	0.002
29.27	144.90	0.03	0.003	0.003	0.49	0.43	0.001
29.37	144.89	0.04	0.004	0.004	0.30	0.26	0.001
29.46	144.88	0.05	0.004	0.005	0.23	0.20	0.001
29.56	144.88	0.05	0.005	0.006	0.38	0.34	0.002
29.66	144.87	0.06	0.006	0.006	0.97	0.84	0.005
29.75	144.86	0.07	0.007	0.007	0.48	0.42	0.003
29.85	144.85	0.08	0.007	0.008	0.95	0.83	0.007
29.95	144.84	0.09	0.009	0.010	1.22	1.07	0.011
30.04	144.81	0.12	0.012	0.012	0.75	0.66	0.008
30.14	144.80	0.13	0.013	0.015	0.46	0.40	0.006
30.23	144.74	0.19	0.018	0.025	0.94	0.82	0.021
30.33	144.61	0.32	0.032	0.033	2.01	1.76	0.059
30.43	144.56	0.37	0.035	0.035	1.97	1.73	0.061
30.52	144.56	0.37	0.035	0.035	2.09	1.82	0.064
30.62	144.56	0.37	0.035	0.031	1.83	1.60	0.050
30.72	144.66	0.27	0.027	0.022	1.73	1.51	0.034
30.81	144.75	0.18	0.017	0.014	1.68	1.47	0.021
30.91	144.81	0.12	0.011	0.011	1.62	1.42	0.016
31.00	144.82	0.11	0.011	0.011	1.45	1.27	0.013
31.10	144.83	0.10	0.010	0.010	1.21	1.06	0.010
31.20	144.83	0.10	0.009	0.009	1.23	1.07	0.010
31.29	144.84	0.09	0.009	0.008	0.89	0.78	0.006
31.39	144.85	0.08	0.008	0.008	0.96	0.84	0.006
31.49	144.85	0.08	0.008	0.007	0.74	0.65	0.005
31.58	144.86	0.07	0.007	0.007	0.17	0.15	0.001
31.68	144.86	0.07	0.007	0.007	0.11	0.09	0.001
31.78	144.86	0.07	0.007	0.006	1.12	0.98	0.006
31.87	144.86	0.07	0.006	0.006	0.47	0.41	0.003
31.97	144.87	0.06	0.006	0.006	0.28	0.25	0.001
32.06	144.87	0.06	0.006	0.006	0.18	0.15	0.001
32.16	144.87	0.06	0.006	0.006	0.10	0.09	0.001
32.26	144.87	0.06	0.006	0.006	0.77	0.67	0.004
32.35	144.87	0.06	0.006	0.005	0.58	0.50	0.003
32.45	144.87	0.06	0.005	0.005	0.71	0.62	0.003
32.55	144.88	0.05	0.005	0.002	0.44	0.38	0.001
32.60	144.93	0.00	0.000	0.000	0.00	0.00	0.000
Cross Section Area (m^2) =			0.413	**Cross Sectional Discharge (m^3/s) =**			0.448

Table B9: Cross Section (c) March 21, 2012 LPIV Discharge Calculation

X (m)	ELV (m)	Depth (m)	Area (m^2)	Effective Area (m^2)	[1]Vel. (m/s)	[2]Avg V (m/s)	Discharge (m^3/s)
28.31	144.95	0.00	0.000	0.000	0.00	0.00	0.000
28.89	144.91	0.04	0.023	0.014	0.05	0.05	0.001
28.98	144.91	0.04	0.004	0.004	0.11	0.10	0.000
29.08	144.90	0.05	0.004	0.004	0.18	0.15	0.001
29.17	144.90	0.05	0.004	0.005	0.16	0.14	0.001
29.27	144.90	0.05	0.005	0.005	0.08	0.07	0.000
29.37	144.90	0.05	0.005	0.005	0.47	0.41	0.002
29.46	144.90	0.05	0.005	0.005	0.40	0.35	0.002
29.56	144.89	0.06	0.005	0.006	0.45	0.39	0.002
29.66	144.89	0.06	0.006	0.006	0.47	0.41	0.002
29.75	144.89	0.06	0.006	0.007	0.68	0.59	0.004
29.85	144.86	0.09	0.008	0.010	0.83	0.73	0.007
29.95	144.83	0.12	0.012	0.013	0.89	0.78	0.010
30.04	144.80	0.15	0.015	0.017	1.02	0.89	0.015
30.14	144.74	0.21	0.020	0.023	0.81	0.71	0.016
30.23	144.68	0.27	0.026	0.028	1.13	0.99	0.028
30.33	144.65	0.30	0.030	0.029	0.56	0.49	0.014
30.43	144.65	0.30	0.029	0.029	1.54	1.34	0.038
30.52	144.65	0.30	0.029	0.028	1.66	1.45	0.041
30.62	144.65	0.30	0.028	0.028	1.40	1.23	0.034
30.72	144.68	0.27	0.027	0.024	0.90	0.79	0.019
30.81	144.72	0.23	0.022	0.020	0.80	0.70	0.014
30.91	144.75	0.20	0.019	0.019	0.79	0.69	0.013
31.00	144.76	0.19	0.018	0.019	0.77	0.68	0.013
31.10	144.76	0.19	0.019	0.018	1.01	0.88	0.016
31.20	144.77	0.18	0.017	0.017	0.86	0.76	0.013
31.29	144.77	0.18	0.017	0.015	0.76	0.67	0.010
31.39	144.82	0.13	0.013	0.009	0.49	0.43	0.004
31.49	144.90	0.05	0.005	0.005	0.22	0.20	0.001
31.58	144.89	0.06	0.005	0.005	0.24	0.21	0.001
31.68	144.90	0.05	0.005	0.005	0.38	0.34	0.002
31.78	144.90	0.05	0.005	0.005	0.33	0.29	0.001
31.87	144.90	0.05	0.005	0.005	0.14	0.13	0.001
31.97	144.90	0.05	0.005	0.005	0.16	0.14	0.001
32.06	144.90	0.05	0.005	0.005	0.14	0.12	0.001
32.16	144.89	0.06	0.006	0.005	0.12	0.10	0.001
32.26	144.89	0.06	0.005	0.006	0.44	0.39	0.002
32.35	144.89	0.06	0.006	0.005	0.13	0.12	0.001
32.45	144.91	0.04	0.004	0.003	-0.06	-0.05	0.000
32.55	144.93	0.02	0.002	0.001	0.01	0.01	0.000
32.59	144.95	0.00	0.000	0.000	0.00	0.00	0.000
Cross Section Area (m^2) =			0.472	**Cross Sectional Discharge (m^3/s) =**			0.332

Table B10: Cross Section (d) March 21, 2012 LPIV Discharge Calculation

X (m)	ELV (m)	Depth (m)	Area (m^2)	Effective Area (m^2)	[1]Vel. (m/s)	[2]Avg V (m/s)	Discharge (m^3/s)
28.10	144.97	0.00	0.000	0.000	0.00	0.00	0.000
28.69	144.92	0.05	0.031	0.018	0.04	0.03	0.001
28.79	144.92	0.05	0.005	0.005	0.05	0.04	0.000
28.89	144.92	0.05	0.005	0.005	0.34	0.30	0.001
28.98	144.92	0.05	0.005	0.005	0.53	0.46	0.002
29.08	144.92	0.05	0.005	0.005	0.55	0.48	0.002
29.17	144.92	0.05	0.005	0.005	0.39	0.34	0.002
29.27	144.92	0.05	0.005	0.005	0.28	0.25	0.001
29.37	144.91	0.06	0.005	0.006	0.44	0.38	0.002
29.46	144.91	0.06	0.006	0.006	0.16	0.14	0.001
29.56	144.91	0.06	0.006	0.006	0.22	0.19	0.001
29.66	144.90	0.07	0.007	0.007	0.24	0.21	0.001
29.75	144.90	0.07	0.007	0.007	0.15	0.13	0.001
29.85	144.89	0.08	0.007	0.009	0.14	0.12	0.001
29.95	144.86	0.11	0.011	0.014	0.19	0.16	0.002
30.04	144.80	0.17	0.016	0.020	0.77	0.67	0.013
30.14	144.72	0.25	0.023	0.027	1.02	0.89	0.024
30.23	144.65	0.32	0.031	0.031	1.02	0.90	0.028
30.33	144.65	0.32	0.032	0.031	1.53	1.34	0.041
30.43	144.66	0.31	0.029	0.029	1.44	1.26	0.036
30.52	144.68	0.29	0.028	0.029	1.37	1.20	0.035
30.62	144.66	0.31	0.030	0.032	1.45	1.27	0.040
30.72	144.63	0.34	0.034	0.034	1.86	1.63	0.055
30.81	144.62	0.35	0.034	0.034	1.06	0.93	0.031
30.91	144.61	0.36	0.034	0.034	0.64	0.56	0.019
31.00	144.61	0.36	0.035	0.030	0.81	0.71	0.021
31.10	144.71	0.26	0.026	0.019	0.42	0.37	0.007
31.20	144.83	0.14	0.013	0.012	0.93	0.82	0.010
31.29	144.85	0.12	0.012	0.011	0.09	0.08	0.001
31.39	144.86	0.11	0.011	0.011	0.21	0.19	0.002
31.49	144.86	0.11	0.011	0.010	0.96	0.84	0.008
31.58	144.87	0.10	0.009	0.009	0.59	0.52	0.005
31.68	144.88	0.09	0.008	0.008	0.76	0.66	0.006
31.78	144.89	0.08	0.008	0.008	0.43	0.37	0.003
31.87	144.89	0.08	0.008	0.007	0.39	0.34	0.002
31.97	144.89	0.08	0.007	0.007	0.20	0.18	0.001
32.06	144.90	0.07	0.007	0.007	0.13	0.11	0.001
32.16	144.90	0.07	0.007	0.006	0.02	0.02	0.000
32.26	144.91	0.06	0.006	0.006	0.29	0.25	0.001
32.35	144.91	0.06	0.006	0.005	0.09	0.08	0.000
32.45	144.93	0.04	0.004	0.003	0.10	0.09	0.000
32.55	144.96	0.01	0.001	0.001	0.02	0.02	0.000
32.60	144.97	0.00	0.000	0.000	0.00	0.00	0.000
Cross Section Area (m^2) =			0.578	**Cross Sectional Discharge (m^3/s) =**			0.412

Table B11: Cross Section (e) March 21, 2012 LPIV Discharge Calculation

X (m)	ELV (m)	Depth (m)	Area (m^2)	Effective Area (m^2)	[1]Vel. (m/s)	[2]Avg V (m/s)	Discharge (m^3/s)
28.10	144.98	0.00	0.000	0.000	0.00	0.00	0.000
28.89	144.93	0.05	0.042	0.023	0.07	0.06	0.001
28.98	144.93	0.05	0.005	0.005	0.19	0.16	0.001
29.08	144.92	0.06	0.005	0.005	0.12	0.11	0.001
29.17	144.92	0.06	0.006	0.006	0.06	0.05	0.000
29.27	144.92	0.06	0.006	0.006	0.04	0.03	0.000
29.37	144.91	0.07	0.006	0.006	0.24	0.21	0.001
29.46	144.91	0.07	0.007	0.007	0.47	0.41	0.003
29.56	144.91	0.07	0.007	0.007	0.54	0.48	0.004
29.66	144.90	0.08	0.008	0.008	0.47	0.41	0.003
29.75	144.90	0.08	0.008	0.008	0.35	0.30	0.002
29.85	144.89	0.09	0.008	0.010	0.57	0.50	0.005
29.95	144.85	0.13	0.013	0.016	0.87	0.76	0.012
30.04	144.77	0.21	0.020	0.024	0.90	0.79	0.019
30.14	144.69	0.29	0.027	0.028	1.02	0.89	0.025
30.23	144.68	0.30	0.028	0.029	1.18	1.04	0.030
30.33	144.68	0.30	0.030	0.030	1.39	1.22	0.036
30.43	144.68	0.30	0.029	0.029	1.50	1.31	0.038
30.52	144.67	0.31	0.029	0.030	1.46	1.27	0.038
30.62	144.67	0.31	0.030	0.031	1.48	1.30	0.040
30.72	144.66	0.32	0.032	0.030	1.38	1.21	0.036
30.81	144.69	0.29	0.028	0.023	1.34	1.17	0.027
30.91	144.79	0.19	0.018	0.015	1.17	1.02	0.015
31.00	144.86	0.12	0.012	0.011	1.09	0.95	0.011
31.10	144.87	0.11	0.011	0.010	0.86	0.75	0.007
31.20	144.88	0.10	0.009	0.009	1.02	0.89	0.008
31.29	144.89	0.09	0.009	0.008	1.03	0.90	0.008
31.39	144.89	0.09	0.008	0.008	0.68	0.59	0.005
31.49	144.90	0.08	0.008	0.008	0.79	0.70	0.005
31.58	144.90	0.08	0.007	0.007	0.85	0.74	0.005
31.68	144.91	0.07	0.007	0.007	0.96	0.84	0.006
31.78	144.91	0.07	0.007	0.006	0.52	0.46	0.003
31.87	144.92	0.06	0.006	0.006	0.37	0.32	0.002
31.97	144.92	0.06	0.005	0.005	0.04	0.03	0.000
32.06	144.93	0.05	0.005	0.005	0.48	0.42	0.002
32.16	144.93	0.05	0.005	0.004	0.14	0.12	0.001
32.26	144.94	0.04	0.004	0.004	0.10	0.08	0.000
32.35	144.94	0.04	0.004	0.004	0.04	0.04	0.000
32.45	144.95	0.03	0.003	0.003	0.05	0.05	0.000
32.55	144.95	0.03	0.003	0.002	0.05	0.04	0.000
32.64	144.97	0.01	0.001	0.001	0.01	0.01	0.000
32.66	144.98	0.00	0.000	0.000	0.00	0.00	0.000
Cross Section Area (m^2) =			0.505	**Cross Sectional Discharge (m^3/s) =**			0.401

Table B12: Cross Section (f) March 21, 2012 LPIV Discharge Calculation

X (m)	ELV (m)	Depth (m)	Area (m^2)	Effective Area (m^2)	[1]Vel. (m/s)	[2]Avg V (m/s)	Discharge (m^3/s)
28.12	144.99	0.00	0.000	0.000	0.00	0.00	0.000
28.79	144.94	0.05	0.035	0.020	0.00	0.00	0.000
28.89	144.93	0.06	0.006	0.005	0.02	0.02	0.000
28.98	144.93	0.06	0.005	0.006	0.00	0.00	0.000
29.08	144.93	0.06	0.006	0.006	0.07	0.06	0.000
29.17	144.93	0.06	0.006	0.006	0.53	0.47	0.003
29.27	144.92	0.07	0.007	0.007	0.24	0.21	0.001
29.37	144.92	0.07	0.007	0.007	0.35	0.31	0.002
29.46	144.92	0.07	0.007	0.007	0.46	0.40	0.003
29.56	144.91	0.08	0.007	0.008	0.30	0.27	0.002
29.66	144.91	0.08	0.008	0.008	0.44	0.38	0.003
29.75	144.90	0.09	0.008	0.010	0.33	0.28	0.003
29.85	144.86	0.13	0.013	0.017	0.38	0.33	0.006
29.95	144.78	0.21	0.021	0.021	0.62	0.54	0.011
30.04	144.77	0.22	0.021	0.021	0.78	0.69	0.015
30.14	144.76	0.23	0.022	0.023	0.92	0.81	0.018
30.23	144.74	0.25	0.023	0.025	1.00	0.88	0.022
30.33	144.73	0.26	0.026	0.025	1.13	0.99	0.025
30.43	144.74	0.25	0.024	0.023	0.91	0.80	0.018
30.52	144.76	0.23	0.022	0.021	1.07	0.93	0.019
30.62	144.79	0.20	0.019	0.019	1.30	1.13	0.022
30.72	144.80	0.19	0.019	0.018	1.55	1.35	0.024
30.81	144.82	0.17	0.016	0.016	1.49	1.30	0.020
30.91	144.83	0.16	0.015	0.014	1.45	1.27	0.018
31.00	144.85	0.14	0.013	0.013	0.74	0.65	0.009
31.10	144.86	0.13	0.013	0.013	0.78	0.68	0.009
31.20	144.86	0.13	0.012	0.012	1.27	1.11	0.013
31.29	144.87	0.12	0.011	0.011	1.30	1.14	0.012
31.39	144.88	0.11	0.011	0.011	1.28	1.12	0.012
31.49	144.88	0.11	0.011	0.010	1.24	1.08	0.011
31.58	144.89	0.10	0.009	0.009	1.22	1.07	0.010
31.68	144.90	0.09	0.009	0.009	0.93	0.81	0.007
31.78	144.90	0.09	0.009	0.008	0.92	0.81	0.007
31.87	144.91	0.08	0.008	0.007	0.50	0.44	0.003
31.97	144.92	0.07	0.007	0.007	-0.01	-0.01	0.000
32.06	144.92	0.07	0.007	0.006	0.03	0.03	0.000
32.16	144.93	0.06	0.006	0.006	0.53	0.47	0.003
32.26	144.93	0.06	0.005	0.005	0.70	0.61	0.003
32.35	144.94	0.05	0.005	0.004	0.43	0.37	0.002
32.45	144.95	0.04	0.004	0.003	0.23	0.20	0.001
32.55	144.97	0.02	0.002	0.001	0.26	0.23	0.000
32.64	144.98	0.01	0.001	0.001	0.03	0.03	0.000
32.74	144.99	0.00	0.000	0.000	0.04	0.03	0.000
32.82	144.99	0.00	0.000	0.000	0.00	0.00	0.000
Cross Section Area (m^2) =			0.485	**Cross Sectional Discharge (m^3/s) =**			0.336

Table B13: Cross Section (g) March 21, 2012 LPIV Discharge Calculation

X (m)	ELV (m)	Depth (m)	Area (m^2)	Effective Area (m^2)	[1]Vel. (m/s)	[2]Avg V (m/s)	Discharge (m^3/s)
28.30	145.00	0.00	0.000	0.000	0.00	0.00	0.000
28.69	144.94	0.06	0.023	0.015	0.01	0.01	0.000
28.79	144.94	0.06	0.006	0.006	0.01	0.01	0.000
28.89	144.94	0.06	0.006	0.006	0.05	0.04	0.000
28.98	144.94	0.06	0.006	0.006	0.01	0.01	0.000
29.08	144.94	0.06	0.006	0.006	0.10	0.08	0.000
29.17	144.94	0.06	0.006	0.007	0.26	0.22	0.002
29.27	144.91	0.09	0.009	0.012	0.30	0.26	0.003
29.37	144.85	0.15	0.014	0.017	0.39	0.34	0.006
29.46	144.79	0.21	0.020	0.018	0.53	0.46	0.008
29.56	144.82	0.18	0.017	0.017	0.55	0.48	0.008
29.66	144.82	0.18	0.018	0.018	0.48	0.42	0.008
29.75	144.80	0.20	0.019	0.020	0.62	0.54	0.011
29.85	144.77	0.23	0.022	0.023	0.63	0.55	0.013
29.95	144.76	0.24	0.024	0.024	0.74	0.65	0.015
30.04	144.76	0.24	0.023	0.023	0.79	0.69	0.016
30.14	144.76	0.24	0.023	0.023	0.83	0.73	0.017
30.23	144.76	0.24	0.023	0.024	0.81	0.71	0.017
30.33	144.76	0.24	0.024	0.023	0.91	0.80	0.019
30.43	144.77	0.23	0.022	0.021	1.05	0.92	0.020
30.52	144.78	0.22	0.021	0.020	0.70	0.61	0.012
30.62	144.80	0.20	0.019	0.019	1.01	0.88	0.017
30.72	144.82	0.18	0.018	0.017	1.28	1.12	0.019
30.81	144.83	0.17	0.016	0.016	1.48	1.30	0.020
30.91	144.84	0.16	0.015	0.016	1.57	1.38	0.022
31.00	144.83	0.17	0.016	0.017	1.54	1.34	0.022
31.10	144.83	0.17	0.017	0.017	1.29	1.13	0.019
31.20	144.82	0.18	0.017	0.017	1.09	0.96	0.016
31.29	144.82	0.18	0.017	0.018	1.16	1.01	0.018
31.39	144.81	0.19	0.018	0.017	1.11	0.97	0.017
31.49	144.83	0.17	0.017	0.016	0.76	0.66	0.011
31.58	144.84	0.16	0.015	0.014	0.71	0.62	0.009
31.68	144.86	0.14	0.014	0.013	0.47	0.41	0.006
31.78	144.87	0.13	0.013	0.012	0.55	0.48	0.006
31.87	144.88	0.12	0.011	0.011	0.48	0.42	0.004
31.97	144.90	0.10	0.010	0.009	0.37	0.32	0.003
32.06	144.90	0.10	0.009	0.009	0.42	0.36	0.003
32.16	144.91	0.09	0.009	0.008	0.43	0.38	0.003
32.26	144.92	0.08	0.007	0.007	0.44	0.38	0.003
32.35	144.93	0.07	0.006	0.006	0.23	0.20	0.001
32.45	144.94	0.06	0.005	0.005	0.22	0.20	0.001
32.55	144.95	0.05	0.005	0.004	0.29	0.25	0.001
32.64	144.96	0.04	0.004	0.003	0.15	0.13	0.000
32.74	144.97	0.03	0.003	0.001	-0.23	-0.20	0.000
32.80	145.00	0.00	0.000	0.000	0.00	0.00	0.000
Cross Section Area (m^2) =			0.613	**Cross Sectional Discharge (m^3/s) =**			0.396

Table B14: Cross Section (h) March 21, 2012 LPIV Discharge Calculation

X (m)	ELV (m)	Depth (m)	Area (m^2)	Effective Area (m^2)	[1]Vel. (m/s)	[2]Avg V (m/s)	Discharge (m^3/s)
28.50	145.02	0.00	0.000	0.000	0.00	0.00	0.000
28.89	144.96	0.05	0.021	0.014	-0.09	-0.08	-0.001
28.98	144.95	0.07	0.006	0.007	0.01	0.01	0.000
29.08	144.93	0.08	0.008	0.008	0.04	0.03	0.000
29.17	144.92	0.09	0.009	0.010	0.15	0.13	0.001
29.27	144.91	0.11	0.011	0.011	0.10	0.09	0.001
29.37	144.89	0.12	0.012	0.012	0.15	0.13	0.002
29.46	144.88	0.13	0.013	0.014	0.32	0.28	0.004
29.56	144.86	0.16	0.015	0.017	0.25	0.22	0.004
29.66	144.82	0.19	0.019	0.020	0.13	0.12	0.002
29.75	144.79	0.22	0.021	0.023	-0.04	-0.03	-0.001
29.85	144.76	0.25	0.024	0.026	-0.01	-0.01	0.000
29.95	144.73	0.29	0.029	0.030	0.07	0.06	0.002
30.04	144.70	0.32	0.030	0.031	0.20	0.17	0.005
30.14	144.69	0.33	0.031	0.031	0.33	0.29	0.009
30.23	144.68	0.33	0.032	0.033	0.39	0.34	0.011
30.33	144.67	0.34	0.034	0.034	0.58	0.50	0.017
30.43	144.67	0.35	0.033	0.033	0.85	0.74	0.025
30.52	144.66	0.36	0.034	0.034	0.87	0.76	0.026
30.62	144.66	0.35	0.033	0.034	1.05	0.92	0.031
30.72	144.67	0.35	0.035	0.034	1.11	0.97	0.033
30.81	144.67	0.34	0.033	0.032	1.31	1.15	0.037
30.91	144.68	0.34	0.032	0.032	1.59	1.39	0.044
31.00	144.68	0.33	0.032	0.032	2.05	1.80	0.058
31.10	144.69	0.33	0.033	0.031	1.75	1.53	0.048
31.20	144.70	0.32	0.030	0.029	1.47	1.29	0.037
31.29	144.72	0.30	0.028	0.027	1.09	0.95	0.026
31.39	144.74	0.28	0.026	0.026	1.16	1.01	0.027
31.49	144.76	0.26	0.026	0.024	0.88	0.77	0.019
31.58	144.77	0.24	0.023	0.022	0.49	0.42	0.009
31.68	144.79	0.23	0.021	0.022	0.23	0.20	0.004
31.78	144.80	0.22	0.022	0.021	0.60	0.52	0.011
31.87	144.81	0.21	0.020	0.019	0.78	0.68	0.013
31.97	144.82	0.20	0.019	0.019	0.69	0.61	0.011
32.06	144.82	0.19	0.018	0.018	0.53	0.46	0.008
32.16	144.83	0.18	0.018	0.017	0.38	0.33	0.006
32.26	144.85	0.16	0.016	0.014	0.36	0.32	0.004
32.35	144.89	0.12	0.012	0.010	0.23	0.20	0.002
32.45	144.93	0.09	0.008	0.006	0.19	0.17	0.001
32.55	144.97	0.05	0.005	0.003	0.06	0.05	0.000
32.64	145.01	0.01	0.001	0.000	0.01	0.00	0.000
32.75	145.02	0.00	0.000	0.000	0.00	0.00	0.000
Cross Section Area (m^2) =			0.871	**Cross Sectional Discharge (m^3/s) =**			0.539

Table B15: Cross Section (a) September 25, 2012 LPIV Discharge Calculation

X (m)	ELV (m)	Depth (m)	Area (m^2)	Effective Area (m^2)	Vel. (m/s)	Avg. V (m/s)	Discharge (m^3/s)
29.94	314.42	0.00	0.000	0.000	0.00	0.00	0.000
29.96	314.42	0.00	0.000	0.000	0.00	0.00	0.000
29.98	314.39	0.03	0.001	0.001	0.00	0.00	0.000
30.00	314.38	0.04	0.001	0.001	0.00	0.00	0.000
30.03	314.38	0.04	0.001	0.001	0.00	0.00	0.000
30.05	314.37	0.05	0.001	0.001	0.01	0.00	0.000
30.07	314.37	0.05	0.001	0.001	0.01	0.01	0.000
30.09	314.36	0.06	0.001	0.001	0.01	0.01	0.000
30.12	314.36	0.06	0.001	0.001	0.01	0.00	0.000
30.14	314.36	0.06	0.001	0.002	0.00	0.00	0.000
30.16	314.32	0.10	0.002	0.003	0.00	0.00	0.000
30.18	314.28	0.14	0.003	0.004	0.01	0.01	0.000
30.21	314.24	0.18	0.004	0.004	0.01	0.01	0.000
30.23	314.22	0.20	0.004	0.005	0.03	0.03	0.000
30.25	314.19	0.23	0.005	0.006	0.18	0.16	0.001
30.27	314.16	0.26	0.006	0.006	0.80	0.70	0.004
30.30	314.14	0.28	0.007	0.006	0.84	0.74	0.004
30.32	314.16	0.26	0.005	0.005	0.94	0.83	0.004
30.34	314.18	0.24	0.006	0.005	0.95	0.83	0.004
30.36	314.20	0.22	0.005	0.005	0.98	0.86	0.004
30.39	314.21	0.21	0.005	0.004	0.98	0.86	0.004
30.41	314.22	0.20	0.004	0.004	1.08	0.94	0.004
30.43	314.24	0.18	0.004	0.004	1.09	0.95	0.004
30.45	314.25	0.17	0.004	0.004	1.10	0.96	0.004
30.48	314.26	0.16	0.004	0.003	1.11	0.97	0.003
30.50	314.28	0.15	0.003	0.004	1.12	0.98	0.004
30.54	314.29	0.13	0.006	0.005	1.10	0.96	0.005
30.57	314.27	0.15	0.003	0.003	1.09	0.95	0.003
30.59	314.25	0.17	0.003	0.004	1.07	0.94	0.004
30.61	314.23	0.19	0.004	0.004	1.01	0.88	0.004
30.63	314.23	0.19	0.004	0.004	0.94	0.82	0.004
30.66	314.23	0.19	0.004	0.004	0.88	0.77	0.003
30.68	314.23	0.19	0.004	0.004	0.88	0.77	0.003
30.70	314.22	0.20	0.005	0.005	0.90	0.79	0.004
30.72	314.22	0.20	0.005	0.005	0.83	0.73	0.003
30.75	314.23	0.19	0.004	0.004	0.85	0.75	0.003
30.77	314.24	0.18	0.004	0.004	0.86	0.75	0.003
30.79	314.23	0.19	0.004	0.004	0.80	0.70	0.003
30.81	314.27	0.15	0.003	0.003	0.56	0.49	0.001
30.84	314.31	0.11	0.003	0.002	0.53	0.47	0.001
30.86	314.32	0.10	0.002	0.002	0.52	0.46	0.001

30.88	314.32	0.10	0.002	0.002	0.62	0.55	0.001
30.90	314.33	0.10	0.002	0.002	0.62	0.54	0.001
30.93	314.33	0.09	0.002	0.002	0.57	0.50	0.001
30.95	314.33	0.09	0.002	0.002	0.01	0.01	0.000
30.97	314.34	0.08	0.002	0.002	0.01	0.01	0.000
30.99	314.35	0.07	0.002	0.002	0.01	0.01	0.000
31.02	314.36	0.07	0.002	0.001	0.01	0.01	0.000
31.04	314.36	0.07	0.001	0.002	0.01	0.01	0.000
31.06	314.34	0.08	0.002	0.002	0.01	0.01	0.000
31.08	314.32	0.10	0.002	0.002	0.01	0.01	0.000
31.11	314.31	0.11	0.003	0.003	0.01	0.01	0.000
31.13	314.29	0.13	0.003	0.003	0.01	0.01	0.000
31.15	314.28	0.15	0.003	0.004	0.31	0.27	0.001
31.17	314.26	0.16	0.004	0.003	0.31	0.27	0.001
31.20	314.31	0.11	0.003	0.002	0.31	0.27	0.001
31.22	314.35	0.07	0.001	0.001	0.34	0.30	0.000
31.24	314.36	0.06	0.001	0.001	0.00	0.00	0.000
31.26	314.36	0.06	0.001	0.001	0.00	0.00	0.000
31.29	314.37	0.05	0.001	0.001	0.00	0.00	0.000
31.31	314.42	0.00	0.000	0.000	0.00	0.00	0.000
Cross Section Area (m^2) =			0.180	**Cross Sectional Discharge ($m^3/3$) =**			0.097

Table B16: Cross Section (b) September 25, 2012 LPIV Discharge Calculation

X (m)	ELV (m)	Depth (m)	Area (m^2)	Effective Area (m^2)	Vel. (m/s)	Avg V (m/s)	Discharge (m^3/s)
29.93	314.42	0.00	0.000	0.000	0.00	0.00	0.000
29.94	314.41	0.00	0.000	0.000	0.00	0.00	0.000
29.96	314.41	0.01	0.000	0.000	0.00	0.00	0.000
29.98	314.40	0.02	0.000	0.000	0.00	0.00	0.000
30.00	314.39	0.02	0.001	0.000	0.01	0.01	0.000
30.03	314.39	0.03	0.001	0.001	0.00	0.00	0.000
30.05	314.38	0.04	0.001	0.001	0.00	0.00	0.000
30.07	314.37	0.04	0.001	0.001	0.00	0.00	0.000
30.09	314.36	0.05	0.001	0.001	0.01	0.01	0.000
30.11	314.35	0.07	0.001	0.001	0.02	0.01	0.000
30.14	314.34	0.08	0.002	0.002	0.02	0.02	0.000
30.16	314.32	0.09	0.002	0.002	0.03	0.03	0.000
30.18	314.31	0.11	0.002	0.002	0.14	0.12	0.000
30.20	314.28	0.14	0.003	0.003	0.32	0.28	0.001
30.23	314.22	0.20	0.005	0.004	0.36	0.31	0.001
30.25	314.17	0.24	0.005	0.005	0.60	0.53	0.003
30.27	314.19	0.23	0.005	0.005	0.72	0.63	0.003
30.29	314.20	0.22	0.005	0.005	0.74	0.65	0.003
30.31	314.21	0.21	0.004	0.005	0.84	0.74	0.003
30.34	314.21	0.21	0.005	0.005	0.92	0.80	0.004
30.36	314.21	0.21	0.004	0.004	0.96	0.84	0.004
30.38	314.21	0.20	0.005	0.004	0.97	0.85	0.004
30.40	314.22	0.20	0.005	0.005	0.91	0.80	0.004
30.42	314.22	0.20	0.004	0.004	0.89	0.78	0.003
30.45	314.22	0.20	0.005	0.004	1.01	0.89	0.004
30.47	314.22	0.20	0.005	0.005	1.04	0.91	0.004
30.49	314.22	0.20	0.004	0.004	1.06	0.93	0.004
30.51	314.22	0.20	0.005	0.004	0.97	0.85	0.004
30.54	314.22	0.20	0.005	0.005	1.01	0.88	0.004
30.56	314.22	0.20	0.004	0.004	0.91	0.80	0.003
30.58	314.22	0.20	0.005	0.004	0.88	0.77	0.003
30.60	314.22	0.20	0.005	0.005	0.83	0.72	0.003
30.62	314.21	0.20	0.004	0.004	0.73	0.64	0.003
30.65	314.20	0.22	0.005	0.005	0.62	0.54	0.002
30.67	314.19	0.23	0.005	0.005	0.55	0.48	0.002
30.69	314.18	0.24	0.005	0.005	0.45	0.40	0.002
30.71	314.16	0.25	0.006	0.005	0.39	0.34	0.002
30.73	314.15	0.26	0.005	0.006	0.38	0.33	0.002
30.76	314.14	0.28	0.006	0.006	0.42	0.37	0.002
30.78	314.13	0.29	0.007	0.007	0.30	0.27	0.002
30.82	314.11	0.30	0.013	0.010	0.00	0.00	0.000
30.85	314.13	0.28	0.007	0.010	0.01	0.01	0.000

30.87	314.15	0.27	0.005	0.006	0.02	0.02	0.000
30.89	314.17	0.25	0.006	0.006	0.04	0.03	0.000
30.91	314.19	0.23	0.005	0.006	0.03	0.03	0.000
30.93	314.20	0.22	0.004	0.005	0.00	0.00	0.000
30.96	314.20	0.21	0.005	0.005	0.01	0.01	0.000
30.98	314.19	0.23	0.005	0.005	0.01	0.00	0.000
31.00	314.18	0.24	0.005	0.005	0.00	0.00	0.000
31.02	314.18	0.23	0.005	0.005	0.00	0.00	0.000
31.04	314.20	0.22	0.004	0.005	0.00	0.00	0.000
31.07	314.21	0.20	0.005	0.005	0.00	0.00	0.000
31.09	314.23	0.19	0.004	0.005	0.00	0.00	0.000
31.11	314.25	0.17	0.003	0.004	0.00	0.00	0.000
31.13	314.26	0.16	0.004	0.004	0.00	0.00	0.000
31.16	314.28	0.14	0.003	0.003	0.00	0.00	0.000
31.18	314.29	0.12	0.002	0.003	0.00	0.00	0.000
31.20	314.33	0.08	0.002	0.002	0.00	0.00	0.000
31.22	314.37	0.05	0.001	0.002	0.00	0.00	0.000
31.24	314.37	0.05	0.001	0.001	0.00	0.00	0.000
31.27	314.37	0.05	0.001	0.001	0.00	0.00	0.000
31.29	314.37	0.05	0.001	0.001	0.00	0.00	0.000
31.31	314.37	0.04	0.001	0.001	0.00	0.00	0.000
31.33	314.38	0.04	0.001	0.001	0.00	0.00	0.000
31.33	314.42	0.00	0.000	0.000	0.00	0.00	0.000
Cross Section Area (m^2) =			0.237	**Cross Sectional Discharge ($m^3/3$) =**			0.081

Table B17: Cross Section (c) September 25, 2012 LPIV Discharge Calculation

X (m)	ELV (m)	Depth (m)	Area (m^2)	Effective Area (m^2)	Vel. (m/s)	Avg. V (m/s)	Discharge (m^3/s)
30.00	314.40	0.00	0.000	0.000	0.00	0.00	0.000
30.03	314.35	0.05	0.001	0.001	0.00	0.00	0.000
30.05	314.34	0.06	0.001	0.001	0.00	0.00	0.000
30.07	314.33	0.07	0.001	0.001	0.00	0.00	0.000
30.15	314.28	0.12	0.010	0.006	0.81	0.71	0.004
30.17	314.27	0.14	0.003	0.007	0.93	0.82	0.005
30.20	314.25	0.15	0.003	0.003	0.83	0.73	0.002
30.22	314.24	0.16	0.003	0.003	0.71	0.62	0.002
30.24	314.23	0.17	0.003	0.003	0.68	0.59	0.002
30.26	314.22	0.18	0.004	0.004	0.69	0.60	0.002
30.28	314.21	0.19	0.005	0.004	0.75	0.66	0.003
30.30	314.20	0.20	0.004	0.004	0.71	0.62	0.003
30.32	314.19	0.21	0.004	0.004	0.70	0.61	0.003
30.34	314.18	0.22	0.004	0.004	0.69	0.61	0.003
30.36	314.18	0.22	0.005	0.005	0.77	0.67	0.003
30.38	314.18	0.22	0.004	0.005	0.83	0.73	0.003
30.40	314.19	0.22	0.004	0.004	0.86	0.75	0.003
30.42	314.19	0.21	0.004	0.004	0.85	0.75	0.003
30.44	314.19	0.21	0.004	0.004	0.74	0.65	0.003
30.47	314.19	0.21	0.005	0.005	0.71	0.62	0.003
30.49	314.19	0.21	0.004	0.005	0.79	0.69	0.003
30.51	314.20	0.20	0.004	0.004	0.82	0.71	0.003
30.53	314.20	0.20	0.004	0.004	0.81	0.71	0.003
30.55	314.20	0.20	0.005	0.004	0.75	0.66	0.003
30.57	314.20	0.20	0.004	0.004	0.68	0.60	0.003
30.59	314.19	0.21	0.004	0.004	0.41	0.36	0.001
30.61	314.18	0.22	0.004	0.004	0.34	0.30	0.001
30.63	314.18	0.23	0.005	0.005	0.30	0.27	0.001
30.65	314.17	0.23	0.005	0.005	0.02	0.02	0.000
30.67	314.16	0.24	0.005	0.005	0.02	0.02	0.000
30.69	314.15	0.25	0.005	0.005	0.03	0.02	0.000
30.71	314.15	0.26	0.005	0.005	0.03	0.02	0.000
30.74	314.15	0.25	0.006	0.006	0.02	0.02	0.000
30.76	314.15	0.25	0.005	0.006	0.02	0.02	0.000
30.78	314.15	0.25	0.005	0.005	0.02	0.01	0.000
30.80	314.15	0.25	0.005	0.005	0.01	0.01	0.000
30.90	314.17	0.23	0.025	0.015	0.00	0.00	0.000
30.92	314.18	0.22	0.004	0.015	0.00	0.00	0.000
30.94	314.19	0.21	0.004	0.004	0.01	0.01	0.000
30.96	314.21	0.20	0.004	0.004	0.01	0.01	0.000
30.98	314.22	0.18	0.004	0.004	0.01	0.01	0.000
31.01	314.23	0.17	0.004	0.004	0.00	0.00	0.000

31.03	314.25	0.16	0.003	0.004	0.00	0.00	0.000
31.05	314.26	0.14	0.003	0.003	0.00	0.00	0.000
31.07	314.27	0.13	0.003	0.003	0.00	0.00	0.000
31.09	314.28	0.12	0.003	0.003	0.00	0.00	0.000
31.11	314.30	0.11	0.002	0.002	0.00	0.00	0.000
31.13	314.31	0.09	0.002	0.002	0.00	0.00	0.000
31.15	314.32	0.08	0.002	0.002	0.00	0.00	0.000
31.25	314.36	0.04	0.004	0.003	0.00	0.00	0.000
31.28	314.37	0.03	0.001	0.002	0.00	0.00	0.000
31.30	314.38	0.02	0.000	0.001	0.00	0.00	0.000
31.32	314.38	0.02	0.000	0.000	0.01	0.01	0.000
31.32	314.40	0.00	0.000	0.000	0.00	0.00	0.000
Cross Section Area (m^2) =			0.218	**Cross Sectional Discharge (m^3/3) =**			0.067

Table B18: Cross Section (d) September 25, 2012 LPIV Discharge Calculation

X (m)	ELV (m)	Depth (m)	Area (m^2)	Effective Area (m^2)	Vel. (m/s)	Avg V (m/s)	Discharge (m^3/s)
29.94	314.44	0.00	0.000	0.000	0.00	0.00	0.000
29.95	314.40	0.04	0.000	0.000	0.01	0.01	0.000
29.97	314.39	0.05	0.001	0.001	0.02	0.02	0.000
29.98	314.38	0.06	0.001	0.001	0.35	0.31	0.000
30.00	314.36	0.07	0.001	0.001	0.35	0.31	0.000
30.02	314.35	0.08	0.001	0.001	0.37	0.32	0.000
30.04	314.34	0.10	0.002	0.002	0.51	0.45	0.001
30.05	314.33	0.11	0.002	0.002	0.70	0.61	0.001
30.07	314.31	0.13	0.002	0.002	0.79	0.69	0.001
30.09	314.30	0.14	0.002	0.002	0.81	0.71	0.002
30.10	314.28	0.15	0.003	0.002	0.85	0.74	0.002
30.12	314.27	0.17	0.003	0.003	0.87	0.76	0.002
30.14	314.26	0.18	0.003	0.003	0.83	0.73	0.002
30.16	314.24	0.20	0.004	0.003	0.83	0.73	0.003
30.17	314.23	0.21	0.004	0.004	0.81	0.71	0.003
30.19	314.21	0.22	0.004	0.004	0.65	0.57	0.002
30.21	314.20	0.23	0.004	0.004	0.66	0.58	0.002
30.22	314.20	0.24	0.004	0.004	0.69	0.60	0.002
30.24	314.19	0.24	0.004	0.004	0.69	0.61	0.002
30.26	314.19	0.25	0.004	0.004	0.66	0.58	0.002
30.27	314.18	0.26	0.004	0.004	0.67	0.58	0.002
30.29	314.18	0.26	0.004	0.004	0.61	0.54	0.002
30.31	314.17	0.27	0.005	0.005	0.67	0.59	0.003
30.33	314.16	0.27	0.005	0.005	0.82	0.72	0.004
30.34	314.16	0.28	0.005	0.005	0.86	0.75	0.003
30.36	314.15	0.28	0.005	0.005	0.87	0.76	0.004
30.38	314.15	0.29	0.005	0.005	0.87	0.76	0.004
30.39	314.14	0.29	0.005	0.005	0.88	0.77	0.004
30.41	314.14	0.30	0.005	0.005	0.98	0.86	0.004
30.43	314.13	0.31	0.005	0.005	0.99	0.87	0.004
30.44	314.13	0.31	0.005	0.005	1.00	0.87	0.004
30.46	314.13	0.31	0.006	0.006	0.82	0.72	0.004
30.48	314.13	0.30	0.005	0.006	0.73	0.64	0.004
30.50	314.14	0.30	0.005	0.005	0.62	0.55	0.003
30.51	314.14	0.30	0.005	0.005	0.59	0.51	0.003
30.53	314.15	0.29	0.005	0.005	0.56	0.49	0.002
30.55	314.15	0.29	0.005	0.005	0.55	0.48	0.002
30.56	314.15	0.28	0.005	0.005	0.58	0.51	0.002
30.58	314.16	0.28	0.005	0.005	0.02	0.02	0.000
30.60	314.16	0.27	0.005	0.005	0.02	0.02	0.000
30.62	314.17	0.27	0.005	0.005	0.03	0.02	0.000
30.63	314.17	0.26	0.004	0.005	0.03	0.02	0.000

30.65	314.18	0.26	0.004	0.004	0.02	0.02	0.000
30.67	314.18	0.26	0.004	0.004	0.01	0.01	0.000
30.68	314.18	0.25	0.004	0.004	0.01	0.01	0.000
30.70	314.19	0.25	0.004	0.004	0.00	0.00	0.000
30.72	314.19	0.25	0.004	0.004	0.00	0.00	0.000
30.73	314.19	0.25	0.004	0.004	0.00	0.00	0.000
30.75	314.19	0.24	0.004	0.004	0.00	0.00	0.000
30.77	314.20	0.24	0.005	0.004	0.00	0.00	0.000
30.79	314.22	0.22	0.004	0.004	0.00	0.00	0.000
30.80	314.24	0.20	0.003	0.003	0.00	0.00	0.000
30.82	314.26	0.18	0.003	0.003	0.01	0.00	0.000
30.84	314.28	0.16	0.003	0.003	0.00	0.00	0.000
30.85	314.30	0.14	0.002	0.002	0.00	0.00	0.000
30.87	314.32	0.12	0.002	0.002	0.00	0.00	0.000
30.90	314.36	0.07	0.002	0.002	0.00	0.00	0.000
30.97	314.38	0.06	0.004	0.003	0.00	0.00	0.000
30.99	314.38	0.06	0.001	0.002	0.00	0.00	0.000
31.01	314.38	0.06	0.001	0.001	0.00	0.00	0.000
31.04	314.38	0.06	0.002	0.001	0.00	0.00	0.000
31.06	314.38	0.06	0.001	0.001	0.00	0.00	0.000
31.08	314.38	0.06	0.001	0.001	0.00	0.00	0.000
31.14	314.38	0.06	0.004	0.002	0.00	0.00	0.000
31.16	314.38	0.06	0.001	0.002	0.00	0.00	0.000
31.16	314.44	0.00	0.000	0.000	0.00	0.00	0.000
Cross Section Area (m^2) =			0.224	**Cross Sectional Discharge ($m^3/3$) =**			0.088

Table B19: Cross Section (e) September 25, 2012 LPIV Discharge Calculation

X (m)	ELV (m)	Depth (m)	Area (m^2)	Effective Area (m^2)	Vel. (m/s)	Avg V (m/s)	Discharge (m^3/s)
29.88	314.48	0.00	0.000	0.000	0.00	0.00	0.000
29.89	314.41	0.07	0.001	0.000	0.00	0.00	0.000
30.01	314.34	0.14	0.017	0.009	0.59	0.52	0.005
30.03	314.32	0.16	0.004	0.010	0.77	0.68	0.007
30.06	314.31	0.17	0.004	0.004	0.72	0.63	0.002
30.08	314.29	0.19	0.004	0.004	0.76	0.66	0.003
30.10	314.28	0.20	0.004	0.004	0.49	0.43	0.002
30.12	314.27	0.21	0.005	0.004	0.40	0.35	0.002
30.15	314.26	0.22	0.005	0.005	0.71	0.62	0.003
30.17	314.25	0.23	0.005	0.005	0.69	0.60	0.003
30.19	314.25	0.23	0.005	0.005	0.66	0.58	0.003
30.22	314.24	0.24	0.006	0.006	0.67	0.59	0.003
30.24	314.23	0.25	0.006	0.006	0.64	0.56	0.003
30.26	314.23	0.25	0.006	0.006	0.58	0.51	0.003
30.29	314.22	0.26	0.006	0.006	0.67	0.59	0.004
30.31	314.22	0.27	0.006	0.006	0.73	0.64	0.004
30.33	314.21	0.27	0.006	0.006	0.86	0.75	0.005
30.35	314.21	0.27	0.005	0.006	0.87	0.76	0.004
30.38	314.20	0.28	0.007	0.006	0.83	0.73	0.004
30.40	314.20	0.28	0.007	0.007	0.83	0.72	0.005
30.42	314.19	0.29	0.007	0.007	0.96	0.84	0.006
30.45	314.19	0.29	0.007	0.007	0.95	0.83	0.006
30.47	314.19	0.30	0.007	0.007	1.09	0.96	0.007
30.49	314.18	0.30	0.007	0.007	1.12	0.98	0.007
30.59	314.23	0.25	0.023	0.015	0.98	0.86	0.013
30.61	314.25	0.23	0.005	0.014	0.89	0.78	0.011
30.63	314.27	0.21	0.005	0.005	0.83	0.72	0.003
30.65	314.29	0.19	0.005	0.005	0.73	0.64	0.003
30.68	314.31	0.18	0.004	0.004	0.67	0.59	0.003
30.70	314.32	0.16	0.004	0.004	0.64	0.56	0.002
30.72	314.34	0.14	0.003	0.003	0.60	0.52	0.002
30.75	314.36	0.12	0.003	0.003	0.51	0.45	0.001
30.77	314.37	0.11	0.003	0.003	0.03	0.03	0.000
30.79	314.34	0.14	0.003	0.003	0.03	0.02	0.000
30.82	314.34	0.14	0.003	0.003	0.02	0.02	0.000
30.84	314.34	0.15	0.003	0.003	0.02	0.01	0.000
30.86	314.33	0.15	0.003	0.003	0.01	0.01	0.000
30.88	314.33	0.15	0.003	0.003	0.00	0.00	0.000
30.91	314.33	0.15	0.004	0.004	0.00	0.00	0.000
30.93	314.33	0.15	0.004	0.004	0.00	0.00	0.000
30.95	314.33	0.16	0.004	0.004	0.00	0.00	0.000
31.05	314.32	0.16	0.015	0.009	0.00	0.00	0.000

31.07	314.32	0.16	0.004	0.009	0.00	0.00	0.000
31.09	314.33	0.15	0.003	0.004	0.00	0.00	0.000
31.11	314.35	0.13	0.003	0.003	0.01	0.00	0.000
31.14	314.38	0.11	0.002	0.003	0.01	0.01	0.000
31.16	314.40	0.08	0.002	0.002	0.00	0.00	0.000
31.21	314.44	0.05	0.002	0.002	0.00	0.00	0.000
31.23	314.45	0.03	0.001	0.001	0.00	0.00	0.000
31.25	314.45	0.03	0.001	0.001	0.00	0.00	0.000
31.39	314.46	0.03	0.004	0.002	0.00	0.00	0.000
31.48	314.46	0.02	0.002	0.003	0.00	0.00	0.000
31.53	314.46	0.02	0.001	0.002	0.00	0.00	0.000
31.55	314.46	0.02	0.000	0.001	0.00	0.00	0.000
31.58	314.46	0.02	0.000	0.000	0.00	0.00	0.000
31.60	314.46	0.02	0.000	0.000	0.00	0.00	0.000
31.64	314.47	0.02	0.001	0.001	0.00	0.00	0.000
31.67	314.47	0.02	0.000	0.001	0.00	0.00	0.000
31.69	314.47	0.01	0.000	0.000	0.00	0.00	0.000
31.70	314.48	0.00	0.000	0.000	0.00	0.00	0.000
Cross Section Area (m^2) =			0.260	**Cross Sectional Discharge ($m^3/3$) =**			0.128

Table B20: Cross Section (f) September 25, 2012 LPIV Discharge Calculation

X (m)	ELV (m)	Depth (m)	Area (m^2)	Effective Area (m^2)	Vel. (m/s)	Avg V (m/s)	Discharge (m^3/s)
29.84	314.49	0.00	0.000	0.000	0.00	0.00	0.000
29.84	314.35	0.14	0.000	0.000	0.00	0.00	0.000
29.87	314.34	0.15	0.003	0.002	0.21	0.18	0.000
29.89	314.34	0.15	0.004	0.003	0.59	0.51	0.002
29.91	314.33	0.16	0.004	0.004	0.51	0.45	0.002
29.94	314.33	0.16	0.004	0.004	0.56	0.49	0.002
29.96	314.32	0.17	0.004	0.004	0.62	0.54	0.002
29.98	314.31	0.18	0.004	0.004	0.62	0.54	0.002
30.01	314.31	0.18	0.004	0.004	0.59	0.52	0.002
30.03	314.30	0.19	0.004	0.004	0.62	0.54	0.002
30.05	314.29	0.20	0.005	0.004	0.59	0.52	0.002
30.08	314.29	0.20	0.005	0.005	0.59	0.52	0.002
30.10	314.28	0.21	0.005	0.005	0.59	0.52	0.003
30.12	314.27	0.22	0.005	0.005	0.48	0.42	0.002
30.15	314.26	0.23	0.005	0.005	0.50	0.44	0.002
30.17	314.26	0.24	0.006	0.005	0.57	0.50	0.003
30.19	314.25	0.24	0.006	0.006	0.61	0.53	0.003
30.22	314.24	0.25	0.006	0.006	0.62	0.54	0.003
30.24	314.23	0.26	0.006	0.006	0.68	0.60	0.004
30.26	314.23	0.26	0.006	0.006	0.71	0.62	0.004
30.29	314.23	0.26	0.006	0.006	0.67	0.59	0.004
30.31	314.23	0.26	0.006	0.006	0.74	0.65	0.004
30.33	314.23	0.26	0.006	0.006	0.72	0.63	0.004
30.36	314.23	0.26	0.006	0.006	0.73	0.64	0.004
30.38	314.23	0.26	0.006	0.006	0.76	0.67	0.004
30.40	314.24	0.26	0.006	0.006	0.82	0.72	0.004
30.43	314.24	0.25	0.006	0.006	0.82	0.72	0.004
30.45	314.24	0.25	0.006	0.006	0.78	0.68	0.004
30.47	314.24	0.25	0.006	0.006	0.80	0.70	0.004
30.50	314.25	0.24	0.006	0.006	0.81	0.71	0.004
30.52	314.26	0.23	0.005	0.005	0.89	0.78	0.004
30.54	314.27	0.22	0.005	0.005	0.84	0.74	0.004
30.57	314.28	0.21	0.005	0.005	0.79	0.69	0.003
30.59	314.29	0.20	0.005	0.005	0.59	0.51	0.002
30.61	314.30	0.19	0.004	0.004	0.57	0.50	0.002
30.64	314.31	0.18	0.004	0.004	0.53	0.47	0.002
30.66	314.33	0.17	0.004	0.004	0.51	0.45	0.002
30.68	314.34	0.16	0.004	0.004	0.52	0.46	0.002
30.71	314.35	0.15	0.003	0.004	0.51	0.45	0.002
30.73	314.35	0.14	0.003	0.003	0.46	0.40	0.001
30.75	314.35	0.14	0.003	0.003	0.53	0.46	0.002
30.78	314.34	0.15	0.003	0.003	0.49	0.43	0.001

30.80	314.34	0.15	0.004	0.004	0.48	0.42	0.001
30.82	314.34	0.15	0.004	0.004	0.56	0.49	0.002
30.85	314.33	0.16	0.004	0.004	0.57	0.50	0.002
30.87	314.33	0.16	0.004	0.004	0.49	0.43	0.002
30.90	314.33	0.16	0.004	0.004	0.60	0.52	0.002
30.92	314.33	0.16	0.004	0.004	0.63	0.55	0.002
30.94	314.33	0.16	0.004	0.004	0.63	0.55	0.002
30.97	314.33	0.17	0.004	0.004	0.55	0.49	0.002
30.99	314.32	0.17	0.004	0.004	0.31	0.27	0.001
31.01	314.32	0.17	0.004	0.004	0.22	0.19	0.001
31.04	314.32	0.17	0.004	0.004	0.33	0.29	0.001
31.06	314.32	0.17	0.004	0.004	0.40	0.35	0.001
31.08	314.33	0.17	0.004	0.004	0.18	0.15	0.001
31.11	314.35	0.14	0.003	0.004	0.02	0.01	0.000
31.13	314.37	0.12	0.003	0.003	0.01	0.01	0.000
31.15	314.39	0.10	0.002	0.003	0.00	0.00	0.000
31.18	314.41	0.08	0.002	0.002	0.00	0.00	0.000
31.20	314.43	0.06	0.001	0.002	0.00	0.00	0.000
31.22	314.45	0.04	0.001	0.001	0.00	0.00	0.000
31.25	314.45	0.04	0.001	0.001	0.00	0.00	0.000
31.27	314.44	0.05	0.001	0.001	0.00	0.00	0.000
31.29	314.44	0.05	0.001	0.001	0.00	0.00	0.000
31.32	314.44	0.06	0.001	0.001	0.00	0.00	0.000
31.34	314.43	0.06	0.001	0.001	0.00	0.00	0.000
31.36	314.43	0.06	0.001	0.001	0.00	0.00	0.000
31.39	314.43	0.07	0.002	0.001	0.00	0.00	0.000
31.41	314.42	0.07	0.002	0.002	0.00	0.00	0.000
31.43	314.42	0.07	0.002	0.002	0.00	0.00	0.000
31.46	314.41	0.08	0.002	0.002	0.00	0.00	0.000
31.48	314.41	0.08	0.002	0.002	0.00	0.00	0.000
31.50	314.41	0.08	0.002	0.002	0.01	0.01	0.000
31.53	314.40	0.09	0.002	0.002	0.01	0.01	0.000
31.55	314.40	0.09	0.002	0.002	0.01	0.01	0.000
31.57	314.40	0.09	0.002	0.002	0.01	0.01	0.000
31.60	314.39	0.10	0.002	0.002	0.01	0.00	0.000
31.62	314.39	0.10	0.002	0.002	0.00	0.00	0.000
31.64	314.39	0.11	0.002	0.002	0.00	0.00	0.000
31.71	314.38	0.11	0.007	0.005	0.00	0.00	0.000
31.74	314.39	0.10	0.002	0.005	0.00	0.00	0.000
31.76	314.40	0.09	0.002	0.002	0.01	0.01	0.000
31.78	314.40	0.09	0.002	0.002	0.01	0.01	0.000
31.78	314.49	0.00	0.000	0.000	0.00	0.00	0.000
Cross Section Area (m^2) =		0.302	**Cross Sectional Discharge ($m^3/3$) =**				0.130

Appendix C: Hydrologic Data of Mud Creek

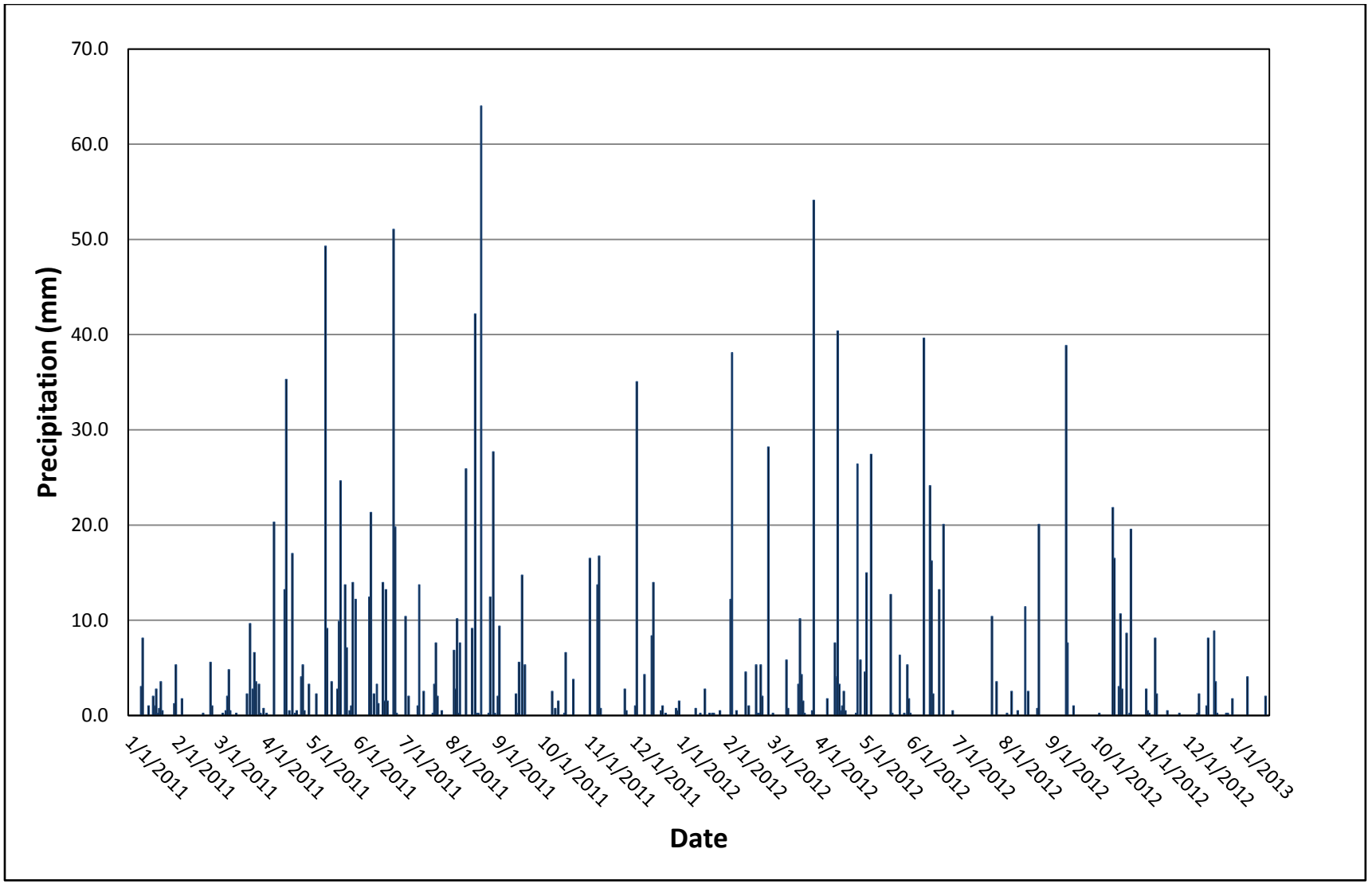

Figure C1: Precipitation data for Mud Creek (January 2011 – January 2013)

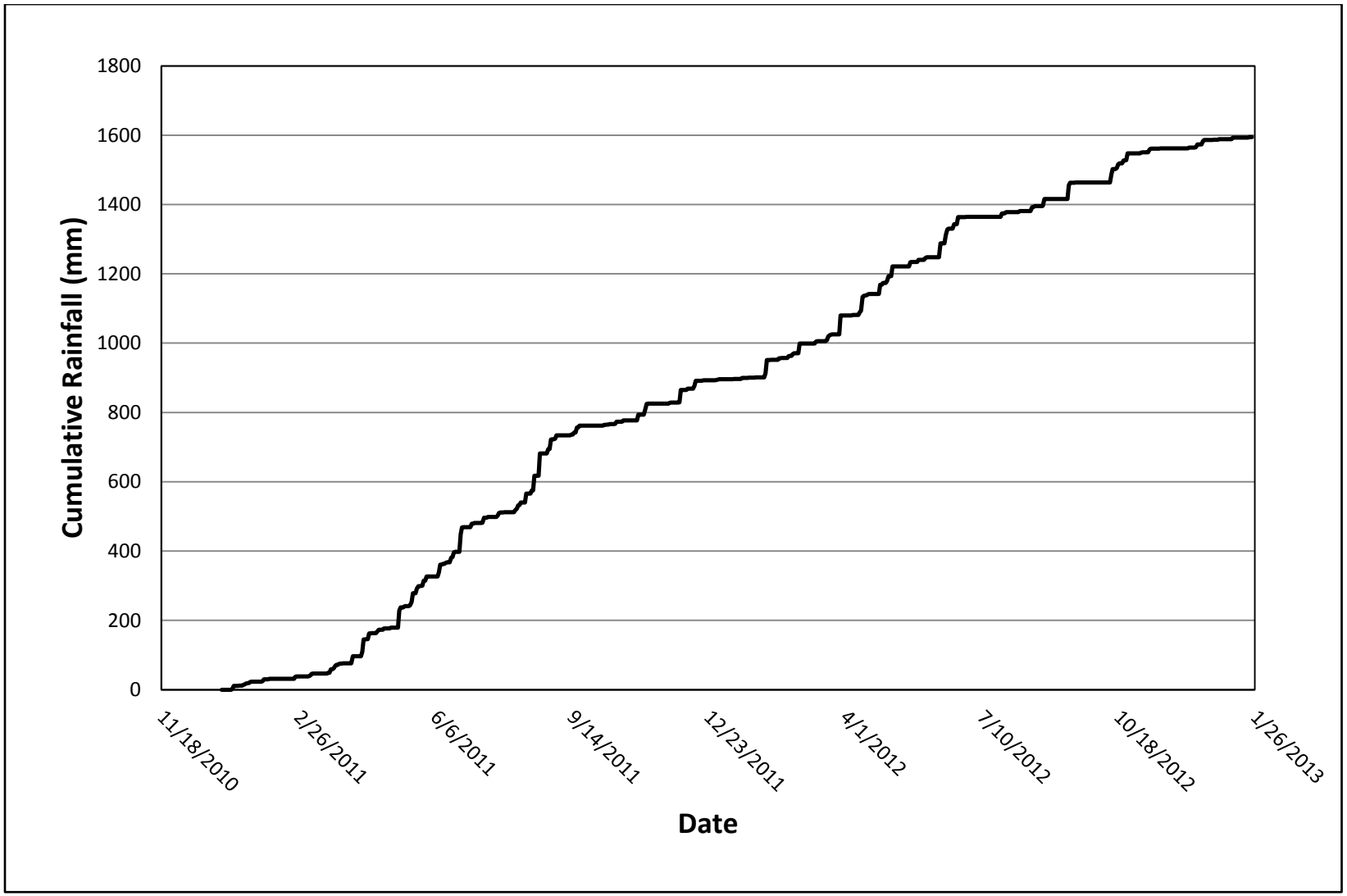

Figure C2: Cumulative rainfall for Mud Creek during study period

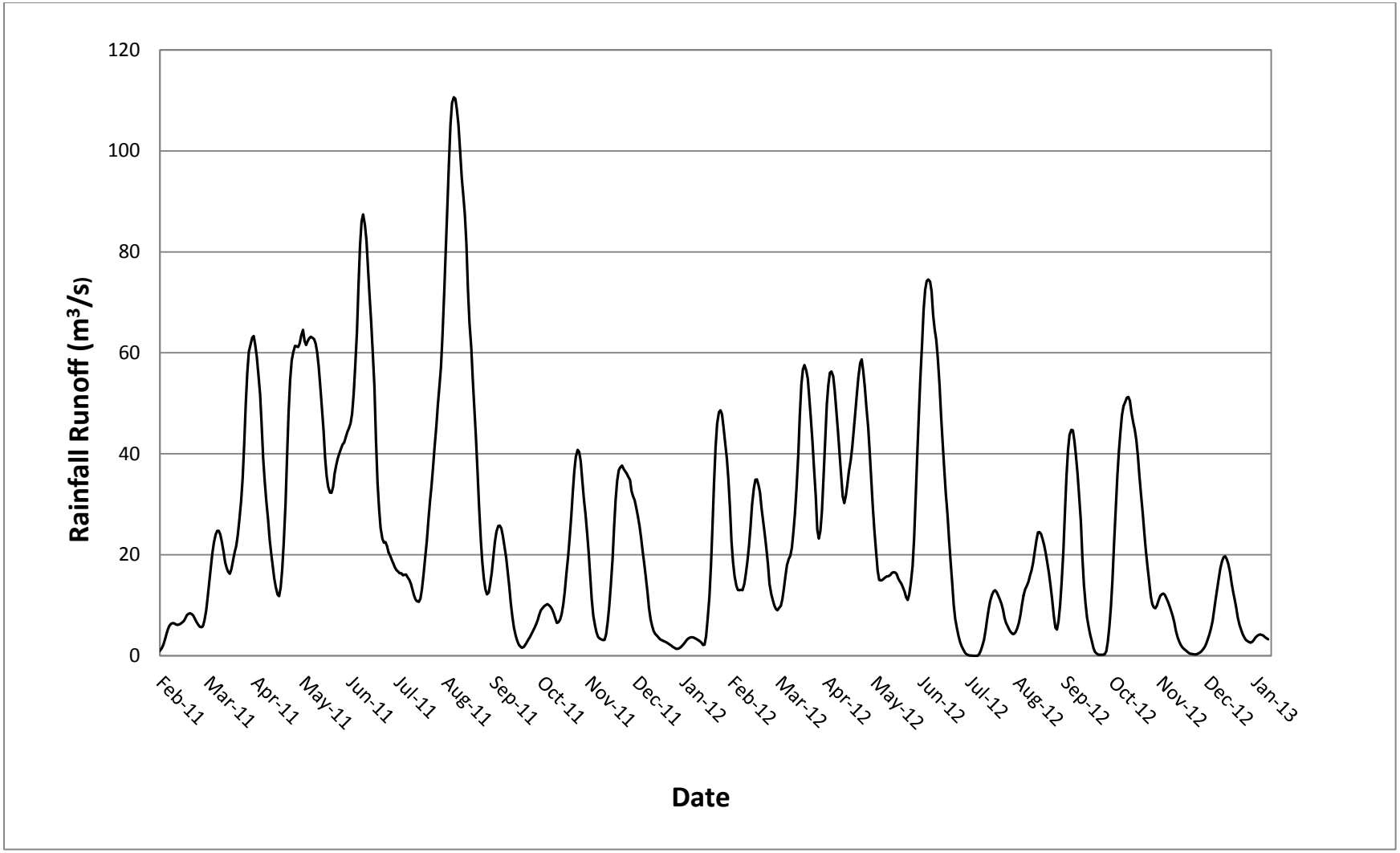

Figure C3: Runoff hydrograph for Mud Creek Watershed obtained using NRCS Unit Hydrograph method

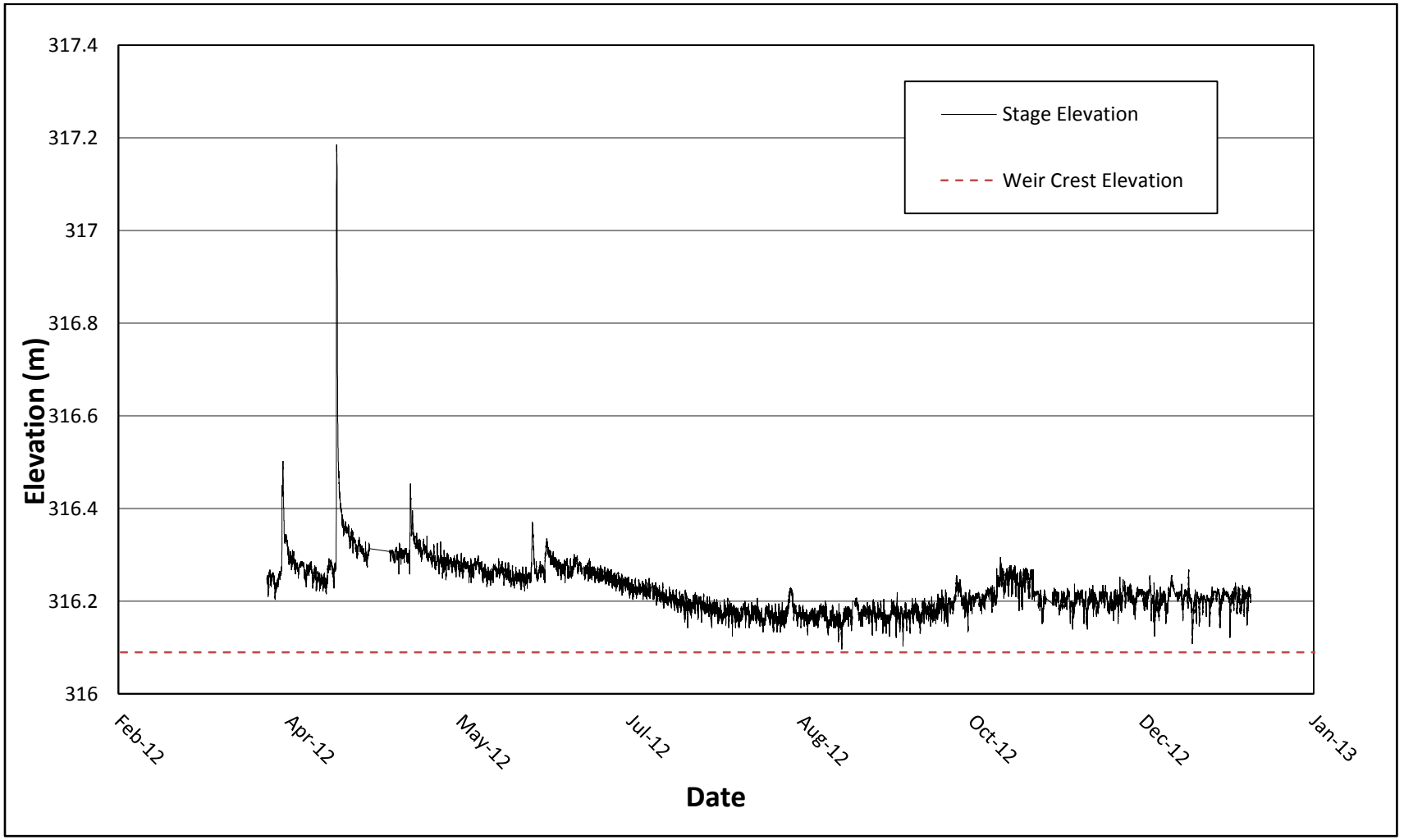

Figure C4: Stage elevation of Mud Creek provided from stage sensor

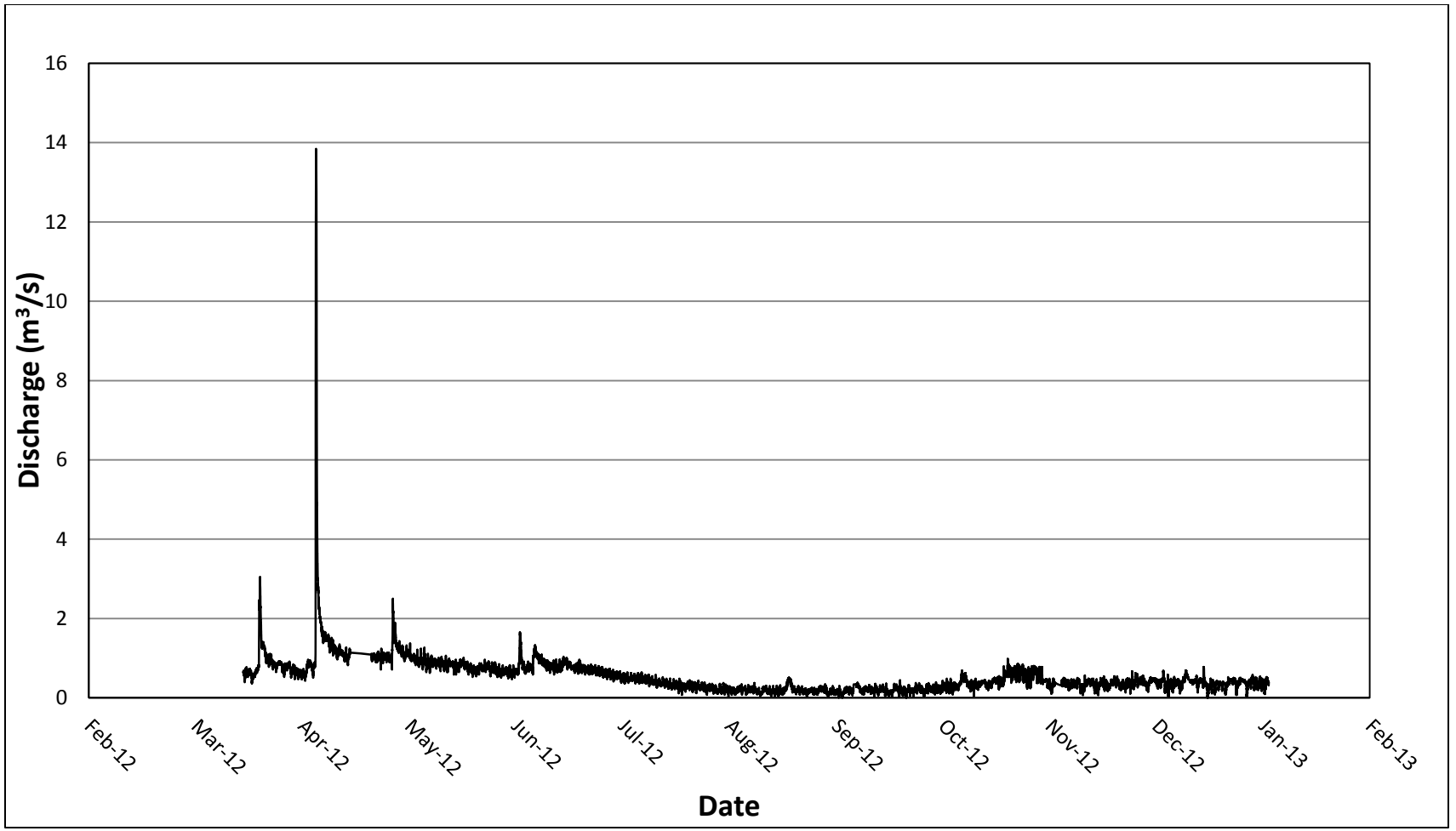

Figure C5: Hydrograph developed from broad crested weir equation